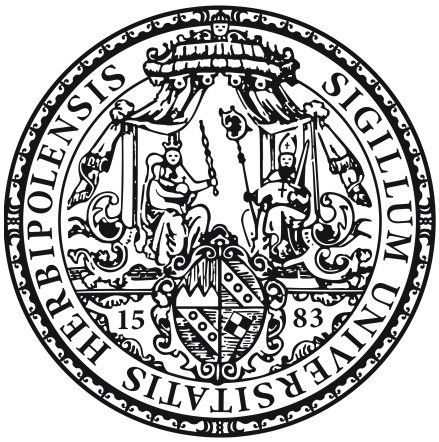

Development of human 3D tissue models for studying *Neisseria gonorrhoeae* infection

***

Entwicklung menschlicher 3D-Gewebemodelle zur Untersuchung der Infektion mit *Neisseria gonorrhoeae*

Doctoral thesis for a doctoral degree
at the Graduate School of Life Sciences,
Julius-Maximilians-Universität Würzburg,
Section Infection and Immunity

submitted by

Motaharehsadat Heydarian

from Tehran

Würzburg, 2019

Submitted on: ……

Members of the Thesis Committee

Chairperson: Prof. Dr. Christian Janzen

Primary Supervisor: PD Dr. Vera Kozjak-Pavlovic

Supervisor (Second): Prof. Dr. Thomas Rudel

Supervisor (Third): Prof. Dr. Heike Walles

Date of Public Defence: ……..……

Date of Receipt of Certificates: ……

Table of Contents

List of Figures

List of Tables

Summary

Gonorrhea is the second most common sexually transmitted infection worldwide and is caused by Gram-negative, human-specific diplococcus *Neisseria gonorrhoeae*. It colonizes the mucosal surface of the female reproductive tract and the male urethra. A rapid increase in antibiotic resistance makes gonorrhea a serious threat to public health worldwide. Since *N. gonorrhoeae* is a human-specific pathogen, animal infection models are not able to recapitulate all the features of infection. Therefore, a realistic in vitro cell culture model is urgently required for studying the gonorrhea infection. In this study, we established and characterized three independent 3D tissue models based on the porcine small intestinal submucosa (SIS) scaffold by co-culturing human dermal fibroblasts with human colorectal carcinoma, endometrial epithelial, and male uroepithelial cells. The histological, immunohistochemical, and ultra-structural analysis showed that the 3D SIS scaffold-based models closely mimic the main characteristics of the site of gonococcal infection in the human host including the formation of epithelial monolayer, underlying connective tissue, mucus production, tight junction (TJ), and microvilli. In addition, functional analysis such as transepithelial electrical resistance (TEER) and barrier permeability indicated high barrier integrity of the cell layer. We infected the established 3D tissue models with different *N. gonorrhoeae* strains and derivatives presenting various phenotypes regarding adhesion and invasion. The results showed disruption of TJs and growing the interleukins production in response to the infection, which depends on the type of strain and cell. In addition, the 3D tissue models supported bacterial survival, which provided an appropriate in vitro model for long-term infection study. This could be mainly because of the high resilience of the 3D tissue models based on the SIS scaffold to the infection in terms of alteration in permeability, cell destruction, and bacterial transmigration.

During gonorrhea infection, a high level of neutrophils migrates to the site of infection. The studies also showed that *N. gonorrhoeae* can survive or even replicate inside the neutrophils. Therefore, studying the interaction between neutrophils and *N. gonorrhoeae* is substantially under scrutiny. For this purpose, we generated a 3D tissue model by triple co-culturing of human primary fibroblast cells, human colorectal carcinoma cells, and human umbilical vein endothelial

cells. The tissue model was subsequently infected by *N. gonorrhoeae*. A perfusion-based bioreactor system was employed to recreate blood flow in the side of endothelial cells and consequently study human neutrophils transmigration to the site of infection. We observed neutrophils activation upon the infection. Furthermore, we demonstrated the uptake of *N. gonorrhoeae* by human neutrophils and reverse transmigration of neutrophils to the basal side carrying *N. gonorrhoeae.* In summary, the introduced 3D tissue models in this research represent a promising tool to investigate *N. gonorrhoeae* infections under close-to-natural conditions.

Zusammenfassung

Tripper ist die zweithäufigste sexuell übertragbare Krankheit weltweit und wird durch Gram negative, humanspezifische Diplokokken *Neisseria gonorrhoeae* verursacht. Das human Pathogen besiedelt die Schleimhautoberfläche des weiblichen Fortpflanzungstraktes und der männlichen Harnröhre. Die rasante Zunahme der Antibiotikaresistenzen macht Gonorrhö zu einer ernsthaften Bedrohung für die öffentliche Gesundheit weltweit. Da *N. gonorrhoeae* ein humanspezifischer Erreger ist, ist es nicht möglich alle Merkmale einer Infektion in Tiermodellen nachzustellen, daher ist ein realistisches In-vitro-Zellkulturmodell für die Untersuchung der Gonorrhö-Infektion dringend erforderlich. In dieser Studie haben wir drei unabhängige 3D-Gewebemodelle etabliert und charakterisiert, die auf dem Gerüst der Schweine-Submukosa (SIS) basieren, indem wir menschliche dermale Fibroblasten mit menschlichen Darmkrebs-, Endometrialepithel- und männlichen Uroepithelzellen kultivieren. Die histologischen, immunhistochemischen und ultrastrukturellen Analysen zeigten, dass die 3D SIS-Gerüstmodelle die Hauptmerkmale der Stelle der Gonokokken Infektion im menschlichen Wirt genau nachahmen, indem sich Epithelien Monoschichten ausbildeten, unter denen sich Bindegewebe erstrechte. Zudem wiesen die Zellen enge Zell-Zell Kontakte auf und es kam zur Produktion von einer Mukosaschicht sowie Mikrovilli in den Modellen. Darüber hinaus zeigten Funktionsanalysen wie die Messung des transepithelialen elektrischen Widerstands (TEER) und die der Barriere Durchlässigkeit eine hohe Barriere Integrität der Zellschicht. Wir haben die etablierten 3D-Gewebemodelle mit verschiedenen *N. gonorrhoeae*-Stämmen und Derivaten infiziert, die verschiedene Phänotypen bezüglich der Adhäsion und der Invasion aufwiesen. Die Ergebnisse zeigten eine Unterbrechung der engen Zellverbindungen und eine Zunahme der Interleukin Produktion als Reaktion auf die Infektion, dessen Ausprägung allerdings stark von der Art des Stammes und des verwendeten Zelltyps abhängig ist. Darüber hinaus unterstützten die 3D-Gewebemodelle das bakterielle Überleben, was ein geeignetes In-vitro-Modell für Langzeit-Infektionsstudien liefert. Dies könnte vor allem auf die hohe Widerstandsfähigkeit der SIS-Gerüstmodelle gegen Infektionen in Bezug auf Veränderung der Permeabilität, Zellzerstörung und Bakterienwanderung zurückzuführen sein.

Während der Gonorrhoe-Infektion wandert ein hoher Anteil an Neutrophilen an den Ort der Infektion. Die Studie zeigte auch, dass *N. gonorrhoeae* in den Neutrophilen überleben konnten oder sich sogar in diesen vermehren konnten. Deshalb wurde besonderes die Interaktion zwischen Neutrophilen und *N. gonorrhoeae* näher betrachtet. Zu diesem Zweck haben wir ein 3D-Gewebemodell mit Hilfe einer dreifache Co-Kultivierung von menschlichen primären Fibroblasten Zellen, menschlichen kolorektalen Karzinomzellen und menschlichen Nabelvenenendothelzellen erstellt. Das Gewebemodell wurde anschließend mit *N. gonorrhoeae* infiziert. Ein perfusionsbasiertes Bioreaktorsystem wurde eingesetzt, um den Blutfluss auf der Seite der Endothelzellen nachzuahmen und somit konnte die Auswanderung menschlicher Neutrophile zur Infektionsstelle untersucht werden. Darüber hinaus konnte mit diesem Modell die Aufnahme von *N. gonorrhoeae* in menschliche Neutrophilen und deren Rückwanderung in den Blutfluss beladen mit *N. gonorrhoeae* nachgewiesen werden. Zusammenfassend lässt sich sagen, dass das in dieser Forschung vorgestellte 3D-Gewebemodell ein vielversprechendes Instrument zur Untersuchung von *N. gonorrhoeae*-Infektionen unter naturnahen Bedingungen darstellt.

Chapter 1 Introduction

1.1 Gonorrhea

The sexually transmitted disease (STD) gonorrhea caused by *N. gonorrhoeae* is the second most common STD in the world (Who 2012). Gonorrhea can also be transmitted from the mothers with gonococcal genital tract infections to their infant during birth and can cause neonatal blindness (Quillin and Seifert 2018; Rees et al. 1977; Woods 2005). More than 100 million new infections per year and the rapid increase of antibiotic resistance make gonorrhea a serious threat to public health worldwide (Liu, Egilmez, and Russell 2013; Ohnishi et al. 2011). The most common sites of *N. gonorrhoeae* infection are the mucosal surface of the female cervix and the male urethra, anorectal, pharyngeal, and conjunctival areas (Miller 2006). The viscoelastic gel-like cervical mucus contains a variety of antimicrobial peptides which prevents pathogen to enter in the deeper layer (Hansen et al. 2014). However, some strains of *N. gonorrhoeae* are capable to pass through the endometrium monolayer and cause systematic infections (Hansen et al. 2014; Łaniewski et al. 2017). The systematic disseminated gonococcal infections (DGI) are reported in the patients (≈ 3%) (Kerle, Mascola, and Miller 1992) and it can also cause endocarditis, meningitis, perihepatitis and permanent joint damage (Cannon, Buchanan, and Sparling 1983; Kerle et al. 1992; Knapp and Holmes 1975).

1.2 Symptoms, diagnosis, and treatment

The risk of STD acquisition differs between males and females. In the case of females, STD may cause infertility, ectopic pregnancy or even genital-tract cancer (Hook 2012). There are two types of symptomatic and asymptomatic gonorrhea infections both in men and women (Quillin and Seifert 2018). In general, the diagnosis of gonorrhea in women is more complicated due to the fact that symptoms in women are various and likely to be non-specific (Hook 2012). There are a variety of symptoms that are associated with gonorrhea in women such as vaginal discharging, vaginal bleeding, and cervicitis (Miller 2006). Nevertheless, many female patients do not show any specific symptoms. Approximately 10-20% of the women with gonorrhea are at risk of pelvic inflammatory disease (PID) such as salpingitis and endometritis which impacts their fertility (Workowski and Bolan 2015). In male patients, gonorrhea disease is normally symptomatic including penile discharge and dysuria (Miller 2006).

Furthermore, sexual dimorphism is playing a key role in STD. For instance, pathogens may quickly dry and lose their viability in men due to a short period of contact with the pathogen during sex (Hook 2012). Hormonal fluctuations in female affect endocervical columnar epithelium cells providing more target cells for *N. gonorrhoeae* (Hook 2012).

The conventional diagnosis method of gonorrhea is a Gram-stain of the purulent exudate from the patient (Quillin and Seifert 2018). The presence of Gram-negative bacteria and high levels of neutrophils are two main signs of the infection. Recently, modern assays have been developed based on the amplification of nucleic acid (Quillin and Seifert 2018).

The history of control and treatment of gonorrhea is back to 1930 with sulfonamides (Quillin and Seifert 2018). However, *N. gonorrhoeae* gained resistance against sulfonamides over time and other classes of antibiotics such as penicillin, ceftriaxone, tetracycline, and cephalosporins (Ohnishi et al. 2011; Unemo and Shafer 2014). Due to the high capacity of *N. gonorrhoeae* to develop the resistance against different types of antibiotics, the untreatable *Neisseria gonorroheae* is highly concerned so that WHO named *N. gonorrhoeae* as a superbug (Ohnishi et al. 2011; Quillin and Seifert 2018).

1.3 *Neisseria gonorrhoeae*

N. gonorrhoeae was discovered by Albert Ludwig Sigismund Neisser for the first time in 1879 (Ligon 2005). *N. gonorrhoeae* is anaerobic, Gram-negative, diplococci and human-specific pathogen which belongs to the *Neisseria* genus of the family of *Neisseriaceae* (Doyle et al. 1984). The genus *Neisseria* is made of a large number of different *Neisseria* species with distribution in humans or another host. *N. meningitidis* and *N. gonorrhoeae* are among two important human-specific pathogens that are a causative agent of meningitis and gonorrhea respectively (Knapp and Clark 1984; Liu, Tang, and Exley 2015). It has been shown that both *N. meningitidis* and *N. gonorrhoeae* obtain iron from human iron-binding proteins (lactoferrin and transferrin), which makes both of these strains human-specific pathogen (Mickelsen, Blackman, and Sparlingl 1982).

1.4 Virulence factors

Bacterial pathogens contain a different set of virulence factors that make the bacteria capable of

infection and survival in the host (Rahme et al. 1995). *N. gonorrhoeae* have different types of virulence factors (Figure 1) such as pili which enable the attachment of bacteria to human epithelial cells (Maier and Wong 2015). The opacity proteins (Opa) proteins are also essential for efficient host cell invasion. Both Pili and Opa are capable of phase and antigenic variation (van Putten 1993). Apart from pili and Opa, another virulence factor expressing by *N. gonorrhoeae* is major outer membrane porin (PorB) including two subtypes ($PorB_{IA}$ or $PorB_{IB}$). Lipooligosaccharides (LOS) and immunoglobulin A1 (IgA1) protease are other virulence factors that are produced by *N. gonorrhoeae.* The immunocompetent cells produce and secrete a variety of antibodies such as human IgA into the human mucosal surface as a human defense mechanism (Plaut et al. 1975). *N. gonorrhoeae* produces IgA1 protease enzyme enabling bacteria to break the hinge of IgA1 (hIgA1) and cleave a major lysosomal-associated membrane protein 1 (LAMP-1). The pathogen debilitates the human immune defense mechanism using this enzyme (Hopper, Vasquez, et al. 2000).

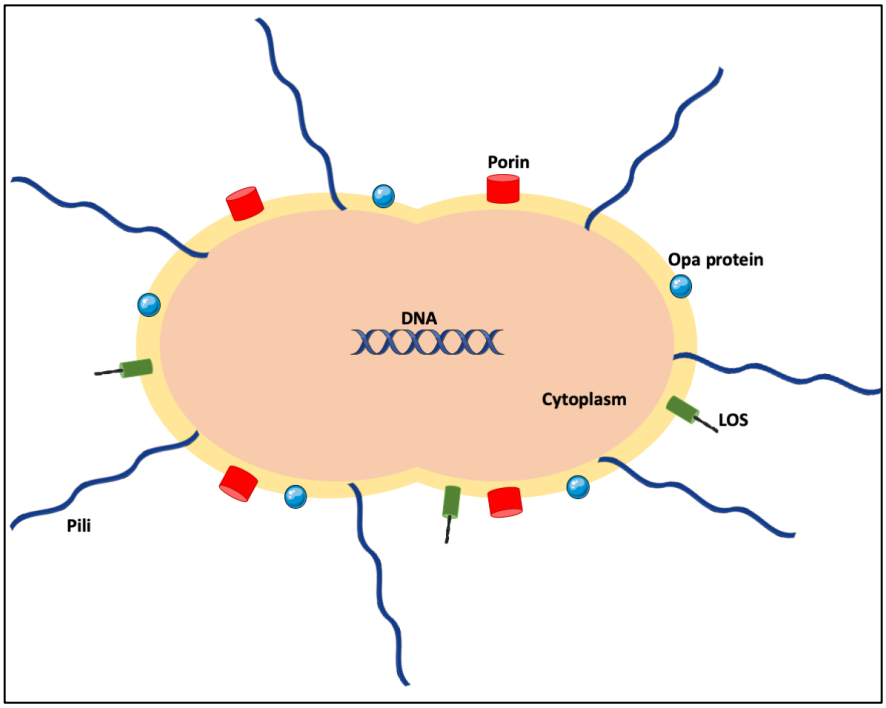

Figure 1. Overview of *Neisseria gonorrhoeae* pathogenesis factors.
N. gonorrhoeae contain different types of virulence factors including pili, Opa, porin, and LOS, which enable the attachment and invasion of bacteria to human epithelial cells. Hair-like pili are responsible for adherence, mobility, DNA uptake, and biofilm formation. Opa proteins mediate cell invasion and immune scaping. Porins, which are characterized by β- barrel structure, are responsible for ion exchanging and modulate the host cell apoptosis. LOS plays a key role in host adhesion and immune evasion.

Different types of strains of *N. gonorrhoeae* may contain a variety of lipopolysaccharide (LPS) components with different structures (Yamasaki et al. 1994). LPS is a pathogen surface component with antigenic variation. They are composed of a backbone of hydrophobic lipid and variable hydrophilic core oligosaccharide units (van Putten 1993). LPS phase variation is responsible for the capacity of bacteria for entrance and translocation through the mucosal lining and subsequently defection from the host immune mechanisms. LPS phenotype of each bacteria is determined based on variations of LPS produced by the pathogen (Moran, Prendergast, and Appelmelk 1996). Since in *N. gonorrhoeae* O-repeating subunits are missing, LPS are called LOS (Griffiss et al. 1988; Moran et al. 1996).

1.4.1 Pili

Pilus is a thin, long filamentous surface structure in many bacteria species including *N. gonorrhoeae* (Fussenegger et al. 1997). Type IV pili is one of the *N. gonorrhoeae* virulence factors, which is responsible for attachment of bacteria to the epithelial cells, human sperm, mucosal surfaces, moving across the human host cells, resistance in the human polymorphonuclear leukocytes, microcolony formation, bacterial aggregation, and transformation (James-Holmquest et al. 1974; Maier and Wong 2015; Merz and So 2000; Punsalang and Sawyer 1973; Rudel et al. 1992). The size of type IV pili filamentous polymers diameter is 6- 9 nm and the length might be different (0.9 ± 0.1 μm) (Craig and Li 2008; Holz et al. 2010).

N. gonorrhoeae pili are made up of different Pilin subunits (18-24 kDa), which are encoded by PilE gene (Freitag, Seifert, and Koomey 1995; Fyfe, Carrick, and Davies 1995). The two major subunits of pili are PilE and PilC, two phase-variable pilus-associated proteins that are responsible for adherence, structural variation, and transformation (Rudel et al. 1992, 1995). *N. gonorrhoeae* is capable of DNA uptake via the presence of PilE. This advantage aids *N. gonorrhoeae* to escape from the immune system and adapt to the new environment. This horizontal genetic exchange also plays a crucial role in the pathogen evolution owing to the fact that *N. gonorrhoeae* is a human-specific pathogen (Fussenegger et al. 1997). *N. gonorrhoeae* is dependent upon PilC for epithelial adherence. It has been shown that the adherence property of the Pili in *N. gonorrhoeae*

is specific and varies between epithelial cells and erythrocytes (Rudel et al. 1992). PilD is an enzyme with peptidase activity, which has the second function of N-methyltransferase activity for modifying the proteins of type IV Pilin family (Strom, Nunn, and Lory 1993).

1.4.2 Opacity-associated proteins (Opa)

Opa are a variable outer membrane protein family involved in pathogenesis and phase variation. In general, there are 11 different OPA gene alleles can be switch on and off independently in terms of expressions (Kupsch et al. 1993). Following the adherence to the epithelial cells with pili, Opa proteins mediate the invasion process (Wang, Meyer, and Rudel 2008). *N. gonorrhoeae* is able to switch the expression of OPA gene on or off, independently. Therefore, different bacteria of the same colony could contain a variety of Opa proteins (Bhat et al. 1991). The human cell receptor for *N. gonorrhoeae* Opa protein is carcinoembryonic antigen-like cellular adhesion molecules (CEACAMs). CEACAMs are parts of immunoglobulin superfamily involved in different cell interactions and signaling. The interaction between *N. gonorrhoeae* Opa protein and CEACAMs could lead to phagocytosis (Martin et al. 2016). CEACAM1 is present in epithelial cells and immune cells such as T cells, B cells, and dendritic cells. Interaction between Opa and CEACAM1 causes phagocytosis of pathogen and protects it from other immune responses. In addition, the interaction between Opa and CEACAM3, which is expressed by neutrophils triggers the immune response by producing granule and reactive oxygen species (ROS) (Stevens and Criss 2018). Another binding receptor of Opa is heparan sulfate proteoglycans (HSPGs). Some types of Opa proteins such as Opa_{30} can bind to HSPG receptors , which leads to pathogen invasion (Merz and So 2000).

1.4.3 Major outer membrane protein (PorB)

Gram-negative bacteria contain a variety of channel-forming proteins so-called porin. The size of porins is approximately 30 kDa in *N. gonorrhoeae*. In general, porins are responsible for the uptake of the small nutrient molecule, which their presence is necessary for the viability of *N. gonorrhoeae* (Merz and So 2000; Zeth et al. 2013). Another virulence factor expressing by *N. gonorrhoeae* with multiple roles during the infection is the PorB (Chen and Seifert 2013). There are two PorB subtypes expressed by *N. gonorrhoeae*, $PorB_{IA}$ or $PorB_{IB}$. DGI is mostly caused by

$PorB_{IA}$ expressing gonococci in a phosphate-sensitive manner (Faulstich et al. 2015). It has also been shown that the growing rate of invasion in epithelial cells and reduction of phagocyte responsiveness can happen by mutation of the porin in *N. gonorrhoeae* (Bauer et al. 1999). Porin (ATP binding protein) with β- barrel structure in *N. gonorrhoeae* is a diffusion channel responsible for the small metabolite transportation. Following the infection, $PorB_{IA}$ transfers to the epithelial cytoplasmic membrane and eventually translocates into the inner membrane of host mitochondria (Zeth et al. 2013). Mitochondrial membrane potential ($\Delta\Psi_m$) then decreases, which induces the inner mitochondrial membrane permeabilization. Afterward, release of cytochrome c leads to the activation of pro-apoptotic factors and consequently host cell apoptosis (Kozjak-Pavlovic et al. 2009; Rudel, Kepp, and Kozjak-Pavlovic 2010).

In a low phosphate environment, *N. gonorrhoeae* binds to the Gp96 binding protein and interacts with cell scavenger receptor I (SREC-I) via Gp96. Following the proper adherence, Gp96 may separate from SREC1 in order to invasion into epithelial cells (Rechner et al. 2007). This process triggers a cascade of cell signaling, which finally causes cytoskeleton rearrangement and uptake of a pathogen. It has also been reported that this type of invasion relies on the activation of neutral sphingomyelinase type 2 (NSM2) and is independent of other virulence factors such as pili and Opa (Faulstich et al. 2015).

Integral ß- barrel outer membrane proteins (OMPs) are present in Gram-negative bacteria which are playing various essential structural and functional roles in nutrient obtaining, secretion, and signaling. Moreover, they are essential for producing membrane vesicles (Sikora et al. 2018). *N. gonorrhoeae* also hires outer membrane vesicles (OMVs) in order to transfer PorB proteins to the mitochondria of macrophages (Deo et al. 2018).

1.5 Anatomy of the female reproductive tract

N. gonorrhoeae is a sexually transmitted pathogen that infects the genital tract. Therefore, the reproductive tract is the primary site of infection of *N. gonorrhoeae*, in which the pathogen can spread through the bloodstream and infect other parts of the body.

The female reproductive tract is divided into five different anatomical parts with diverse functions including fallopian tubes, uterus, endocervix, ectocervix, and vagina (Wira, Rodriguez-

Garcia, and Patel 2015) (Figure 2). The female reproductive tract has a mesodermal origin. Each part develops to special epithelial form during the development process. The uterus is composed of a simple columnar epithelium and the cervix and vagina are made out of the stratified squamous epithelium. The meeting area of these two parts is called the transformation zone. Although all anatomical regions of the female reproductive tract have the same origin, each part has the unique morphology and gene expression (Kurita 2011; Nguyen et al. 2014; Wessels et al. 2018).

The menstrual cycle is the vital regular natural change that happens in the female reproductive system and makes pregnancy possible. The cycle is divided into two main phases, namely proliferative and secretory. Throughout this cycle, ovarian follicular development, ovulation and remodeling of the endometrium (regeneration, differentiation and shedding) occur. In addition, metabolism of amino acid, lipid, carbohydrate, energy and vitamin is fluctuated over the different phases of this cycle (Draper et al. 2018; Mihm, Gangooly, and Muttukrishna 2011; Turco et al. 2017).

In addition, ovarian steroid hormones alter during the pregnancy and menstruation cycle. Therefore, the morphology, cellular and extracellular constitutions of human endometrium, which consists of two parts namely as epithelium and stroma, are influenced by hormones fluctuation (Ghosh and Sengupta 1995; Wira et al. 2015).

Among different cells in the connective tissue, fibroblasts are responsible for the structure and shape of the connective tissue by producing and secreting the extracellular matrix (ECM) components such as collagen, glycosaminoglycans, and proteoglycans (Le and Brown 2012). Fibroblasts also play an important role in immune responses by producing and responding to a variety of cytokines (Delves, Peter 1999). In the cervix, fibroblasts are responsible for regulating the ECM and pro-inflammatory cytokine (e.g. IL-1B) and hormones (e.g. progesterone) (Shukla et al. 2018).

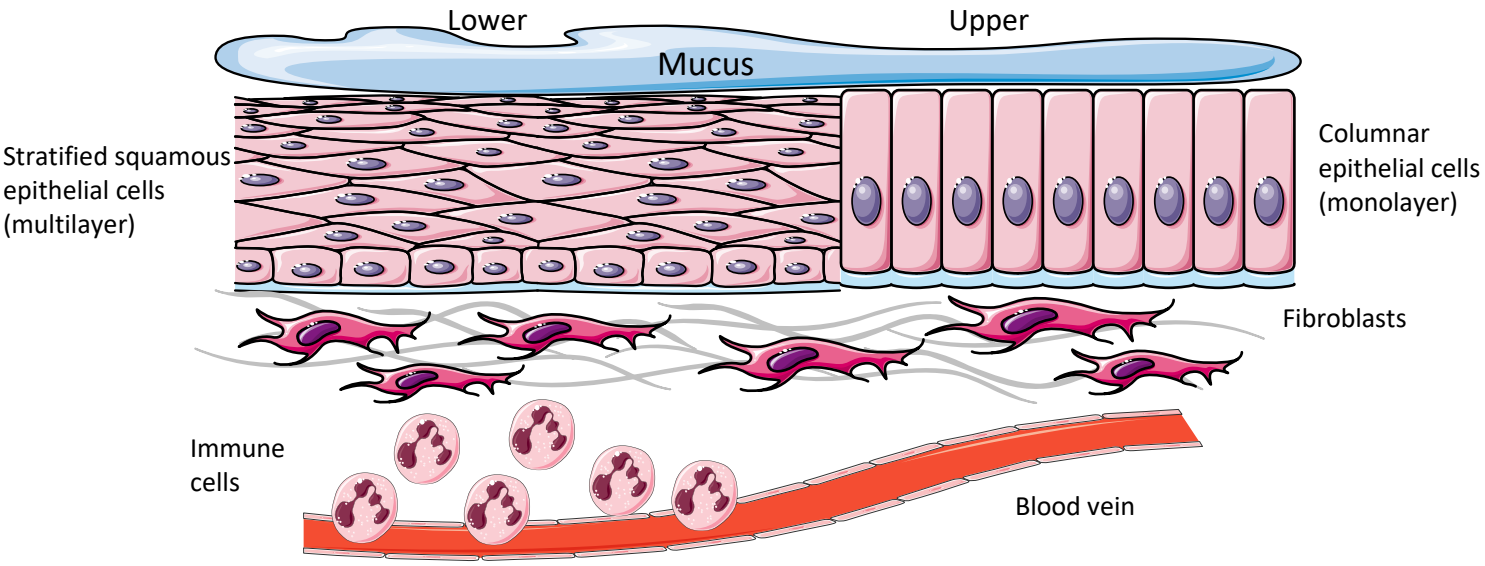

Figure 2. The female reproductive tract epithelium.

The female reproductive tract is divided into two main parts, namely the upper tract and lower tract. The lower tract (vagina and ectocervix) has a multilayer structure of stratified squamous epithelial cells (basal, intermediate and superficial epithelial cells). This part is not changing during the menstrual cycle. The upper tract (endocervix, endometrium, and fallopian tube) structure is made of a monolayer of columnar epithelial cells. Proliferation and gland formation of endometrium columnar epithelial cells occur during the menstrual cycle. The meeting area of these two parts is the transformation zone. Mucus covers the epithelial surface mostly lower tract with different thicknesses during the cycle. Residence bacteria such as *Lactobacillus* are also present in the female reproductive tract. Connective tissue under beneath epithelium contains compact fibroblast layers. Blood vessels supply the immune cells especially with a higher rate in the transformation zone.

1.5.1 Mucus

Epithelial cell layer covers the female reproductive tract, offering an appropriate condition for sperm and ovum movement and fertilization. The proper function of the female reproductive tract organ depends on the formation and secretion of a fluidic layer by epithelial cells that cover the cervical canal. The properties of this fluidic layer or so-called mucus are influenced by environmental parameters such as pH, the content of water, electrolytes, and carbohydrates (Gorodeski 1996). Mucosal epithelial cells of the female reproductive tract secrete a high quantity of mucins, which are extremely glycosylated, with high molecular weight (≥ 200 kDa). The amount of mucus production in the endocervix is variable to mediate the sperm migration process.

(Gipson 2001; Meseguer, Pellicer, and Simo 1998; Navabi, McGuckin, and Lindén 2013). Two types of mucus are covering the female reproductive tract, namely estrogenic (over the proliferative phase) or progestational mucus (over the secretory phase). Estrogenic mucus is a thin layer of mucus with low viscosity to facilitate the movement of sperm. In contrast, progestational mucus is a dense layer to obstruct the sperm transition (Hickey et al. 2011). Moreover, the mucus contains a variety of anti-microbial peptides (AMPs). The AMPs are produced and released by epithelial cells in the female genital tract and possess different mechanisms of actions, such as bacterial opsonization or recruitment of immune cells. The number of AMPs varies during hormonal regulation over various stages of the female menstrual cycle (Yarbrough, Winkle, and Herbst-Kralovetz 2015).

1.5.2 Microbiota

The inside of the female genital tract has been considered as a no resident bacteria zone or sterile region due to the limitation in detection techniques. However, novel technologies, such as next-generation sequencing (NGS) revealed that the different types of microbes exist in this region (Rampersaud, Randis, and Ratner 2012; Simon 2018). Microbiota in different sites of the female reproductive tract (cervix, fallopian tube, fluids, and vagina) are not similar. It has been shown that there is a relation between microbiota and menstrual cycle. During different phases of the menstrual cycle, the microbiota presents at the vagina and uterus are dissimilar (Chen et al. 2017; Forsgren-brusk 2006). The existing bacteria in the female genital tract have a major modulatory role in the host inflammatory reactions. For example, *Lactobacillus jensenii* produces different materials such as lactic acid which is crucial for vagina health (Anahtar et al. 2015; Mirmonsef et al. 2011). It has also been shown that the presence of *L. jensenii* prevents the *N. gonorrhoeae* adherence and invasion to the epithelial cells of the female genital tract with different mechanisms such as acidification (Graver and Wade 2011; Spurbeck and Arvidson 2010). *In vitro* gonococcal growth is difficult to achieve due to the complex nutritional growth requirements including the source of glucose, glutamine, thiamine, phosphate, iron and carbon dioxide which are normally present in the site of infection. Therefore *N. gonorrhoeae* have to compete with residence microbiota for gaining access to nutrients (Quillin and Seifert 2018).

1.5.3 Hormones

The endometrium changes over the menstrual cycle in response to hormones including estrogen and progesterone. The hormone estrogen is produced by the ovaries throughout the first part of the cycle. Estrogen has different responsibilities such as epithelial proliferation, the attraction of immune cells to stroma and provoking the progesterone receptors. In contrast, progesterone is involved in the differentiation process of epithelial cells implantation. These two hormones have their own receptors and duties. Upregulation and downregulation of their expression are essential for the whole cycle. Microvilli on the surface of epithelial cells can be influenced by hormones changes during the menstrual cycle (Stavreus-Evers et al. 2001; Wada-Hiraike et al. 2006). Furthermore, estrogen and progesterone are effective in the decidual transformation of the stromal cells (Irwin et al. 1989; Young 2013). It has been studied that hormonal fluctuations indirectly affect the gonorrhea infection via endometrium alternation. However, the estrogen and progestogen hormones can directly affect *N. gonorrhoeae* by inhibition of oxygen consumption and glucose catabolism (Lysko and Morse 1980).

1.5.4 Cell junctions and cytoskeleton

Zonula occludens (ZO) proteins, comprising ZO-1, -2, and -3, are high molecular weight (e.g. ZO-1 is a 220 kDa) peripheral membrane protein localizing at junctional sites (Li and Poznansky 1990). The female reproductive tract epithelium layer in different areas such as endocervix, uterus, and fallopian tubes are tightly sealed by these junctions. Therefore, the polarized epithelial cells in the female reproductive tract are known as the first line of defense against pathogens (Wira, Grant-Tschudy, and Crane-Godreau 2005). It has been shown that *N. gonorrhoeae* has developed a mechanism to disrupt the TJs and adherence junctions in epithelial cells in order to migrate through the cell monolayer for colonization (Edwards et al. 2013; Maisey et al. 2012). In addition, cytoskeletal rearrangement and microvilli elongation in epithelial cells can occur during *N. gonorrhoeae* infection (Giardina et al. 1998; Grassmé, Ireland, and van Putten 1996).

1.6 Male reproductive tract

The male reproductive tract is made of two major parts, namely penile urethra and testes. The penile opening region is composed of a stratified squamous epithelium which is similar to the lower tract in the female. The bulbous and spongy parts are lined by a pseudostratified glandular columnar epithelium which is responsible for producing the liquids (Figure 3). Production of sperm and sex hormones happen in testis. Penile urethra is the main region of infection with *N. gonorrhoeae* in males. The presence of mucus and AMPs and different types of Toll-like receptors (TLRs) are also features of the male reproductive tract (Anderson, Politch, and Pudney 2011; Nguyen et al. 2014; Pudney and Anderson 2011).

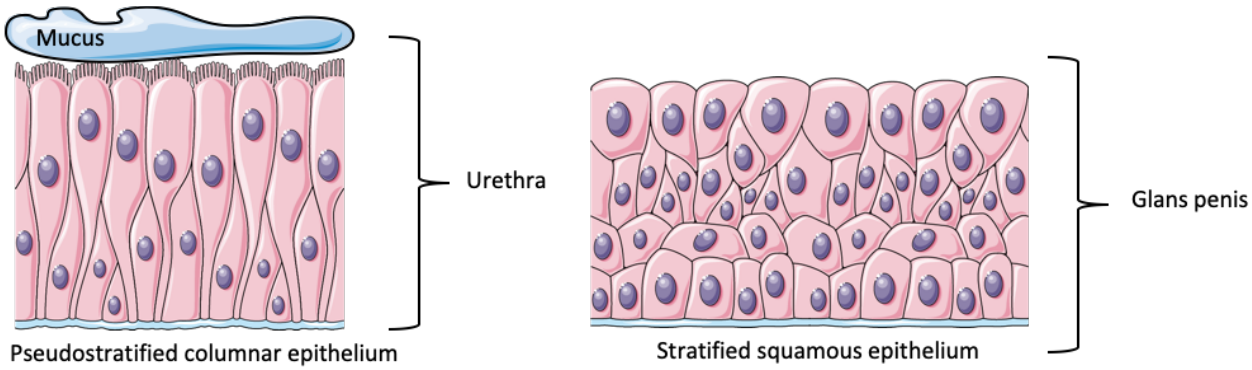

Figure 3. The male reproductive cellular structure.
The male reproductive tract is made of two major parts namely penile urethra and testes. The opening part of the penile is made out of stratified squamous epithelium and the inside part is made of pseudostratified columnar epithelium. Inside the urethra, the penile small gland produces mucus and AMPs are present in this part.

1.7 Host-cell interaction

N. gonorrhoeae use different mechanisms in order to interact with the host epithelium including adhesion to the surface, exocytosis and intracellular penetration (Mosleh et al. 1997). The transmigration of *N. gonorrhoeae* across the human epithelial cells is the process that has not been completely clarified yet. The pathogen may stay inside intracellular vacuole or may escape into the cell cytosol indicating host and pathogen dependency of the infection. The interaction between *N. gonorrhoeae* and host cells is triggered by pili, which are responsible for bringing *N.*

gonorrhoeae physically close to host cells. In the next step, Opa mediates bacterial-host cell interaction and facilitate the invasion of bacteria to the host cell. As a result of infection, epithelial shading occurs due to the induction of apoptosis (L. C. Wang et al. 2017).

1.8 Immune response

The presence of the immune system in the female reproductive tract protects the organ against a variety of sexually transmitted infections. Various types of innate immune actions exist in the female reproductive tract such as secretion of antimicrobial peptides and cytokines (secreted proteins and signal molecules), mucus layer and TJs in epithelial cells (Hickey et al. 2011). The secretion of different hormones such as estradiol and progesterone affect the immune system by increasing the number of circulating immune cells.

Rapid exfoliation in response to bacterial infection is a defense mechanism of host cells to hinder the bacteria to spread. During this process, the contaminated host epithelial cells are detached from the epithelial layer causing substitution with new epithelial cells (Kim et al. 2010). Once the pathogen passes the epithelial cells, it encounters the fibroblasts. These fibroblasts have the capacity to become activated by inflammatory cytokines. Subsequently, they secrete different cytokines in order to recruit the immune cells to the site of infection (Wira et al. 2015).

Interleukins (ILs) are a group of cytokines that mostly expressed by white blood cells during the innate response with a variety of functions (Jerse, Bash, and Russell 2014). Interleukin 8 (IL-8) is a neutrophil activator peptide and neutrophil chemotactic stimulant (Smith et al. 1991). Interleukin 6 (IL-6) is a cytokine with anti-inflammatory properties, conducting neutrophils trafficking during inflammation (Fielding et al. 2008; Kishimoto 1989). Tumor necrosis factor alpha (TNFα) is an inflammatory cytokine mostly produced by macrophages during the acute inflammation, which is involved in a variety of cell signaling especially for infection resistance (Idriss and Naismith 2000).

Type of tissues and gender affect the inflammatory responses (Edwards and Apicella 2004). Inflammatory cytokines IL-6, IL-8, and tumor necrosis factor alpha (TNF-α) are present at the local site of infection before the onset of symptoms after challenge with gonococci (Ramsey et al. 1995). Harvey et al. developed a model for studying the inflammatory cytokine response to *N.*

gonorrhoeae infection using immortalized human urethral epithelial cells. They found that the immortalized urethral epithelial cells secreted higher levels of IL-6 and IL-8 following gonococcal infection. In addition, IL-6 and IL-8 levels in the primary urethral epithelial cell supernatants increase after challenge with *N. gonorrhoeae* (Harvey, Post, and Apicella 2002).

Fichorova et al. showed an upregulation of IL-8 and IL-6 after 4h of infection with both piliated and non-pilated *N. gonorrhoeae* in female cervical cells. They also showed the presence of *N. gonorrhoeae* itself stimulate the increasing level of IL-6 and IL-8 and is independent of pathogen uptake (Fichorova et al. 2001). Christodoulides et al. also showed that the level of TNFα secretion increases upon infection with *N. gonorrhoeae* regardless of pilus expression (Christodoulides et al. 2000).

TLRs are important innate immune response receptors upon the presence of pathogens. Studies showed that they are not expressed at the same level through the female reproductive tract. Different expression pattern aids us to understand the regulation of immunity upon infection (Pioli et al. 2004). Especially TLR 4 in the female genital tract is responsible for recognizing the Gram-negative bacterial compositions such as LOS leading to NF-kB signaling pathway activation and eventually the inflammation and production of a variety of chemokines. TLR activation promotes the immune cells to migrate to the site of infection (Anahtar et al. 2015; Wira et al. 2005).

It has also been reported that some intracellular *N. gonorrhoeae* suppress autophagy repressor mammalian target of rapamycin complex 1 (mTORC1) enabling escape from autophagy-mediated killing inside the epithelial cell (Lu et al. 2018).

1.8.1 Neutrophils

Neutrophils or polymorphonuclear lymphocytes (PMNLs) are the most frequent leukocytes in the blood and are considered as the first line of innate immune defense against pathogens (Kumar and Sharma 2010). Neutrophils are produced in the bone marrow and released to the blood. In non-infection conditions, neutrophils stay in blood circulation for a just few hours (the half-life is estimated at 6-12 h) before they leave into tissues (Rosales 2018).

In infection conditions, subpopulations of neutrophils transmigrate across the endothelial layer to the site of infection. This transendothelial migration process requires the bonding interaction between neutrophils ligands such as CD44 with ICAMs receptors, which are expressed on endothelial cells (Borregaard 2010). The mechanisms are used by neutrophils to control infection are a phagocytic activity, releasing antimicrobial molecules, and forming neutrophil extracellular traps (NETs) (Kumar and Sharma 2010). Although many neutrophils reach the site of infection, pathogens evade the neutrophils immune response via an unknown mechanism (Simons et al. 2005). A probable hypothesis about the survival of *N. gonorrhoeae* taken up by *human* neutrophils would be that *N. gonorrhoeae* remain undetected inside the neutrophils leading to infection dissemination between the partners. However, the role of neutrophils in gonococcal disease is still not fully understood due to the absence of relevant *in vitro* models (Quillin and Seifert 2018).

1.8.2 Macrophages

Macrophages are the primary mediators of granulomatous inflammation in the immune system that are formed through the differentiation of monocytes in response to infection (Gordon and Taylor 2005). A significant number of tissue macrophages can be presented in the cervix upon infection (Deo et al. 2018). However, high numbers of *N. gonorrhoeae* are able to survive and replicate inside the macrophages. *N. gonorrhoeae* can inhibit the macrophage apoptosis process. Therefore, macrophages could be considered as a niche for *N. gonorrhoeae* (Château and Seifert 2016). Macrophage infectivity potentiator (MIPs) is a surface-exposed lipoprotein of *N. gonorrhoeae*. Its main characteristic is the peptidyl-prolyl cis/trans isomerase (PPIase) activity and involvement in persistence in macrophages (Leuzzi et al. 2005). It has also been revealed that inhibitors of macrophage infectivity potentiator-like PPIases affect *N. gonorrhoeae* pathogenicity (Reimer et al. 2016). *N. gonorrhoeae* can induce macrophage apoptosis independently of entering the macrophages. In addition, *N. gonorrhoeae* release the outer membrane vesicles (OMVs) in order to transport PorB proteins to the mitochondria of macrophages, resulting in a loss of mitochondrial membrane potential, cytochrome c release and induction of apoptotic caspases, leading to cell apoptosis (Deo et al. 2018).

1.9 Tissue engineering

Translational research is limited by the lack of relevant tissue models, mimicking the site of infection in gonococcal infection. The advent of tissue engineering techniques enables researchers to recreate infection models to understand the mechanism of infection (Mills and Estes 2016).

Tissue engineering is an evolving and interdisciplinary field for developing functional biological tissues using a combination of cells, biomaterials, suitable biochemical and physicochemical factors and engineering. The main concept of tissue engineering is illustrated in Figure 4. Tissue engineering aims to manufacture a new viable tissues for application in medical research (Langer and Vacanti 1993). Three main components of tissue engineering are I. a scaffold which is a 3D structure that can be fabricated by biodegradable natural/synthetic-based biomaterials, II. cell sources that can be isolated cells or cell lines, and III. growth factors, which are necessary for cell activities and cell signaling (Langer and Vacanti 1993). Tissue engineering based on acellular scaffolds is one of the efficient strategies toward the development of new engineered tissues.

These matrices are mainly produced by mechanical or chemical removal of the cells and cellular components from the tissue in order to produce acellular collagen-rich matrices (Kloppot et al. 2015).

Scaffolds are the first requirement in tissue engineering. A scaffold is a porous matrix providing the 3D structural support for cell attachment, growth and subsequent tissue development. Scaffolds are typically manufactured from biocompatible and biodegradable polymeric biomaterials (natural or synthetic-based). The structural, biophysical and mechanical properties of the fabricated scaffolds are extremely important for the generation and development of new tissue (Yang et al. 2001). One of the major roles of the scaffold is to mimic the native architecture of ECM for cells (Li, Shanti, and Tuan 2007).

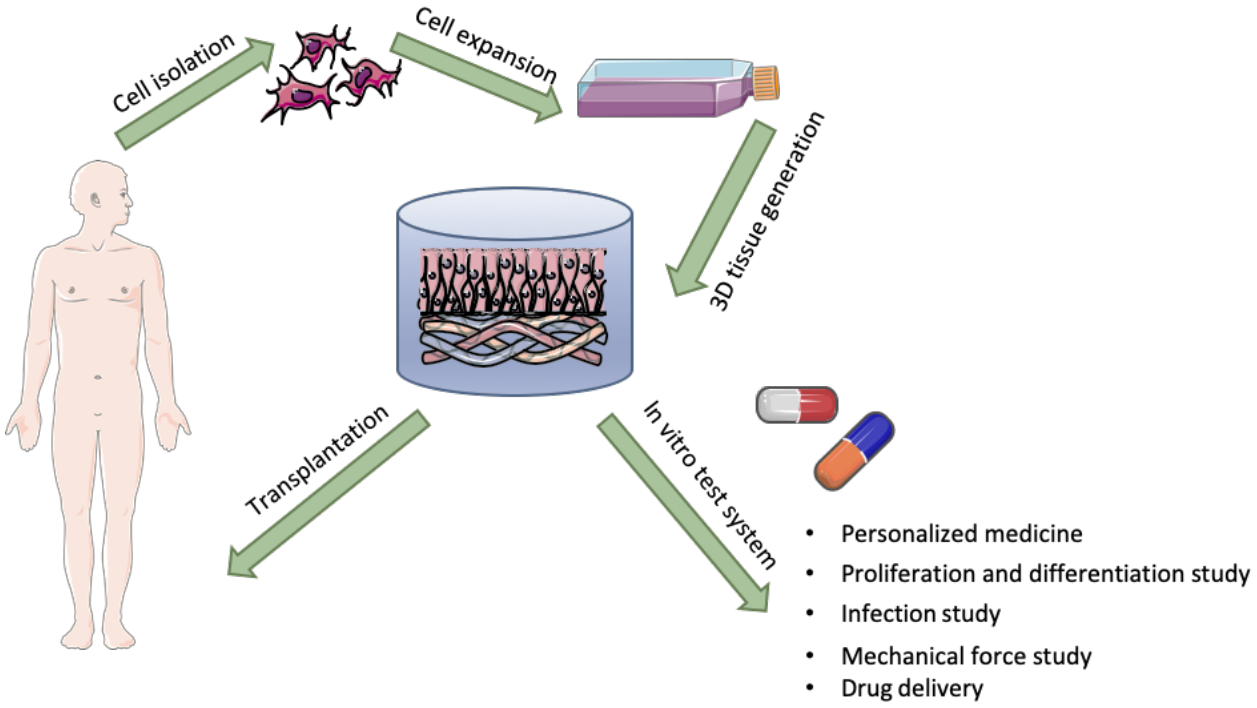

Figure 4. The general concept of tissue engineering.

Tissue engineering is a multidisciplinary field and combines the principles of cell biology, engineering, and materials methods to improve or replace damaged tissue and recovery organ function. Tissue engineering is comprised of different steps, from isolation and expansion of the cells to develop a tissue and organ substitutes for clinical transplantation. Tissue engineering covers a broad range of applications such as *in vitro* test systems for discovering new drugs and treatments.

Scaffolds are mainly fabricated from natural or synthetic materials. Natural-based scaffold materials such as collagen, fibrin, agarose, alginate, chitosan contain particular amino acids that facilitate cell attachment and support cell growth. In spite of this advantage, natural polymers are suffering from bench-to-bench variation (Drury and Mooney 2003; Langer and Vacanti 1993). Synthetic materials allow accurate control over the physical and mechanical properties of the final scaffold by playing with parameters such as molecular weight, concentration, and manufacturing method. Among synthetic polymers, polycaprolactone (PCL), polyethylene oxide (PEO), polylactide (PLA) are widely used.

Natural-based scaffolds such as decellularized tissue are currently being investigated as scaffolds for ex-vivo models. They are able to keep ECM characteristics of the native organ and provide suitable conditions for cell proliferation and differentiation (Gilbert, Sellaro, and Badylak 2006).

The acellular scaffold can be derived from different tissues such as heart valves, liver, blood vessel, nerves, skin, and skeletal muscle (Badylak 2007). Among them, porcine small intestinal scaffold (SIS) has been frequently used in many studies in order to establish a human tissue barrier for drug delivery investigations (Massie et al. 2017; Shi et al. 2013; Steinke et al. 2014; D. Wang et al. 2017). This type of scaffold is comparable to the commercially available *in vitro* cell culture model such as Transwell® insert system due to the high degree of cell parallelization (Schweinlin et al. 2017; Schweinlin, Wilhelm, and Schwedhelm 2016). SIS contains collagen, fibronectin, laminin, elastin, glycosaminoglycans, proteoglycans, and essential growth factors such as fibroblast growth factor-2 (FGF-2), transforming growth factor-beta1 (TGF-ß1) and vascular endothelial growth factor (VEGF). In addition, the SIS scaffolds provide an appropriate 3D porous structure with an interconnected pore size of ≤ 30µm in diameters and a thickness of 0.05-0.22 mm (Shi et al. 2013).

1.10 Models for studying *N. gonorrhoeae*

1.10.1 Animal models

Several studies have been conducted using animal models to investigate important host cell factors regarding the gonorrhea infection. These findings were crucial for understanding invasion and dissemination of *N. gonorrhoeae* and the corresponding immune responses (Table 1) (Arko 1972, 1974; Johnson, Taylor-Robinson, and McGee 1977; Lucas 1971). Particular animal models such as chimpanzees were successfully infected by *N. gonorrhoeae* (Arko 1989; Jerse et al. 2011). Physiology of the mouse reproductive tract is to some extent similar to the human female reproductive tract in oxygen tension reduction and glucose and lactate supplement. Nevertheless, there are differences between animal and human female reproductive tracts such as normal vaginal flora and the absence of serum factors releasing over the menstrual bleeding (Noguchi, Tsukumi, and Urano 2003). The average pH in the human vagina is 3.5-4.5 and in the cervix is 6.1 (during the secretory stage) and 6.8 (during the proliferation stage) (Jerse et al. 2011). It has been shown that β-estradiol treated mice can be infected with *N. gonorrhoeae* with the average pH of 6.6 (Muench et al. 2009). Another major difference between human and mice is the absence of special host-specific receptors which are a binding target of different virulence

factors in *N. gonorrhoeae* (Jerse et al. 2011). Several transgenic mice have been generated for expressing a variety of receptors such as human CEACAM1 expressing transgenic mice (Table 1). Using a humanized transgenic mice, it was shown that *N. gonorrhoeae* is able to bind the neutrophils via CEACAM1 ligands (Gu et al. 2010). Recently, Kim et al. modified animal models via estradiol treatment to explore the mechanism that commensal *Neisseria* use to kill *N. gonorrhoeae* (Kim et al. 2019). Transgenic animal models open a new window to understand the gonorrhea infection. These models were successful to create the early stages of *N. gonorrhoeae* infection (Francis et al. 2018; Gu et al. 2010; Wang et al. 2008). However, they cannot fully recapitulate all the features of the *N. gonorrhoeae* infection in the human (Quillin and Seifert 2018; Stevens and Criss 2018; L. C. Wang et al. 2017).

Table 1: Animal and *in vitro* cell culture models that have been used for studying Gonorrhea.

Models For studying *N. gonorrhoeae*

References	NG Strain	Animal model/*in vitro* model	The used Platform	Key results
(Lucas et al. 1971)	NA	Chimpanzee	Animal model	Chimpanzee was Introduced as a model for studying *N. gonorrhoeae* infection.
(Arko 1972)	NA	Rabbit, Guinea pigs, Hamsters, Mice	Animal model	infecting various laboratory animals with *N. gonorrhoeae*.
(Arko 1974)	NA	Rabbit, Guinea pigs, Hamsters, Mice	Animal model	Guinea pig was introduced as a most relevant model for studying immune responses in *N. gonorrhoeae*
(Johnson et al. 1977)	GC 2686	Human oviduct, Rabbit oviduc, Porcine pviduct	Animal model	Studying the species were caused damage by *N. gonorrhoeae*
(Shaw and Falkow 1988)	F62 , MS11	Hec1-B	2D cell culture	The HEC1B cell line was introduced as a model for studying the invasion of *N. gonorrhoeae*
(Rudel et al. 1992)	MS11	Corneal epithelial cells	2D cell culture	The requirement of interaction between PiLE and PiLC for pilus mediated adherence of *N. gonorrhoeae* to the host was studied.
(Grassmé et al. 1996)	VP1($Pili^{-}Opa^{-}$), MS11($Pili^{+}Opa^{-}$)	Chang cells	2D cell culture	The role of Opa was studied in rearrangements of the epithelial cell actin cytoskeleton
(Mosleh et al. 1997)	N137($Pili^{+}$ Opa^{30}), N263($Pili^{-}$ Opa^{30})	Distal ureters excised from healthy adult kidney donors	Ex-vivo model	The mechanisms of colonization and invasion of *N. gonorrhoeae* were revealed.
(Giardina et al. 1998)	FA1090, VP1, 1291	Primary urethral squamous epithelium	2D collagen-coated glass coverslips	The induction of actin focal polymerization was investigated by *N. gonorrhoeae*
(Wang et al. 1998)	N302–N313, MS11-B2.1, N483 MS11-F3, N496, N541, and N547	T84 cells	Transwell insert	The role of Opa binding to CD66 receptors was studied in transcellular traversal of *N. gonorrhoeae*.
(Wang et al. 2008)	N309 ($Pili^{-}$, Opa^{+}), N302 ($Pili^{-}$, Opa^{-}), N303 ($Pili^{-}$, Opa^{50})	T84 cells	Transwell insert	the role of cytoskeleton and motor proteins were examined in transcytosis of *N. gonorrhoeae*
(Gu et al. 2010)	E. coli-Opa^{+}	Transgenic mouse	Animal model	A human CEACAM1 transgenic mice was generated which *N. gonorrhoeae* Opa protein can bind to the neutrophils

(Li et al. 2011)	WHO-A NICPBP29106, YZ1006 and YZ1228	Transgenic mice	Animal model	Using human CEACAM1 transgenic mouse model for studying *N. gonorrhoeae* infections
(Maisey et al. 2012)	MS11 ($Pili^+/Opa^-$), FA1090 ($Pili^-/Opa^-$)	Ishikawa cell line	2D cell culture	Cell junction disruption in human genital epithelial cells is independent to Opa and Pili.
(Edwards et al. 2013)	MS11 ($Pili^+$ Opa^+)	T84 and HEC1B	Transwell insert	*N. gonorrhoeae* breaches the apical junction of polarized epithelial cells for transmigration by activating EGFR.
(Łaniewski et al. 2017)	MS11 ($Pili^+$ Opa^-)	HEC1A	Bioreactor	A bioreactor model was developed for studying *N. gonorrhoeae* infection under dynamic conditions
(L. C. Wang et al. 2017)	MS11 ($Pili^+$ Opa^-) MS11 ($Pili^+$ Opa^+)	Human endocervical tissue explants, T84	Transwell insert	*N. gonorrhoeae* activates non-muscle myosin II-mediated epithelial exfoliation
(Francis et al. 2018)	MS11 N313($Pili^-Opa^{57}$) and non-opaque MS11 N302 ($Pili^-$ Opa^-)	Wild and transgenic mice (hCEACAM1 CEABAC2 hCEACAM5)	Animal model	The effect of CEACAMs during *N. gonorrhoeae* infection was studied.
(Kim et al. 2019)	MS11, MS11/ΔpilT	Modified estradiol treated mice	Animal model	How *commensal Neisseria* kill *N. gonorrhoeae*

1.10.2 In *vitro* cell systems

Multiple *in vitro* cell culture models have been developed to study the interaction between the host cell and *N. gonorrhoeae* during infection. Table 1 presents *in vitro* cell culture models that have been used for studying *N. gonorrhoeae.* To our knowledge, Shaw and Falkow in 1998 reported the first *in vitro* model for studying the invasion of *N. gonorrhoeae* (Shaw and Falkow 1988). They developed a mono-culture model based on human endometrial adenocarcinoma (HEC-1-B) cell line. Further mono-culture models were also developed based on corneal epithelial cells (Rudel et al. 1992) and human conjunctival epithelial (Chang) cells (Grassmé et al. 1996). In 1998, Wang et al. established an *in vitro* epithelial model (human colorectal carcinoma cells (T84) cell line) on a Transwell® insert (Wang et al. 1998). The author investigated the role of Opa binding to CD66 receptors in the transcellular traversal of *N. gonorrhoeae*.

In 2008, Wang *et al* established an *in vitro* cell culture model using T84 cells on Transwell® insert. They studied the role of the cytoskeleton and motor proteins in transcytosis of different strains of *N. gonorrhoeae* ((N309 ($Pili^-$, Opa^+), N302 ($Pili^-$, Opa^-) N303 ($Pili^-$, Opa^{50})) (Wang et al. 2008).

In addition to the traditional cell culture models, bioreactor systems are widely employed in tissue engineering. Bioreactors are well-controlled cell culture platforms that support cell growth under dynamic culture conditions (Bancroft, Sikavitsas, and Mikos 2003). In 2017, Łaniewski et al. hired a rotating wall vessel (RWV) bioreactor system to study the colonization of the endometrium by *N. gonorrhoeae.* They indicated that infection with *N. gonorrhoeae* significantly induced proinflammatory mediators and caused ultrastructural alteration of the epithelial cells (Łaniewski et al. 2017).

The commonly used cell lines in gonorrhea infection study are HEC-1-B, T84, Chang, and human Asian endometrial adenocarcinoma cells (Ishikawa) (Grassmé et al. 1996; Shaw and Falkow 1988; Wang et al. 1998, 2008). Moreover, primary cells such as urethral epithelium (Giardina et al. 1998) and ex-vivo explants culture such as kidney and endocervix (Mosleh et al. 1997; L. C. Wang et al. 2017) have been recruited to study the *N. gonorrhoeae* infection.

In spite of many efforts to develop a suitable cell culture model, a biomimetic tissue model recreating the main feature of the site of infection during gonorrhea infection is not available.

All the major studies to date developed a mono-culture *in vitro* model based on the epithelial cells. However, as described in section 1.5 (Figure 2), the female reproductive tract made out of multilayers of epithelial and fibroblast cells providing barriers against pathogen invasion.

In this study, therefore, we aimed to:

a) establish a 3D tissue model based on the SIS scaffold in order to resemble functional and morphological features of the site of infection in the human body;
b) study the host cell-pathogen interaction via various bacterial strains and cell types in closer to natural conditions and
c) investigate the immune response to the pathogens in a more realistic model under dynamic culture conditions.

Chapter 2 Materials and Methods

2.1 Materials

The full details of materials, cell lines, bacteria strains, culture media, reagent, buffers, antibodies, kits, chemical and solution, and equipment have been used in this shown are listed in table 2-14.

Table 2. Antibodies

Name	Source	Ref. number
Anti E-Cadherin	Proteintech	20874-1-AP
Anti ZO1 Antibody	Proteintech	21773-1-AP
Anti- Fibroblast	Antikörper.online	ABIN4311698
Anti- *N. gonorrhoeae*	Antikörper.online	ABIN110874
Anti- NCF2 antibody (Neutrophil Cytosolic Factor 2) (Cy3)	Antikörper.online	ABIN750721
Anti- VE cadherin	Thermo Fisher	14-1441-82
Anti-CD11b	MACS	130-091-240
Anti-CD31 antibody	Abcam	ab24590
Anti-CD66b	Becton Dickinson	561650
Anti-MUC1 antibody	Abcam	ab45167
AntiPAX8 antibody	Abcam	ab97477
CY (2,3,5) Mouse CY (2,3,5) Rabbit	Dianova	111-225-144 115-225-146 111-165-144 115-165-146 115-175-146 115 175 146
DAPI	Sigma Aldrich	D9542-5MG
Phalloidin	MoBiTec GmbH	MFP-D555-33

Table 3. Bacteria strains

Strain	Phenotype
MS11	$PorB_{IB}$, $Pili^{+}$, Opa^{+}
MS11 ΔOpa	$PorB_{IB}$, $Pili^{+}$, Opa^{-}
N924	$PorB_{IB}$, $Pili^{-}$, Opa^{-}
N927	$PorB_{IA}$, $Pili^{-}$, Opa^{-}
N927 GFP	$PorB_{IA}$, $Pili^{-}$, Opa^{-}
VP1	$PorB_{IA}$, $Pili^{-}$, Opa^{-}

Table 4. Biological materials

Biological materials	Source
HEC1-B cell line	ATCC® HTB113TM
T84 cell line	ATCC® CCL-248TM
SV-HUC-1 cell line	ATCC®CRL-9520TM
HUVEC cell line	Invitrogen C-003-5C
Human primary neutrophils	Isolated from healthy volunteer donors base on Ficoll-Gradient
Primary human dermal fibroblasts (HDFib)	Isolated according to the published protocol from foreskin biopsies of healthy donors (Pudlas et al. 2011)
Female reproductive tract biopsies	Frauenklinik, Würzburg
SIS scaffold	Pig (6 weeks, male) (TERM)

Table 5. Cell culture medium, supplements

Culture medium	Source	Catalog number
Advanced DMEM/F-12	Thermo Fisher	12634010
DMEM/F12	Gibco/Thermo Fisher scientific	31331093
Dulbecco's Modified Eagle Medium (DMEM)	Gibco/Thermo Fisher scientific	D6429
Fetal calf serum (FCS)	Sigma Aldrich	F7524
Ham's F12 Nutrient Mixture	Invitrogen	31765068
Hanks' Balanced Salt Solution (HBSS)	Thermo Fisher	14190169 14175095 14025100
Low serum growth supplement (LSGS)	Thermo Fisher	S00310
MCDB 105 Medium	Sigma Aldrich	M6395-1L
Medium200	Thermo Fisher	M200500
PBS	Thermo Fisher	14190169

Table 6. Chemical and solution

Chemical/solution	Source	Catalog number
Absolute ethanol	Sigma Aldrich	32221-2.5L
Accutase® solution	Sigma Aldrich	A6964
Acetone	Carl Roth	9372.6
Albumin Fraction	Carl Roth	8076.3
B27 supplement	Thermo Fisher	12587010
Benzyl alcohol	Sigma Aldrich	305197-1L

Benzyl benzoate	Sigma Aldrich	W213810-100G-K
Beta - estradiol	Sigma Aldrich	E4389
Cell Recovery Solution, 100 mL	Corning	354253
Citric Acid	Carl Roth	X863.2
Collagenase, Type I, powder	Thermo Fisher	17018029
Dako Glycergel Mounting Medium	Agilent	C0563
Dimethyl Sulfoxide (DMSO)	Carl Roth	A994.2
Dispase II	Sigma Aldrich	4942078001
Eosin	Morphisto	10177.01000
Ficoll® Paque Plus	Sigma Aldrich	GE17-1440-03
FITC- Dextran	Sigma Aldrich	46944-100MG-F
GC Medium	Becton Dickinson	228950
Gentamicin	Sigma Aldrich	G1397-10ML
Glutamax	Thermo Fisher	35050061
Glycerol	Carl Roth	3783.2
Hematoxylin	Morphisto	10231.01000
Hyaluronidase	STEMCELL	07461
Isopropanol	Carl Roth	6752.4
Matrigel Matrix	Corning	356231
Mounting Medium (Entellan)	Merck Millipore	1079600500
MOWIOL	Carl Roth	0713.2
N- Hexane	Sigma Aldrich	1043682511
N-Acetyl-L-cysteine	Sigma Aldrich	A9165-5G
N2 Supplement	Thermo Fisher	17502001
Nicotinamide	Sigma Aldrich	N3376-100G
Penicillin/Streptomycin	Thermo Fisher	15140122
PFA 4%	Morphisto	10303.01000
Poly (vinyl alcohol)	Sigma Aldrich	341584-25G
Primocin	Invitrogen	ant-pm-1
Recombinant Human Epidermal Growth Factor (EGF)	Peprotech	AF-100-15
Recombinant Human Fibroblast Growth Factor (FGF)	Peprotech	100-26
Recombinant Human Hepatocyte Growth Factor (HGF)	Peprotech	100-39
Saponin	Sigma Aldrich	47036-50G-F
Sodium Deoxycholic Acid	Carl Roth	3484.7
Sodium hydroxide solution	Sigma Aldrich	S2770
Sodium Pyruvate	Thermo Fisher	11360088
TEMED	Sigma Aldrich	T9281-100ML
TGF beta inhibitor	Tocris Bioscience	A-83-01/2939

Triton- X 100	Carl Roth	3051.4
Trypan Blue	Sigma Aldrich	T8154-20ML
TryplE Express	Thermo Fisher	12604039
Tween-20	Carl Roth	9127.2
Xylene	Sigma Aldrich	A5597-1GAL

Table 7. Disposable materials

Materials	**Source**
Aluminum Foil	Carl Roth GmBH, Karlsruhe (GER)
Biopsy Foam Pads	VWR, Darmstadt (GER)
Cell Culture Flasks: T25, T75, T175	Corning, Hickory, NC (USA)
Cell Culture Multiwell Plates: (6 well, 12 well, 24 well, 96 well)	Corning, Hickory, NC (USA)
Cell scraper	Sarstedt, Nümbrecht (GER)
Cell strainer 40um	SigmaAldrich, St. Louis, MO, (USA)
Centrifuge Tubes 50 ml, 15 ml	Corning, Hickory, NC (USA)
Cover Slips for Object Slides	VWR, Darmstadt (GER)
Cryo Tubes: 1.8 ml	Sarstedt, Nümbrecht (GER)
Disposal Bags	Sarstedt, Nümbrecht (GER)
Embedding Cassettes	Thermo Scientific
Embedding Foam Pad	VWR, Darmstadt (GER)
Eppendorf® Low Bind microcentrifuge tubes	SigmaAldrich, St. Louis, MO, (USA)
Gloves	SigmaAldrich, St. Louis, MO, (USA)
Imaging dish	Ibidi
Inoculation cotton	Hartenstein, Würzburg (GER)
Inoculation loop	Sarstedt, Nümbrecht (GER)
Ismaprene tubing	Ismatec, WertheimMondfeld (GER)
Microscope slides	VWR, Darmstadt (GER)
Microtome blades	Hartenstein, Würzburg (GER)
Microtome Disposable Blades	Carl Roth, Karlsruhe (GER)
Object Slides	VWR, Darmstadt (GER)
Parafilm	Carl Roth, Karlsruhe (GER)
Pasteur Pipettes	Hartenstein, Würzburg (GER)
Pestle for Cell Strainer	SigmaAldrich, St. Louis, MO, (USA)
Petri Dishes	Sarstedt, Nümbrecht (GER)
Pipette Tips	Sarstedt, Nümbrecht (GER)
S-Monovette® 9ml LH	Sarstedt, Nümbrecht (GER)
Scalpel Blades, rounded	Carl Roth, Karlsruhe (GER)
Silicone tube	Carl Roth, Karlsruhe (GER)
Sterile Filter	Corning, Hickory, NC (USA)
Sterile surgical blade	Carl Roth, Karlsruhe (GER)

Syringes: 5 ml, 10 ml, 20 ml	VWR, Darmstadt (GER)
Weighing Dish	Hartenstein, Würzburg (GER)

Table 8. Equipment

Equipment	Source
6.5mm Transwell® with 3.0µm Pore Polyester Membrane Insert, Sterile	Corning, Hickory, NC (USA)
Cell counting chamber	Hartenstein ZK06
Centrifuges: Eppendorf 5417 R Eppendorf 5424 Megafuge	 Eppendorf, Hamburg (GER) Eppendorf, Hamburg (GER) Heraeus
Drying oven	Memmert, Schwabach (GER)
Embedding Station	Thermo Fisher Scientific, Dreieich (GER)
Flow cytometer	FACS ARIA III (BD)
Fume Hood	Prutscher Laboratory Systems, Neudörfl (AUT)
Hera Safe sterile bench	Thermo Fisher Scientific, Dreieich (GER)
Incubator	Thermo Ficher
Luminex (MAGPIX®)	Luminexcrop
Magnetic Stirrer	Topolino (IKA)
Microscopes	Confocal TCS SP5 Leica, Wetzlar (GER) Light microscope Leica Leica, Wetzlar (GER) JEM-2100 JEOL microscopes JSM-7500F JEOL microscopes
Millicell ERS volt-ohm Meter	Millipore, Billerica, MA (USA)
Nanodrop 1000 spectrophotometer	Peqlab Biotechnology
Neubauer Cell Counting Chamber	Hartenstein, Würzburg (GER)
Plate reader	TECAN
Shaker incubator Celltron	INFORS GmbH
Sliding microtome	Leica, Wetzlar (GER)
Ultrapure water system	Millipore, Schwalbach (GER)
Ultrospec 3100 pro Spectrophotometer	Amersham Bioscience
Vortex	Carl Roth GmBH, Karlsruhe (GER)

Table 9. Kits

Kits	Source
Cytotoxicity Detection Kit PLUS (LDH)	Roche

Luminex Assay Magnetic Human Premixed, split based on dilution of Cell culture Supernates, IL-1B, IL-8, TNF, CCL20, IL-6, Custom	R&D

Table 10. Laboratory material

Materials	**Source**
Beaker	Hartenstein
Cell Crowns for static 3D Culture	Chair of Tissue Engineering and Regenerative Medicine, Würzburg (GER)
Embedding Tissue Casting Molds	Leica
Erlenmeyer flasks	Hartenstein
Funnels	Hartenstein
Measuring cylinder	Hartenstein
Protective Goggles	Carl Roth
Scalpel	Bayha
Slide holder	VWR
Spoon Spatula	Hartenstein
Spray Flask (Ethanol, 70 %)	Hartenstein
Staining rack made of glass	Hartenstein
Super PAP Pen Liquid Blocker	Science Services GmbH
Tweezers	Assistant

Table 11. Software

Software	**Source**
Flowing	http://flowingsoftware.btk.fi
GraphPad Prism Software	GraphPad Software, Inc.
FIJI (Image J)	https://imagej.nih.gov/ij
IMARIS	Version 8.4.1
Luminex	Luminex® software
Mendeley	Mendeley, Version 1.19.4
Office word 2016 Office PowerPoint Office Word 2016	Microsoft® Word for Mac Microsoft® PowerPoint for Mac
Smart PP	https://smart.servier.com
Tecan-I-control TM 1.7	Tecan plate reader software

Table 12. Bacteria culture buffers recipes

Bacteria culture protocol	Ingredients
GC Agar (1L)	36.23 g GC agar base, autoclaving, cooling and adding 1% vitamin mix
HEPES -Solution I	0.1% L-Alanine, 0.15% L-Arginine, 0.025% L-Asparagine, 0.025% Glycine, 0.018% L-Histidine, 0.05% L-Lysine, 0.015% L-Methionine, 0.05% Proline, 0.05% L-Serine, 0.05%L-Threonin, 0.061% L-Cysteine, 0.036% L-Cysteine, 0.05% L-Glutamine, 0.046% reduced Glutathione (GSH), 0.0032% Hypoxanthine, 0.008% Uracil, 0.004% D-Biotin, add 18% 1 N NaOH and 82% H_2O
HEPES -Solution II	375 g/L Glucose
HEPES -Solution III	10 g/L Fe $(NO_3)_3$·9H2O
HEPES -Solution IV/V	0.33% Nicotinamide adenine dinucleotide (NAD), 0.33% Carboxylase, 0.33% Thiamin, 0.33% Ca-Pantothenate, 0.188% CaCl2· 2H2O, 4.17% Na-Lactate, 15.33% Glycerin, 3.33% Oxaloacetate
HEPES -Solution VI	50 g/L $MgCl_2$·7H2O
HEPES -Solution VII	50 g NaCl, 34 g Na-Acetat in 1 L H_2O
HEPES -Solution VIII	23.8 g/L HEPES
HEPES Medium (Low phosphate medium)	50 ml solution I, 10 ml solution II, 200 µl solution III, 3 ml solution IV/V, 5 ml solution VI, 50 ml solution VII, 50 ml solution VIII Up to 500 ml H_2O, regulate pH 7.3, filter sterilization
PPM Medium (1L)	15g Protease peptone; 5g sodium chloride; 0.5g soluble starch; 1g Potassium dihydrogen phosphate; 4g dipotassium hydrogen phosphate for 1l; pH 7.2; 1% vitamin mix, 0.5% Sodium hydrogen carbonate, 10mM magnesium chloride, sterilized by filtration
Vitamin Mix Solution I	200 g D (+)-glucose, 20 g L-glutamine, 0.026 g 4-aminobenzoic acid, 0.2 g cocarboxylase, 0.04 g iron (III) nitrate nonahydrate, 0.006 g Thiamine hydrochloride (vitamin B1), 0.5 g NAD, 0.02 g vitamin B12, 52 g L-cysteine hydrochloride monohydrate; add 1 L dH_2O

Vitamin Mix Solution II	2.2 g L-cystine, 0.3 g L-arginine monohydrochloride, 1 g Uracil, 0.06 g Guanine-hydrochloride, 2 g adenine hemisulfate, add 600 mL dH_2O, 30 mL 32% HCl

Table 13. Biopsy and Organoid

Transfer medium	90% MCDB-105, 10% FBS,1x Pen/Strep
Cervix organoid medium	Advanced DMEM/F12 (1X), N2 supplement (1X), B27 supplement minus vitamin A(1X), Primocin (100 µg/ml), Recombinant human WNT (500 ng/ml), Recombinant human EGF (50 ng/ml), Recombinant human Noggin (100 ng/ml), Recombinant human Rspondin-1 (500 ng/ml), Recombinant human FGF-10 (100 ng/ml) , ALK-4, -5, -7 inhibitor, A83-01 (500 nM), Nicotinamide (10 nM) (Chumduri et al. 2018).
Digestion medium	0.5 mg collagenase I+ 20ul hyaluronidase in HBSS
Endometrium organoid medium	Advanced DMEM/F12 (1X), N2 supplement (1X), B27 supplement minus vitamin A(1X), Primocin (100 µg/ml), N-Acetyl-L-cysteine (1.25 mM), L-glutamine (2 mM), Recombinant human EGF (50 ng/ml), Recombinant human Noggin (100 ng/ml), Recombinant human Rspondin-1 (500 ng/ml), Recombinant human FGF-10 (100 ng/ml) , Recombinant human HGF (50 ng/ml), ALK-4, -5, -7 inhibitor, A83-01 (500 nM), Nicotinamide (10 nM) (Turco et al. 2017)

Table 14. Buffers

Buffer	**Ingredients**
10% SDS lower gel solution	for 10 mL: 3.3 mL 30% acrylamide, 2.5 mL 4x lower buffer, 4.1 mL H2O, 100 µL 10% (w/v) APS, 10 µL TEMED
10x SDS Electrophoresis buffer (1 L)	30.25 g Tris, 144 g glycine, 10 g SDS
10x semi dry buffer (1 L)	24 g Tris, 113 g glycine, 2 g SDS

10x TAE (1L)	48.5 g Tris, 11.4 mL glacial acetic acid, 20 ml 0.5 M EDTA (pH 8.0)
10x TBE (1L)	54 g Tris, 27.5 g Boric acid, 20 ml 0.5 M EDTA (pH 8.0)
10x TBS-T (1 L)	48.5 g Tris, 175 g NaCl, 10 mL Tween-20, adjust to pH 7.5 with HCl
2x Laemmli buffer	4% (w/v) SDS, 20% (v/v) glycerol, 120 mM Tris/HCl (pH 6.8), 0.2 mg/mL bromophenol blue, 0.1 M DTT
4x SDS lower buffer (1 L)	1.5 M Tris/HCl (pH 8.8), 0.4% (w/v) SDS
4x SDS upper buffer (1 L)	0.5 M Tris/HCl (pH 6.8), 0.4% (w/v) SDS
Blocking solution for immunofluorescence staining (IF)	1x PBS, 1% (w/v) BSA
Blocking solution for WB	1x TBS-T, 3% (w/v) BSA
Coomassie Destaining solution	20% methanol, 7% acetic acid
Coomassie Staining solution	4% methanol, 11% acetic acid, 0.2% Coomassie blue R250
Corresponding buffer for IF	1.92 g Citric acid in 1000 ml dH2O, pH 6, 0.5ml Tween 20
Permeabilization solution for IF	1x PBS, 1% (w/v) Saponin
Semi dry transfer buffer	1x semi dry buffer, 20% (v/v) methanol
Washing buffer for IF	1x PBS, 0.5% Tween 20

2.2 Methods

2.2.1 Cell culture

All cell cultures were performed under sterile conditions using a laminar airflow safety hood. The materials and tools contacting the cells were autoclaved (121 °C, 1.5 h) or baked (180 °C, 8 h). SIS scaffolds were disinfected by gamma sterilization (25 kGy). The human endometrial adenocarcinoma cell line (HEC-1-B) and Primary human dermal fibroblasts (HDFib) were cultured in Dulbecco's Modified Eagle Medium (DMEM). Human ureter uroepithelial SV40 immortalized cells (SV-HUC-1) were cultured in Ham's F12 nutrient mixture and human colorectal carcinoma cells (T84) were cultured in DMEM/F12. All media were supplemented with 10% heat-inactivated fetal calf serum (FCS) and 1% Penicillin/Streptomycin. Human Umbilical Vein Endothelial Cells (HUVEC) was cultured in M200 medium supplemented with 10% low serum growth supplement (LSGS) and 1% Penicillin/Streptomycin.

2.2.2 Generation of the human 3D tissue models

Preparation of porcine small intestinal submucosa scaffold (SIS) and decellularization were performed according to the established protocol (Schweinlin et al. 2017). Briefly, porcine intestine tissue from 6 to 8 weeks old pig was received after surgery. The intestine lumen was washed using tap water followed by cutting it into pieces with a length of approximately 10-15 cm. All the pieces were turned inside out with tweezers and pulled onto a 25 mL pipette tube. Scraping off the mucosa was performed using tweezers in order to remove the mucosa. Then the pieces of tissues were transferred to a solution of (PBS- + 1 % PenStrep) and kept on rocking shaker at 4 °C, for an overnight. The next day, two ends of the gut pieces were clamped and filled with desoxycholate solution using a syringe and incubated for 1.5 hours at room temperature (RT). Afterward, the solution was replaced by PBS^- buffer and placed on a shaker, 4 °C for 1 hour. Afterward, the clamps were opened and the tissue pieces were washed for 4 to 5 times with PBS buffer. Finally, the tissue pieces were transferred to PBS buffer without any antibiotic and subsequently were disinfected by gamma sterilization (25 kGy, BBF Sterilisationsservice GmbH, Rommelshausen, Germany). The SIS scaffold was then kept in fresh PBS at 4 °C.

For generating the 3D tissue models, an intact piece of SIS scaffold was mounted on the 6.5 mm

diameter Cell Crowns and fibroblasts cells ($3x10^5$ cell/cm^2) were seeded on the apical side of each cell crown in the DMEM medium. After 48 h, epithelial cells ($9x10^5$ cell/cm^2) were seeded on the apical side of the model (Figure 5). Tissue models were cultured under submerged static conditions or with shaking on an orbital shaker at 25 rpm for 12 days in the case of T84 or SV-HUC-1 cells, or 14 days in the case of HEC-1-B cells at 37 °C / 5% CO_2 in the tissue culture incubator. The medium was exchanged every two days. In some cases, the different culture medium was required for fibroblasts and epithelial cells. In these cases, the models were cultured in the medium consisting of 50:50 fibroblasts: epithelial cell medium.

For generating Transwell® insert models (6.5 mm diameter, 3 µm pore size polyester Transwell® inserts) were coated with rat tail collagen type I. Fibroblasts cells ($3x10^5$ cell/cm^2) were seeded on the basal side and 48 h later epithelial cells ($6x10^5$ cell/cm^2) were seeded on the apical side of the Transwell® membrane. Models were grown for 10 days under submerged static conditions at 37 °C / 5% CO_2 in the tissue culture incubator.

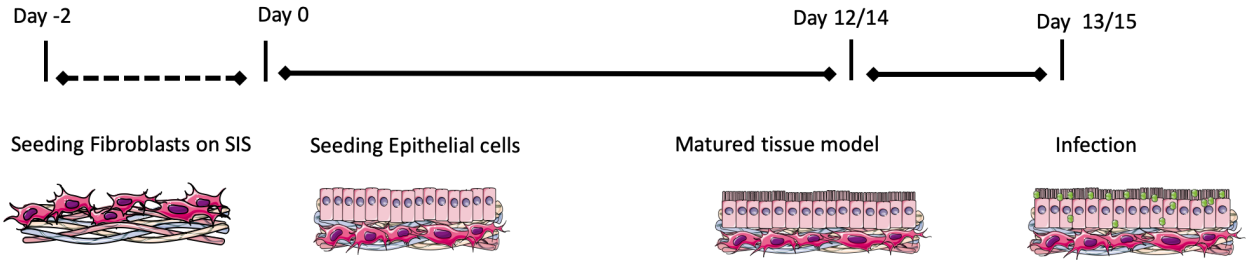

Figure 5. Establishment of mucosal tissue models on the SIS Scaffold.

The workflow of the preparation of 3D tissue models on the SIS scaffold. After preparation of the SIS scaffold (section 2.2.2), the scaffold was fixed between two cylinders so-called Cell Crown. Primary human dermal fibroblasts (HDFib) cells then seeded on the SIS scaffold and cells incubated (37 °C / 5% CO_2) (day -2). After 2 days of incubation, the epithelial cells seeded to apical compartment (day 0). The culture medium was exchanged every 2 days until the matured tissue model obtained (day 12/14). TEER measurements have been performed during the cultivation to find the maturation time. After establishing the co-culture model of epithelial/ fibroblast, the models were infected with various types of *N. gonorrhoeae* (section 2.2.4) over 6 days.

2.2.3 Barrier integrity assessment

Transepithelial electrical resistance (TEER) was measured using Millicell® ERS-2 Volt-Ohm Meter in order to evaluate the barrier integrity of the epithelial cell monolayer over the cell culture. This method also helps to have an overview of the time is needed for each cell line to make a fully polarized monolayer. SIS scaffold (between 80 $\Omega*cm^2$ and 90 $\Omega*cm^2$) and empty Transwell® insert (between 50 $\Omega*cm^2$ and 60 $\Omega*cm^2$) are considered as a blank control and their values were subtracted from the final TEER values. Before each measurement, the device was calibrated and sterilized based on the manufacturer protocol. During the measurement, the short electrode places inside the Cell Crown without touching the cells and the long one outside the Cell Crown. In addition, the integrity of the monolayer was assessed using 4 kDa fluorescein isothiocyanate (FITC)-dextran permeability assay. FITC-dextran is a substrate of sugar chain and covalently coupled with a FITC. After 14 days of cultivation for HEC-1-B and 12 days of cultivation for T84 and SV-HUC-1 cell lines, the FITC assay was performed. First, 0.25 mg/ml FITC-dextran was dissolved in cell culture medium and sterilized by filtration. The culture media were removed from the apical and basal sides of the cell crown or Transwell®. Then, 1 mL of fresh medium was added to the basal side, and 300 µL of FITC-dextran containing medium to the apical side. After 30 min of incubation, 200 µL from the lower compartment was collected into a 96 well plate and fluorescence was analyzed using TECAN reader (absorption 490 nm, emission 525 nm). The results were normalized by an empty SIS scaffold or a Transwell® membrane.

2.2.4 *N. gonorrhoeae* strains and culture conditions

N. gonorrhoeae N927 ($PorB_{IA}$, $Pili^-$, Opa^-), N924 ($PorB_{IB}$, $Pili^-$, Opa^-), MS11 ($PorB_{IB}$, Opa^+, $Pili^+$), MS11 ΔOpa ($PorB_{IB}$, Opa^-, $Pili^+$), VP1 clinical strain ($PorB_{IA}$, $Pili^-$, Opa^-) were grown on the GC agar plates supplemented with 1% vitamin mix for 14–17 h at 37 °C in 5% CO2. For growth curve measurements, bacteria were grown overnight on GC-agar plate, resuspended in PPM medium to OD550=0.2 and allowed to grow to OD550 between 0.5 and 0.6. All cultures were diluted to OD550=0.1 in PPM medium and incubated with shaking at 37 °C. OD550 was measured at different time points to assess growth. This section was done in collaboration with Tao Yang.

2.2.5 Histology

Tissue models were fixed in 4% paraformaldehyde at RT. After paraffin embedding, samples were sectioned to 6 µm thickness. Hematoxylin and Eosin staining were performed in order to have a study tissue morphology following the standard protocol (Table 15). Samples were mounted with Entellan® and dried overnight before microscopy.

Table 15. H&E staining steps used in this study.

Steps	Solution	Duration (min)
De-paraffining, Rehydration	Xylene 1	10
De-paraffining, Rehydration	Xylene 2	10
De-paraffining, Rehydration	Ethanol 96 %	3 X dip in and out
De-paraffining, Rehydration	Ethanol 96 %	3 X dip in and out
De-paraffining, Rehydration	Ethanol 70 %	3 X dip in and out
De-paraffining, Rehydration	Ethanol 50 %	3 X dip in and out
Rinsing	VE- Water	Swirl until turbulences disappear
Cell nuclei staining	Hematoxylin	6
Rinsing	VE- Water	Flow weakly until no color is washed out
Bluing	Tap water	5
Staining	Eosin	6
Rinsing	VE- Water	Flow weakly until no color is washed out
Dehydration	Ethanol 70 %	2 X dip in and out
Dehydration	Ethanol 96 %	2
Dehydration	Isopropanol 1	5
Dehydration	Isopropanol 2	5
Dehydration	Xylene 1	5
Dehydration	Xylene 2	5

2.2.6 Immunofluorescence study

Tissue models were fixed with 4% paraformaldehyde for 2 hours. The tissue models were then washed with phosphate-buffered saline (PBS), permeated using 1% saponin, blocked with 1% BSA in PBS and stained with primary antibodies overnight. This was followed by decoration with fluorophore-coupled secondary antibodies, Phalloidin and DAPI. Z-stacks of images were obtained through 25 µm from the top of monolayer using Leica SP5 and processed by FIJI and FIJI Plugin 3D Viewer (Schindelin et al. 2017; Schmid et al. 2010).

2.2.7 Immunohistochemistry

Tissue models were fixed in 4% paraformaldehyde at RT. After paraffin embedding, samples were sectioned to 6 µm thickness. Immunohistochemistry staining were performed in order to stain different parts of tissue samples specifically following the standard protocol (Table 16).
Then samples were incubated with blocking solution (1% BSA/ PBS) for 20 minutes in order to avoid any unspecific binding of the secondary antibody. Each of the primary antibodies was diluted according to their protocol and the secondary antibody was diluted 1:100. Primary mouse antibodies and primary rabbit antibodies were mixed in the same solution and were added at once. After overnight incubation at 4 °C, samples were washed 3 times with washing buffer on a shaker, 5 minutes for each. Then again different mouse and rabbit secondary antibodies were mixed together wilt DAPI and Phalloidin and added on samples following 1 h of incubation at RT. Final samples were washed in washing buffer, 5 minutes for each. The samples were mounted using DAKO on a coverslip.

Table 16. Immunohistochemistry staining steps used in this study

Steps	Solution	Duration (min)
De-paraffining, Dehydration	Xylene 1	10
De-paraffining, Dehydration	Xylene 2	10
De-paraffining, Dehydration	Ethanol 96 %	3 X dip in and out
De-paraffining, Dehydration	Ethanol 70 %	3 X dip in and out
De-paraffining, Dehydration	Ethanol 50 %	3 X dip in and out

Rinsing	VE- Water	Swirling
Washing	Washing buffer	Swirling
Unmasking the epitopes	Corresponding buffer (100°C) (citrate buffer pH 6)	20
Washing	Washing buffer	Swirling

2.2.8 Scanning electron microscopy / Transmission electron microscopy

Tissues were washed with PBS and then fixed with 6.5% glutaraldehyde for 1 h at RT. Then samples were washed 5 times, every 5 minutes with 50 mM cacodylic acid (pH 7.2). Dehydration is done using a graduated series of acetone following the standards protocol (Table 17). Samples were then dried with CO_2 using a critical point dryer (BAL-TEC CPD 030) and coated with gold/ palladium using a sputter machine (sputter coater BAL-TEC SCD 005).

Table 17. Dehydration steps used for SEM samples this study.

Solution	Duration (min)
30% Acetone	15
50% Acetone	20
75% Acetone	30
90% Acetone	45
100% Acetone	30
100% Acetone	30
100% Acetone	30
100% Acetone	30
100% water free Acetone	30
100% water free Acetone	30

For TEM samples, following the fixation in 2.5 % glutaraldehyde for 12-18 h at 4 °C, samples were washed 3 times with 50 mM sodium cacodylic acid (pH 7.2), each for 3 minutes. The samples were then fixed with 2% osmium tetroxide for 90-120 minutes at 4 °C. Afterward, samples were washed with deionized water. Post-fixation is done using 0.5 % aqueous uranyl acetate overnight. The dehydration process was performed according to standard protocol (Table 18).

Samples were then ultrathin sectioned and analyzed using JEM-2100 and JSM-7500F JEOL microscopes (Ott et al. 2012; Spiliotis et al. 2008).

Table 18. Dehydration steps used for TEM samples this study.

Solution	Duration (min)
30% Ethanol	30
50% Ethanol	30
70% Ethanol	30
90% Ethanol	30
100% Ethanol	30
100% Ethanol	30
100% Ethanol	30
Propylene oxide	30
Propylene oxide	30
Propylene oxide	30
Propylene oxide: Epon 1:1	Overnight
Epon	120
Epon	120
Epon/ Embedding form	60
Polymerization at 60°C	48 h

2.2.9 Bacterial infection and colonization assays

After evaluating the models for barrier integrity, the tissue models were infected (MOI 20) in the phosphate-free HEPES medium, as described before (Kuhlewein et al. 2006). To assess the transmigration of *N. gonorrhoeae* across the polarized epithelial monolayer after different infection time points, the medium from the bottom compartment was collected. For Transwell® inserts, 50 µL of medium were plated directly onto the GC agar plate. For tissue models, the total culture media was centrifuged at 100xg and the pellet was resuspended in the remaining 50 µL of medium and then plated on GC agar. For assessment of bacterial adhesion, the infected tissues were incubated for 30 minutes with 1% saponin and dilution series were cultured on GC agar. For invasion assay, the infected tissues were treated by Gentamicin and then incubated for 30 minutes with 1% saponin and dilution series were cultured on GC agar.

2.2.10 LDH assay

Cytotoxicity detection kit was used in order to quantify the cell death and cell lysis rate based on lactate dehydrogenase (LDH) activity in the supernatants. The LDH activity is quantified by an enzymatic reaction. During this reaction, LDH oxidizes lactate to pyruvate, generating NADH. A coupled enzymatic reaction at the same time converts iodonitrotetrazolium into formazan with red color. The experiment was performed according to the manufactureŕs instructions.

2.2.11 Cytokine quantification

A highly sensitive customized Luminex assay kit was used in order to detect and quantify TNFα, IL-6, and IL-8. The protocol was performed according to the customized Luminex assay kit and measurements were performed using Luminex® in collaboration with Dr. Tobias Hertlein.

2.2.12 Neutrophil isolation

Neutrophil isolation from the blood was carried out based on the Ficoll® separation method. 10 mL of blood was slowly added on 15 mL of Ficoll®. Following the centrifuge at 1500 rpm (no break) for 30 minutes at 22 °C, the blood formed a layer-by-layer of (from top) the plasma, monocytes, Ficoll®, neutrophils, and red blood cells (Figure 6).

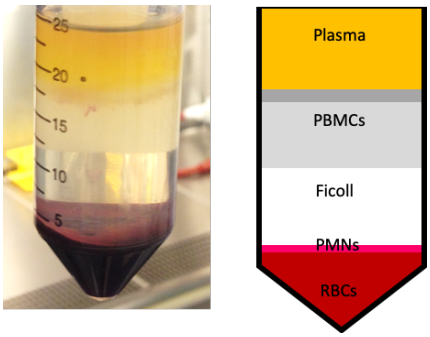

Figure 6. Neutrophils isolation from human blood based on the Ficoll® gradients.
Separation of whole human peripheral blood cells was performed using Ficoll-Paque. Layering of the blood done over the Ficoll® gradients. The very bottom layer contains aggregated red blood cells. The thin layer above the erythrocyte layer includes the neutrophils. Above the neutrophils layer, the Ficoll-Paque media stand. Peripheral blood mononuclear cells are found on top of Ficoll-Paque media. The plasma is the top layer.

All the layers above the neutrophils were slowly removed. Poly (vinyl alcohol) solution (30 mL) was added to the neutrophils and red blood cells. Following 45 minutes of incubation at RT, a two-layer solution is formed i.e. the upper layer (light red) and bottom layer (dark red). The upper layer was carefully transferred to a new falcon and centrifuged at 1000 rpm for 5 minutes at 22 °C. After the formation of a new red pellet, the supernatant is discarded and the pellet is resuspended with Millipore water. Following another round of centrifugation, the white pellet containing neutrophils was resuspended in 10 mL HBSS solution. The number of neutrophils was counted using the counting chamber. The activation and purity of neutrophils were measured by FACS for CD11b and CD66, respectively.

2.2.13 Bioreactor setup

A perfusion-based bioreactor system was designed for studying the immune response (neutrophils) to the pathogens under dynamic culture conditions. The bioreactor consists of a main chamber including two parts i.e. apical and basolateral, an extra reservoir and a neutrophils chamber (Figure 7). The culture media is circulated (perfusion rate of 2.5 mL/min) through the apical chamber (epithelial cells) and the human isolated neutrophils are delivered to the endothelial cells in the basolateral chamber via a perfusion pump (perfusion rate of 0.5 mL/min). All the system was autoclaved before cell culturing and the bioreactor was then transferred to a custom-designed incubator (37 °C and 5% CO_2).

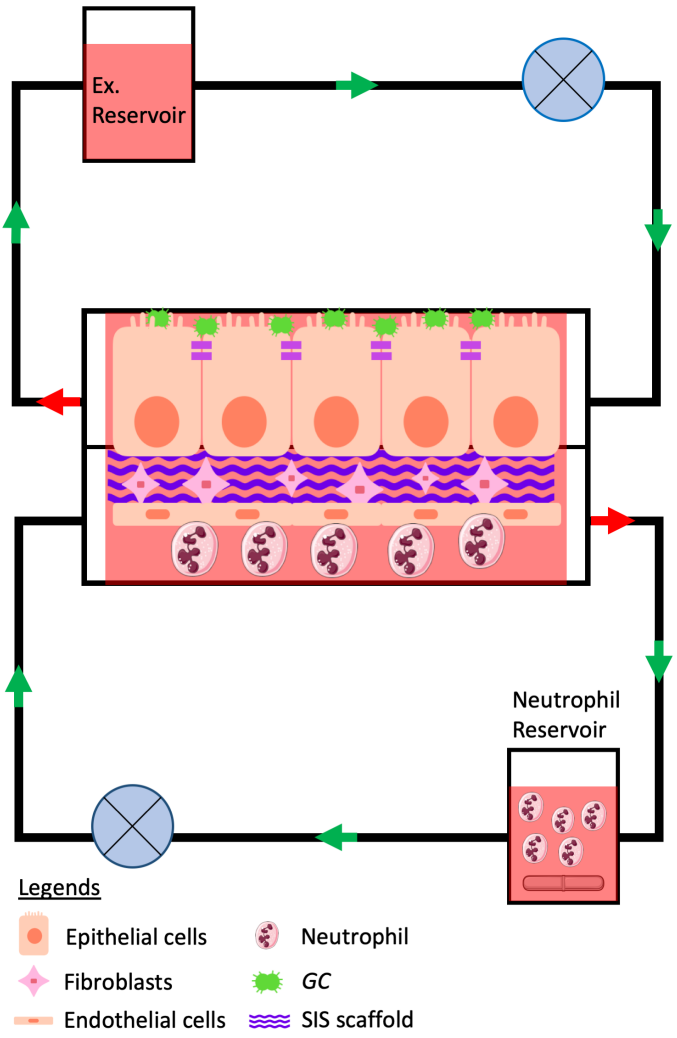

Figure 7. Schematic of the bioreactor used in this study.

We developed a triple co-culture of epithelial (top), fibroblast (middle) and endothelial (bottom) cells on the SIS scaffold. The triple co-culture model was then infected with GFP-expressing N927 and placed into the bioreactor setup. The bioreactor has a main chamber consists of two compartments. The medium exchanges through the cell culture using a perfusion pump (perfusion rate of 2.5 mL/min). At the same time, the isolated human neutrophils are circulated) perfusion rate of 0.5 mL/min) in the system through the basal chamber for 2 hours. A custom-designed incubator was used to provide the culture conditions (37 °C and 5% CO2). All the experiments were performed under sterilized conditions.

2.2.14 Triple co-culture

We modified the 3D tissue model to study neutrophils transmigration into the site of infection by triple co-culturing of HDFib, T84, and HUVECs. After the generation of the 3D tissue models

(section 2.2.2), on day 7, the co-culture models were inverted and HUVECs ($6x10^5$ cell/cm^2) were seeded on the basolateral side of the scaffold (Figure 8).

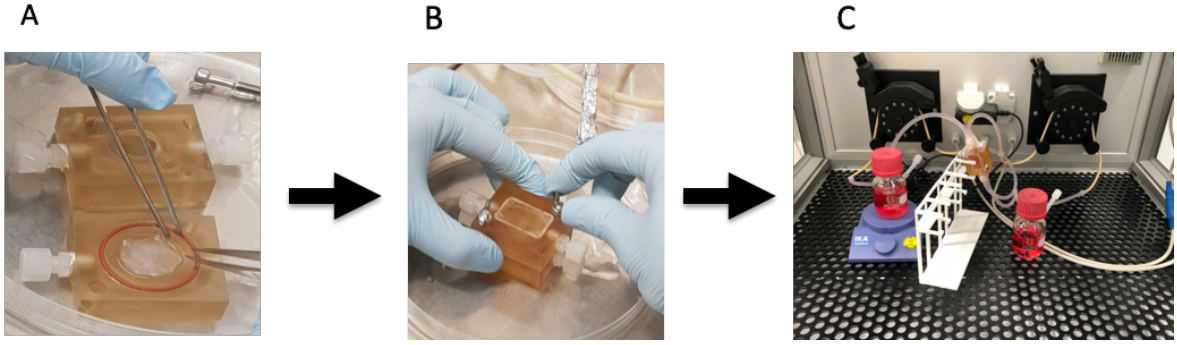

Figure 8. The workflow of handling the 3D tissue model into the perfusion-based bioreactor system.

The triple co-culture model was infected with GFP-expressing N927 ($PorB_{IA}$, $Pili^-$, Opa^-) in static condition. After 24 h, the two cylinders of Cell Crown were separated and (A) the infected tissue transferred to the holder. (B) The holders then fasten tightly and placed to the bioreactor system. (C) The fresh human isolated neutrophils were administered to the endothelial side (basal compartment) via perfusion the neutrophils to the supplier of the basal chamber in the perfusion-based bioreactor system.

The model then transferred on a shaker (50 rpm/min) to aid the formation of a mature endothelial cell monolayer. The barrier integrity of the new model was assessed (section 2.2.3). The established triple co-culture model was then infected with *N. gonorrhoeae* (MOI 20) in static condition for 24 h. Fresh human isolated neutrophils (section 2.2.12) ($1x10^6$ cells/mL) were administered to the endothelial side via adding the neutrophils to the supplier of the basal chamber in the perfusion-based bioreactor system (see section 2.2.13). The bioreactor system run for 2 h and the culture media were then taken for further downstream analysis.

2.2.15 Flow cytometry

Flow cytometry was used to characterize isolated neutrophils using CD66 marker and activation state of neutrophils using CD11b after isolation. Neutrophils were also characterized after circulation through the perfusion-based bioreactor. GFP positive neutrophils were sorted using flow cytometry. Neutrophils were transferred into a falcon and centrifuged 5 minutes, 250 g in order to get the pellet. The pellet was resuspended in 100 µL of the corresponding buffer and the antibody was added according to the manufacturer's instruction. Measurement performed with

FACS Aria III and the data were analyzed by Flowing software. FACS Aria III was operated by Dr. Katrin Stelzner, Elke Maier, and Franziska Solger.

2.2.16 Light-sheet fluorescence microscopy (LSFM)

The samples were fixed using PFA (4%) in PBS and then washed 3 times with PBS at RT. After that, the tissues were stained with primary and secondary antibody as described in Table 19. After staining, the tissues were cleared using the BABB method based on the standard protocol (Figure 9). A custom-designed setup was used for light-sheet fluorescence microscopy (LSFM), which has already described by Prof. Beihalk's lab (Amich et al. 2019; Brede et al. 2012). LSFM imaging has been performed in collaboration with Dr. Zeinab Mokhtari.

Table 19: Staining and clearance steps for light sheet microscopy.

Step	Duration	Repeat	Temperature	Shake	Solution
Washing	30 min	3	RT	no	PBS
Blocking	24 h	-	4 °C	no	2% FCS and 0,1 % Triton-X100/PBS
Primary antibody	24 h	-	4 °C	yes	Antibody 1:100 in PBS
Washing	30 min	3	4 °C	no	PBS
Secondary antibody	24 h	-	4 °C	yes	Antibody 1:100 in PBS
Washing	30 min	3	4 °C	no	PBS
Alcohol row	2 h	5	RT	no	30, 50, 70, 80, 90% Ethanol (each 2h)
Secondary antibody	Over night	-	4 °C	no	100% Ethanol
N-Hexane	2 h	-	RT	no	N-Hexane
Clearing	30 min	3	RT	no	BABB: (1-part Benzyl alcohol and 2 parts Benzyl benzoate)

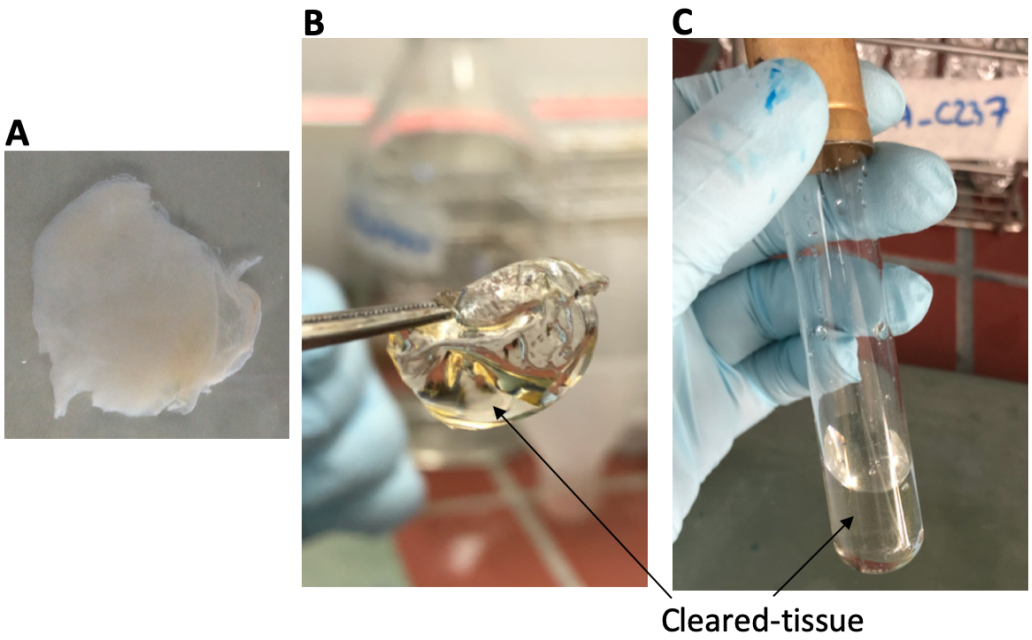

Figure 9. Tissue clearance for LSFM.

(A) After administration of the human neutrophils (for 2h) over the infected triple co-culture tissue (T84/HDFib/HUVECs) with *N. gonorrhoeae*, the tissue model removed from bioreactor setup and fixed with PFA (4%) in PBS and at RT. After that, the tissue was stained with primary and secondary antibody as described in Table 19. (B and C) For LSFM analysis, the tissues were cleared using the clearance protocol (Table 19). After clearing the tissue, the entire sample was completely transparent.

2.2.17 Isolation of primary cells from female reproductive tract

Biopsies were obtained from different parts of the female reproductive tract (endometrium and cervix). The biopsies were taken from women clinic, University Hospital Würzburg.

For primary fibroblasts cell isolation, following the surgery, the tissue biopsy transferred into sterile petri dich and wash three times with PBS. We removed the fat using scalpel and washed again with PBS. We then cut the tissue biopsy into stripes of 2 mm and put them into 15 mL Falcon tube containing 10 mL Dispase II (2U/mL) for 16-18 h incubation at 4 °C. Afterward, we spinned down the tissue pieces at 800 rpm for 5 minutes and aspirated the Dispase II solution. The tissue pieces placed into a to petri dish with DMEM/ 10%FCS/ PIS for 5 days. We then aspirated the culture media and rinsed the tissues with PBS to remove dead and not attached cells and tissue debris.

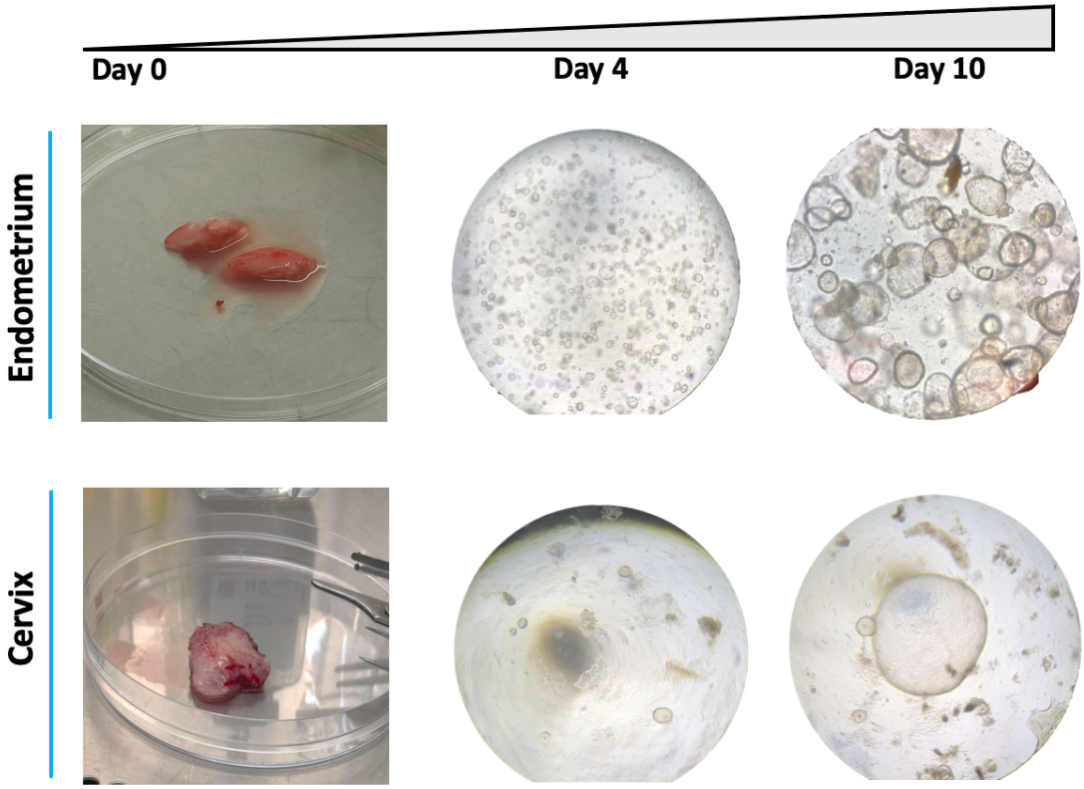

Figure 10. Isolation of primary fibroblasts and epithelial cells from the female reproductive tract.

The primary fibroblast isolated directly from fresh tissue biopsy (cervix and endometrium) and expanded in the normal cell culture flask. Endometrium and cervix tissue biopsies were cut into small pieces. Following the enzymatically digestion process in digestion buffer, the tissue was placed on a shaker at 37 °C for 1 h. The cells were resuspended in 10 mL of DMEM medium and spun down for 5 minutes, 800 rpm. The cervix and the endometrium organoids were developed in Matrigel® to grow and proliferate well enough. The primary cells were then seeded on the SIS scaffold and make 3D tissue model base on primary cells.

For primary epithelial cells, the biopsies with different range of a size (2-10 cm) were transported in transfer buffer on ice. The tissues were washed several times with PBS in order to remove the blood. The biopsy cut using scalpel into small pieces and transferred to a 50 mL Falcon tube containing a digesting solution. After 45 minutes of shaker incubation in an incubator, the tissue pieces were transferred to the cell strainer and cells were separated from the tissue using a pestle. The cells were resuspended in 10 mL of DMEM medium and spun down for 5 minutes, 800 rpm. The pellet was resuspended in Matrigel® and drops of 50 µL were placed in a 24 well plate. After 20 minutes of incubation at 37 °C, 500 µL of organoid culture media was added to

each well. The culture media for endometrium organoids contains advanced DMEM/F12, N2 supplement, B27 supplement, N-Acetyl-L-cysteine, L-glutamine, ALK inhibitor, nicotinamide, and recombinant human EGF, Noggin, R-spondin-1, FGF-10, and HGF. The culture media for the proliferation of cervix organoids contain advanced DMEM/F12, N2 supplement, B27 supplement, ALK inhibitor, nicotinamide, and recombinant human EGF, Noggin, R-spondin-1, FGF-10, and WNT. The medium was exchanged every two days and organoids were split weekly (Figure 10). The endometrium organoids can be expanded at a passage ratio of 1:2, every 10 days.

For seeding isolated primary cells on the SIS scaffold, first, the isolated fibroblast cells ($3x10^5$ cell/cm^2) from the same donor were seeded on the SIS scaffold. After 48 h, the isolated primary epithelial cells ($1.2x10^6$ cell/cm^2) were seeded on the same side of the SIS scaffold.

2.2.18 Statistical analysis

Statistical analysis was performed with one-way ANOVA, Tukey's multiple comparison test, using GraphPad Prism Software (GraphPad Software, Inc.). Each data point was expressed as mean ± standard deviation (SD).

Chapter 3 Results

3.1 Establishment of SIS-based 3D tissue models

We established three independent co-culture mucosal tissue models in order to study gonococcal infection following different approaches: I. A co-culture model of T84 (colon carcinoma cell line) and HDFib that is considered as a tight epithelial barrier model with highly polarized cells. II. A co-culture model of HEC-1-B (endometrial adenocarcinoma cell line) and HDFib that is regarded as a mucosal model of female reproductive tract tissue. III. A co-culture model of SV-HUC-1 (immortalized uroepithelial cell line) and HDFib mimicking the male urogenital tissue. In all the 3D tissue models, epithelial cell lines were co-cultured with primary human dermal fibroblasts, as a supportive layer and mimic the connective tissue, on the SIS scaffold. Light microscopy of a 2D culture of each cell line is depicted in Figure 11.

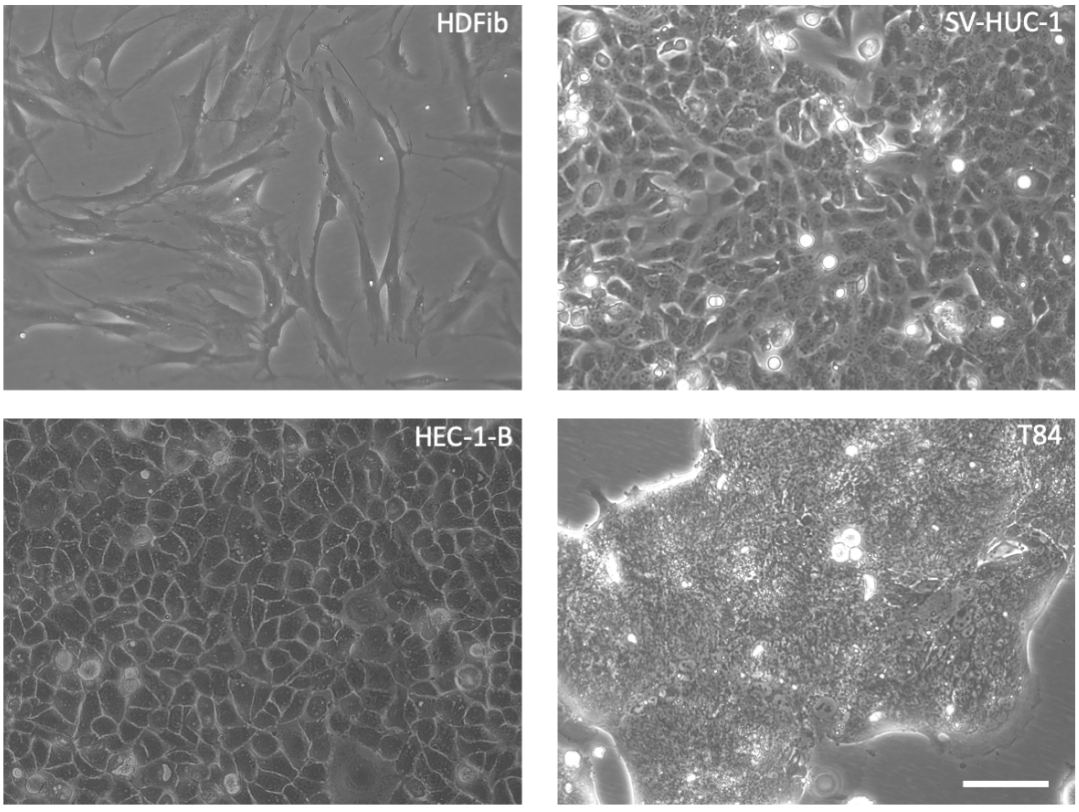

Figure 11. Light microscopy of cell lines used for the generation of tissue models in this study. HDFib; primary human dermal fibroblasts, T84; human colon carcinoma cell line; HEC-1-B, human endometrial adenocarcinoma cell line; SV-HUC-1, human uroepithelium SV40 immortalized cell line. Cells were grown in tissue culture flasks and the images were made using an inverted phase-contrast microscope. The scale bar is 100 µm.

3.2 Characterization of SIS-based 3D tissue models

3.2.1 Structural analysis

The morphology of the established 3D tissue models is evaluated by histological, immunohistochemical and immunofluorescence analysis.

3.2.1.1 Histological characterization

Histological characterization of the established tissue was performed using H&E staining after fixation and paraffin embedding of the tissue models. The results show an overview of the structure of the models. T84 cells form a polarized and tall columnar monolayer. HEC-1-B cells do not always grow as a monolayer and are not as polarized as T84 cells. SV-HUC-1 cells build up a thin and flat monolayer (Figure 12).

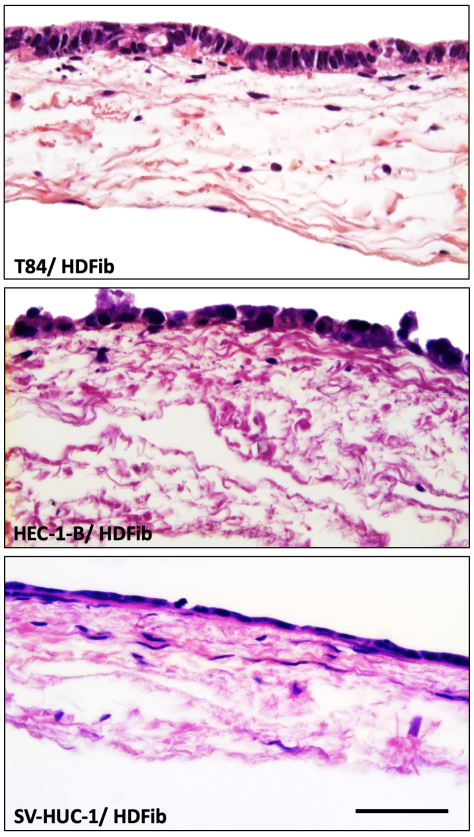

Figure 12. Histological characterization of the 3D tissue models.
H&E staining of the 3D tissue models based on the SIS mucosal scaffold. Epithelial/fibroblast co-culture tissue models of T84/HDFib, HEC-1-B/ HDFib, SV-HUC-1/ HDFib were established as described in Figure 5. T84 and HEC-1-B grew as a columnar epithelial monolayer while SV-HUC-1 cells formed a squamous epithelial layer. The scale bar is 50 µm.

3.2.1.2 Immunohistochemical characterization

The paraffin-embedded tissues were stained with E-cadherin and mucin 1 (Muc1) antibodies in order to observe the cell-cell contacts and mucus production. The results of immunohistochemistry showed that all three tissue models produce mucus. Mucus could be occasionally identified in large vesicles inside cells for the T84 model. In addition to Muc1, all models were also positive for E-cadherin and anti-fibroblast staining. In general, the immunofluorescence on tissue sections made after paraffin embedding showed a monolayer of epithelial cells located on the apical side of the scaffold, where occasionally fibroblasts could be observed growing within the SIS scaffold (Figure 13).

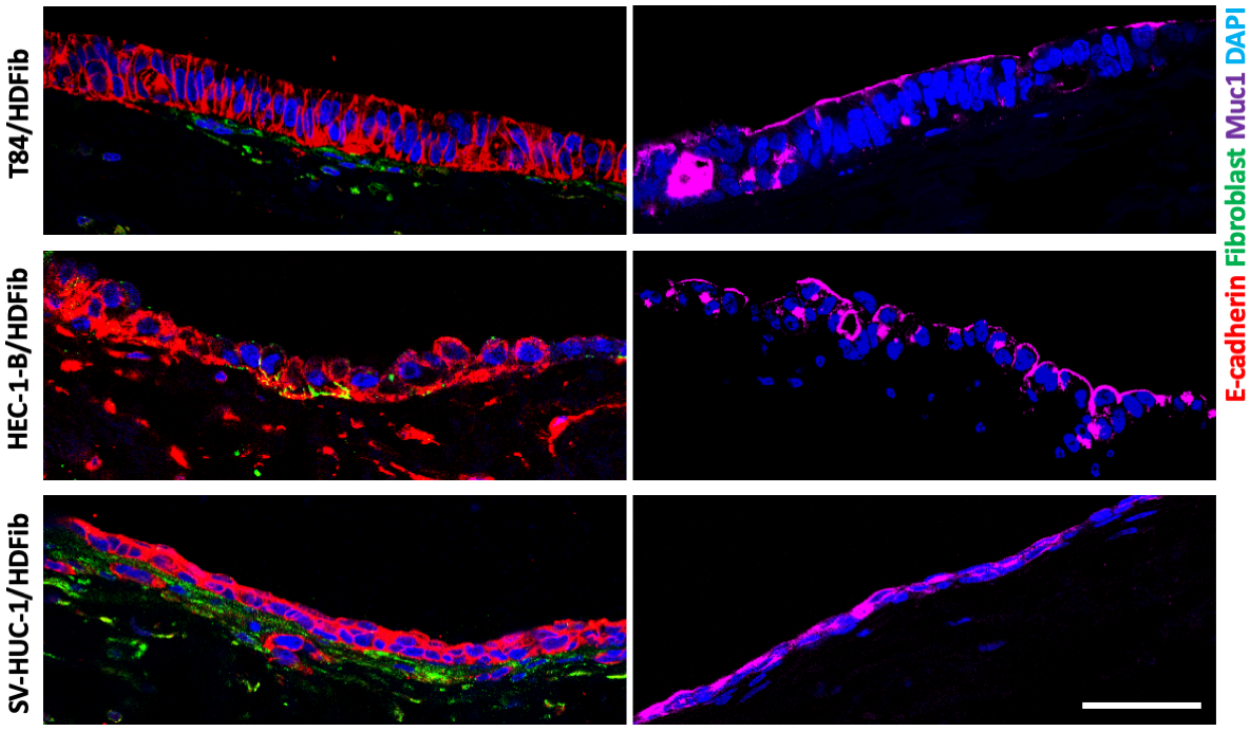

Figure 13. Immunofluorescence staining of models.

Immunofluorescence staining of the 3D tissue models based on the SIS mucosal scaffold. Epithelial/fibroblast co-culture tissue models of T84/HDFib, HEC-1-B/HDFib, SV-HUC-1/HDFib were established as described in Figure 5. The 3D Tissue models stained with anti-E-cadherin (red), anti-mucin 1 (Muc1, magenta) and anti-fibroblast (green). Cell nuclei were stained with DAPI (blue). The scale bar is 50 µm.

3.2.1.3 Immunofluorescence characterization

We adapted the technique for immunofluorescence staining after paraformaldehyde fixation followed by confocal microscopy to 3D tissue models and analyzed the morphology of the tissues as well as the distribution of the TJ marker ZO-1 (Figure 14a-c).

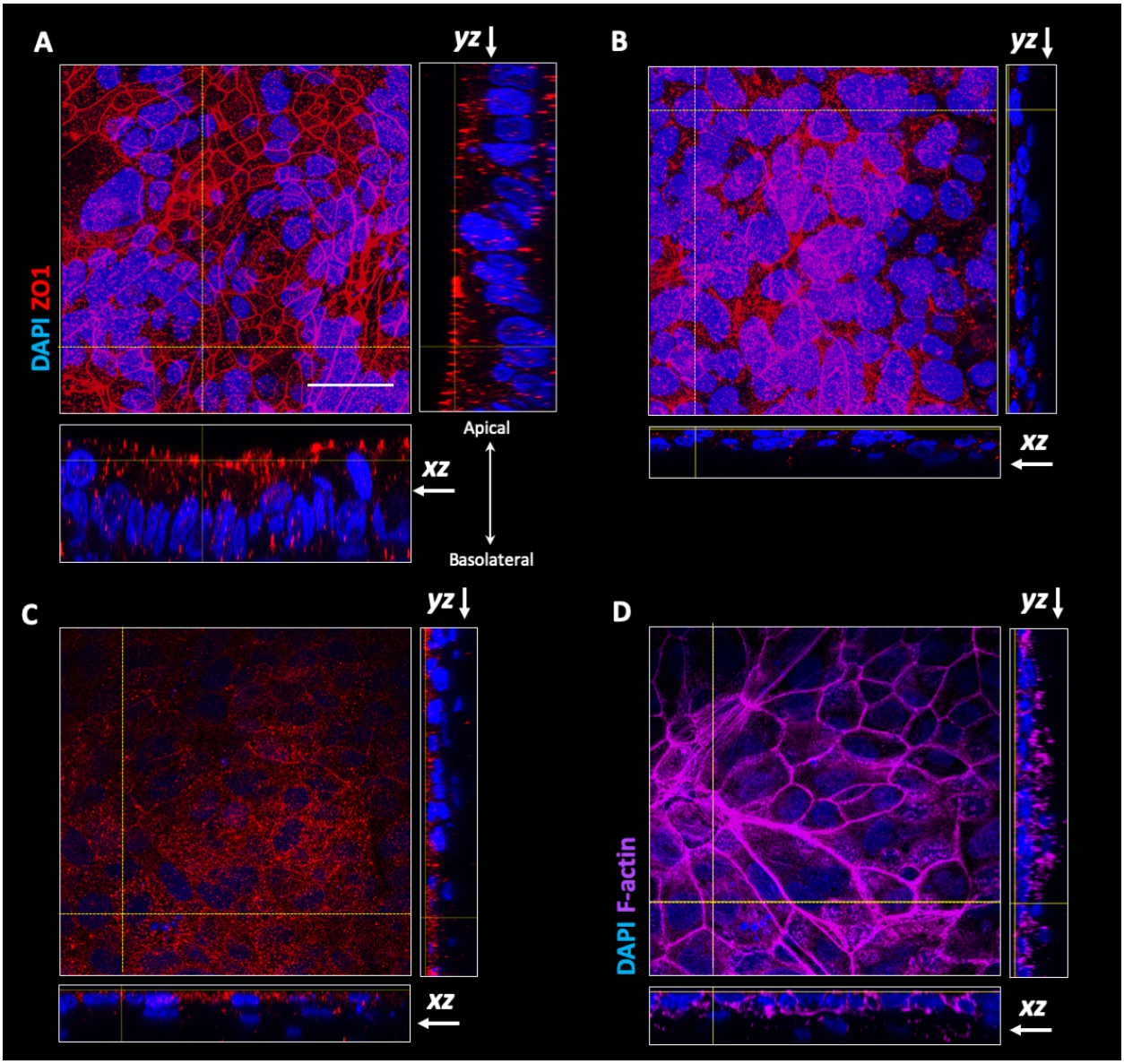

Figure 14. Immunofluorescence analysis using confocal microscopy of the 3D tissue models based on the SIS scaffold.

Immunofluorescence analysis of the 3D tissue models (epithelial/fibroblast co-culture tissue models) were cultured for 12 days (T84 and SV-HUC-1 cells) or 14 days (HEC-1-B cells) as described in Figure 5. ZO-1 TJ stating of (A) T84/HDFib, (B) HEC-1-B/HDFib, and (C) SV-HUC-1/HDFib. (D) F-actin staining of the co-culture

of SV-HUC-1/HDFib on the SIS scaffold. Z-stacks were made using confocal fluorescence microscopy from the top of the epithelial layer to the beginning of the SIS scaffold and reconstructed using FIJI. Orthogonal view of confocal microscopy (XY) with side views of YZ (right) and XZ (bottom). ZO-1 (red), phalloidin (f-actin, magenta), and DAP (blue). The scale bar is 25 µm.

T84 cells showed a strong expression of ZO-1 at the very apex of the cell layer. The ZO-1 TJ did well-expressed in HEC-1-B cells. Regarding the SV-HUC-1/HDFib model, the ZO-1 was expressed but was hard to visualize by confocal microscopy due to the formation of a thin flat layer by SV-HUC-1 cells. Figure 14D shows the continuous layer of the f-actin formation of SV-HUC-1 cells. The side view of yz and xz of 3D reconstruction of stacks of confocal images showed continuous layers of columnar T84, cuboidal layer of HEC-1-B, and squamous SV-HUC-1 epithelial cells.

3.3 Functional analysis

3.3.1 Transepithelial electrical resistance (TEER)

We measured the TEER of the established tissue models based on the SIS scaffold and Transwell® models. For Transwell® models, we measured the TEER on day 4, 7 and 10 after seeding the cells. Transwell® inserts were coated with collagen on both sides of the membrane. The TEER values for the Transwell® models showed an increase with time up to 10 days and after that the value kept constant. The TEER values for T84/HDFib, HEC-1-B/HDFib, and SV-HUC-1/HDFib on day 10 were 320 ± 12, 159 ± 11, and 134 ± 5 $\Omega.cm^2$, respectively.

We also measured the TEER values for the tissue models on day 7, 12 and 14 of cell culturing. The maximum TEER values obtained for T84/HDFib (318 ± 18 $\Omega.cm^2$) and SV-HUC-1/HDFib (122 ± 7 $\Omega.cm^2$) on day 12 and for the HEC-1-B/HDFib (182 ± 8 $\Omega.cm^2$) on day 14 of cultivation.

In the separate experiments, tissue models were also placed on an orbital shaker to examine the effect of shear stress on the maturation of the 3D tissue models. The results showed that the TEER value has slightly improved for T84/HDFib and SV-HUC-1/HDFib models and decreased in HEC-1-B/HDFib but they were not significant (Figure 15).

In addition, the result showed that the tissue models of T84/HDFib, SV-HUC-1/HDFib, and HEC-1-B/HDFib formed the barrier and reached the maturation state on days 12, 12, 14, respectively after the cell seeding.

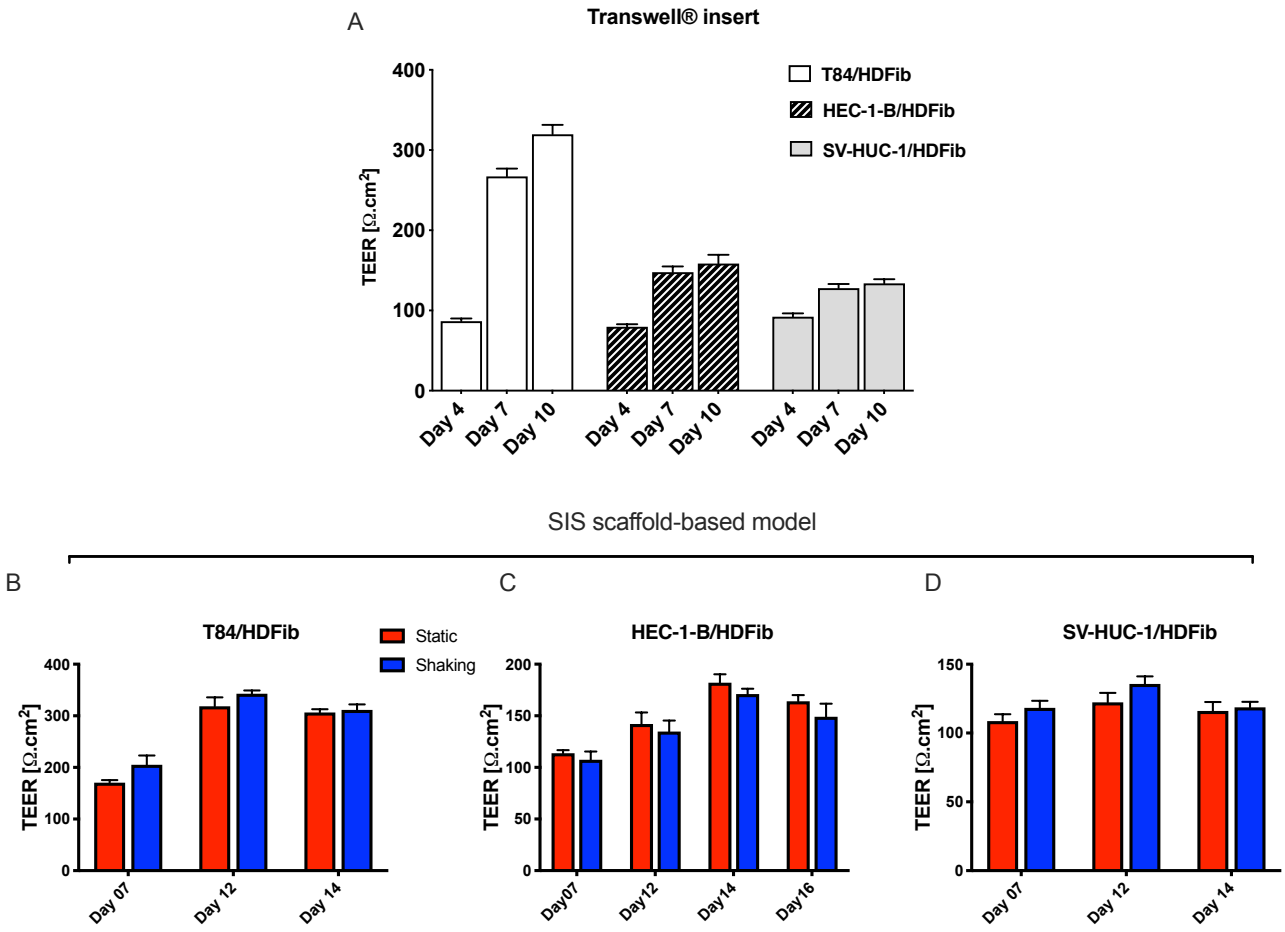

Figure 15. TEER measurements of Transwell® inserts and the 3D tissue models.

TEER was measured at indicated time points for (A) Transwell® inserts and (B, C, D) HDFib and specified epithelial cells (T84, HEC-1-B, and SV-HUC-1). Tissue models were grown either under static conditions or shaking using an orbital shaker. TEER was measured at indicated time intervals. All graphs represent the mean values ± SD from at least three independent replicates.

3.3.2 Permeability

According to the TEER results, all subsequent 3D tissue models were grown under static culture conditions. After the maturation time (day 12-14), the permeability of both Transwell® and the 3D tissue models was tested using the FITC-dextran permeability assay. The results showed that the mature 3D tissue models with epithelial cells were much less permeable with 1-2% translocation of FITC-dextran in comparison to only the SIS scaffold with HDFib (12%). The

permeability of Transwell® models was measured as 3-5% (Figure 16).

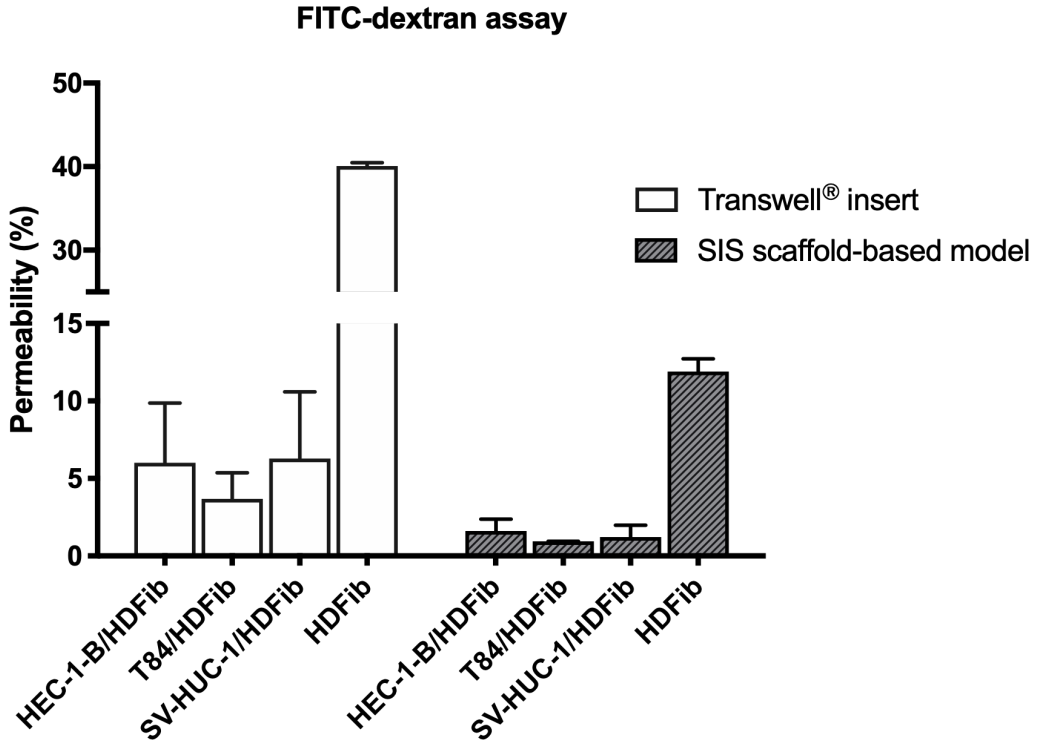

Figure 16. Permeability measurement using FITC- dextran assay.

Permeability was measured by FITC-dextran (FD; 4 kDa) assay at day 10 for co-culture Transwell® models, at day 12 and co-culture tissue models of T84/HDFib, SV-HUC-1/HDFib (at day 12), and HEC-1-B/HDFib (at day 14), based on the SIS scaffold as described in Figure 5. The graph shows fluorescence intensity from the lower compartment normalized by the fluorescence intensity obtained when empty Transwell® or SIS were used. The graph represents the mean values ± SD from at least three independent replicates.

3.4 Ultrastructural analysis

We examined the ultrastructure of the established 3D tissue models using TEM and SEM. The SIS scaffold was seen as a mesh of fibers (Figure 17, first column). TEM analysis also showed formation of apical junctions between the epithelial cells (Figure 17, white arrowheads).

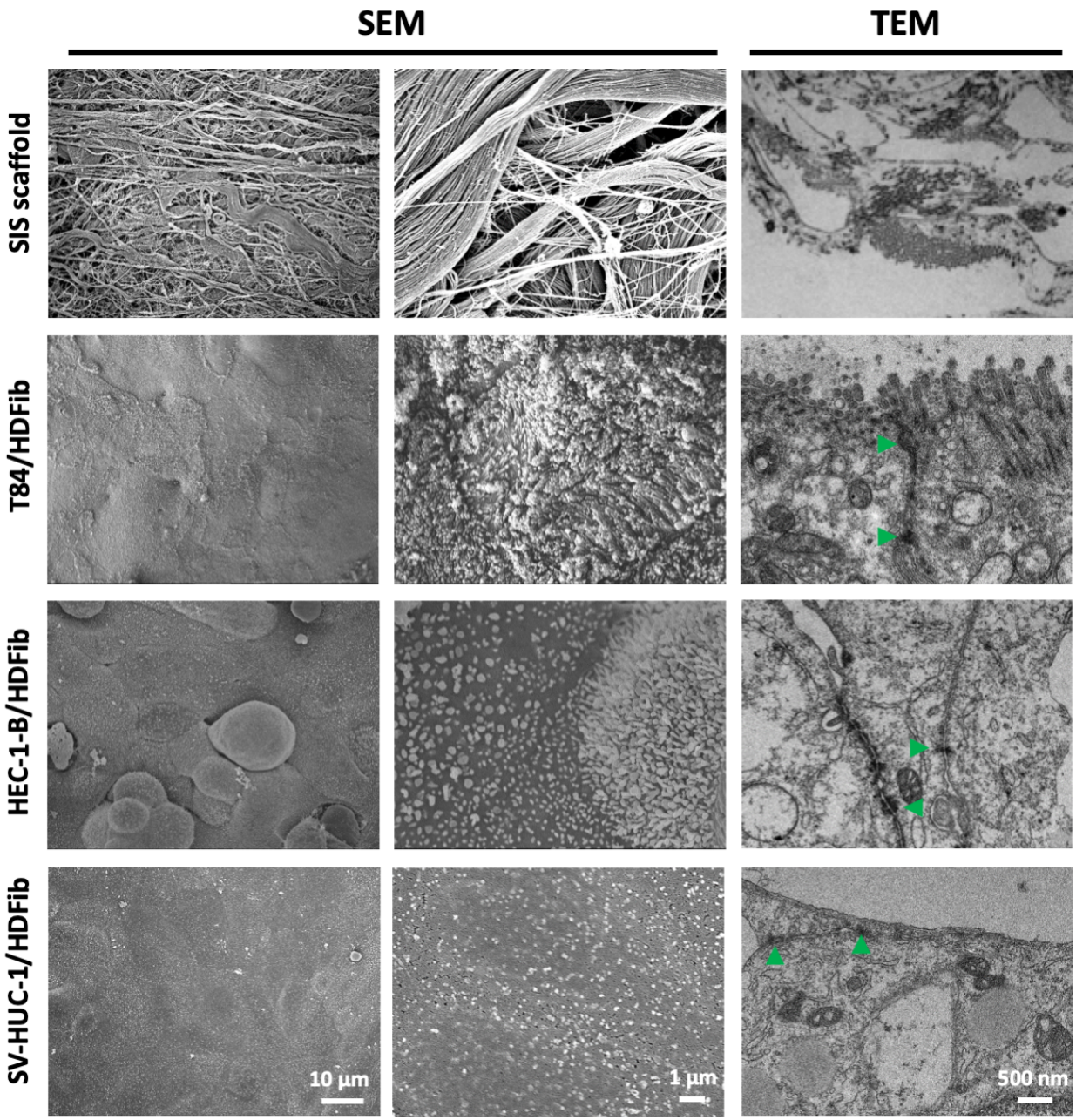

Figure 17. Morphology and ultra-structure of 3D mucosal tissue models.

Tissue models on the SIS scaffold were generated and analyzed by SEM and TEM. The co-culture tissue models of T84/HDFib, HEC-1-B/HDFib, and SV-HUC-1/HDFib based on the SIS scaffold were established as described in Figure 5. The SIS scaffold is a 3D porous structure contains mesh fibers of collagen, fibronectin, laminin, elastin, and glycosaminoglycans. SEM analysis depicted the microvilli on the surface of the T84 cell and HEC-1-B cells are more pronounced while they are shorter on SV-HUC-1 cells. TEM analysis also showed formation of TJs between the epithelial cells (green arrows).

T84 and SV-HUC-1 cells appeared as a continuous monolayer, whereas groups of HEC-1-B cells occasionally protruded from the underlying monolayer. We observed microvilli formation on the apical surface of the cells via higher magnification. The microvilli were most pronounced on T84 cells, followed by HEC-1-B cells, whereas on SV-HUC- 1 cells they were less and shorter.

Epithelial cells grew confluently and adhered firmly to the SIS scaffold. As shown in Figure 18a, the blue arrow marks the edges of the epithelial cell layer on the mesh of fibers of the SIS scaffold revealing a transition to the underlying scaffold. It also showed a fully grown tight continues epithelial cells. Figure 18b shows a monoculture of fibroblast cells on the SIS scaffold. The multipolar, elongated shapes of fibroblast growing on the scaffold showing the empty holes between the fibroblast cells. These holes might increase barrier permeability which agrees with the data of FITC dextran assay (Figure 16).

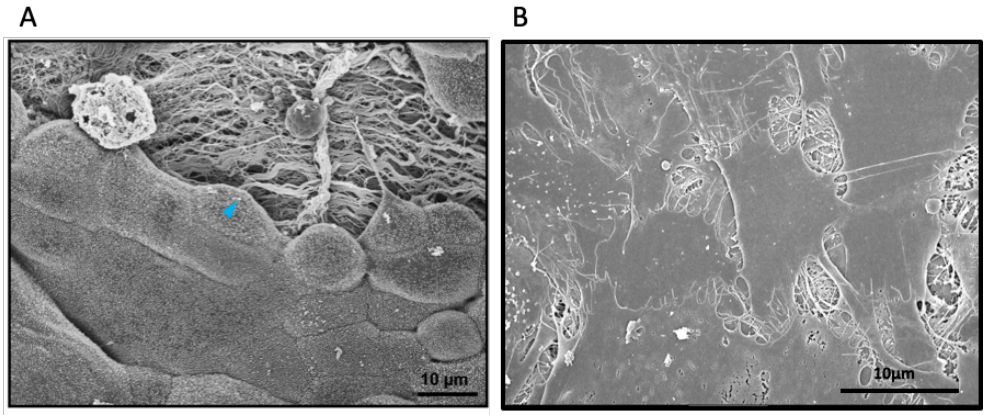

Figure 18. Morphology of the HEC-1-B/HDFib model and monoculture of Fibroblasts on the SIS scaffold.

SEM analysis of the co-culture of HEC-1-B and HDFib on the SIS scaffold. (A) The edge of HEC-1-B cells on the SIS scaffold marked with blue arrow, revealing the continuous contacts between the epithelial cells (B) HDFib cell seeded and grew on the SIS scaffold. The monoculture of fibroblast on the SIS scaffold showing the empty gaps between the cells.

3.5 infection Study

3.5.1 Bacterial strains

We used different laboratory derivatives and a clinical isolate for infection study. The MS11 strain derivatives N927 and N924 were selected to be Opa^- and $Pili^-$ and differed only in the expressed

PorB variant, N924 expresses $PorB_{IB}$ whereas N927 expresses $PorB_{IA}$. For MS11 wildtype and the related ΔOpa derivative that is devoid of any Opa proteins (Stein et al. 2015). $Pili^{+}$ colonies were selected; however, subsequent western blot showed that the bacteria used for infection were unpiliated, since they did not express pilin. VP1 is a clinical isolate expressing (Makino, van Putten, and Meyer 1991; van Putten 1993) and Opa^{-} and $Pili^{-}$ colonies were selected for this strain. Measurements showed comparable growth of all strains and derivatives.

3.5.2 Bacterial transmigration

The infection was performed in the HEPES medium, which is phosphate and serum-free and permits host cell invasion via the phosphate sensitive interaction with $PorB_{IA}$.

As a readout for infection, we assessed the number of bacteria that transmigrated across the tissue model to the basal side.

In the Transwell® model, we collected all the bacteria strains from the basal compartment after 6h of infection (Figure 19a). The highest level of transmigration was ΔOpa regardless of the co-culture model. In addition, the lowest level of transmigration occurred in N924 for co-culture models of HEC-1-B/HDFib, and SV-HUC-1/HDFib. However, we could not detect a significant difference between various strains of *N. gonorrhoeae* in all the Transwell® models.

In the tissue models based on the SIS scaffold, we collected the bacteria strains from the basal compartment after 144h of infection (Figure 19b). The transmigration efficiency of VP1 and ΔOpa in all the tissue models were greater than other strains (≥9000 CFU/mL in T84/HDFib and HEC-1-B/HDFib, and ≥500 CFU/mL in SV-HUC-1/HDFib). The lowest transmigration in all the tissue models happened in N924. However, no transmigration was detected in the SV-HUC-1/HDFib tissue model. The similar levels of transmigration efficiency N924 and MS11 were detected in T84/HDFib and HEC-1-B/HDFib tissue models.

In spite of Transwell® models, a significant difference is detected in transmigration efficiency of various strains in the tissue models based on the SIS scaffold.

Nevertheless, VP1 and ΔOpa could transmigrate across the tissue models only after 48h of infection. Figure 20 shows the transmigration efficiency of VP1 and ΔOpa in 6, 24, 48, 72, 96 and 144h after infection in all the tissue models.

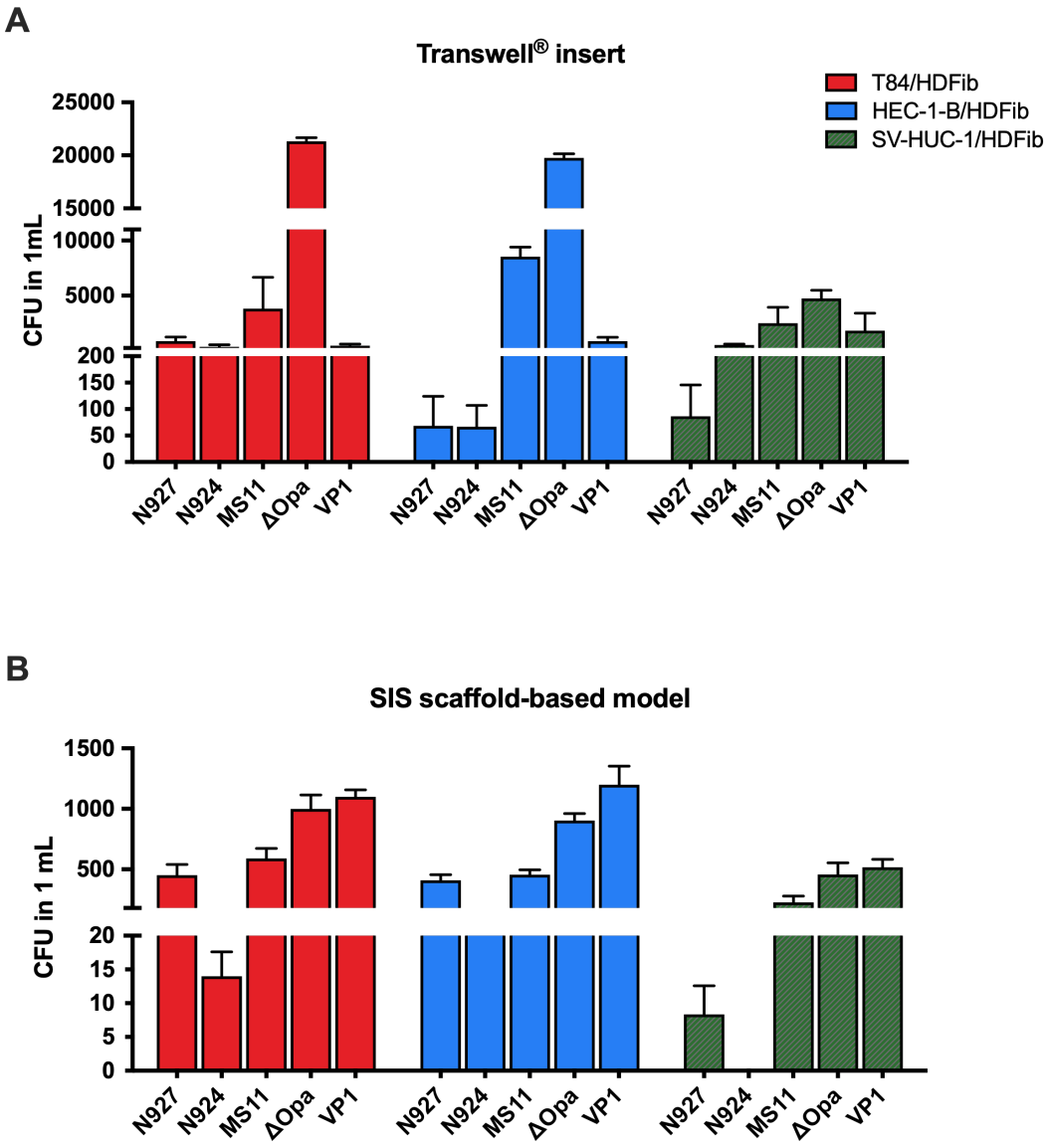

Figure 19. Bacterial transmigration assay.

Bacterial transmigration through the Transwell® and 3D tissue models-based on SIS scaffold. (A) Eleven days after seeding of the epithelial cells on Transwell® inserts, co-culture models were infected with indicated strains of *N. gonorrhoeae* at MOI 20 for 6 h. The number of bacteria in the basal compartment was calculated by plating and counting colony forming units (CFU). (A) Tissue models based on the SIS scaffold were generated as described in Figure 5. After thirteen (T84 and SV-HUC-1 cells) and fifteen (HEC-1-B cells) days of seeding epithelial cells, models were infected with indicated strains of *N. gonorrhoeae* at MOI 20 for 144 h and the number of bacteria present in the medium from the basal compartment was calculated. All graphs represent the mean values ± SD from at least three independent replicates.

The results showed that the transmigration of VP1 started at 6 h after infection in T84/HDFib and 24 h in HEC-1-B/HDFib tissue models. We observed the transmigration of ΔOpa after 72 h and 24 h of infection in T84/HDFib and HEC-1-B/HDFib tissue models, respectively.

However, SV-HUC-1/HDFib tissue model presented the most resistant barrier for bacterial transmigration even after 144 h of infection.

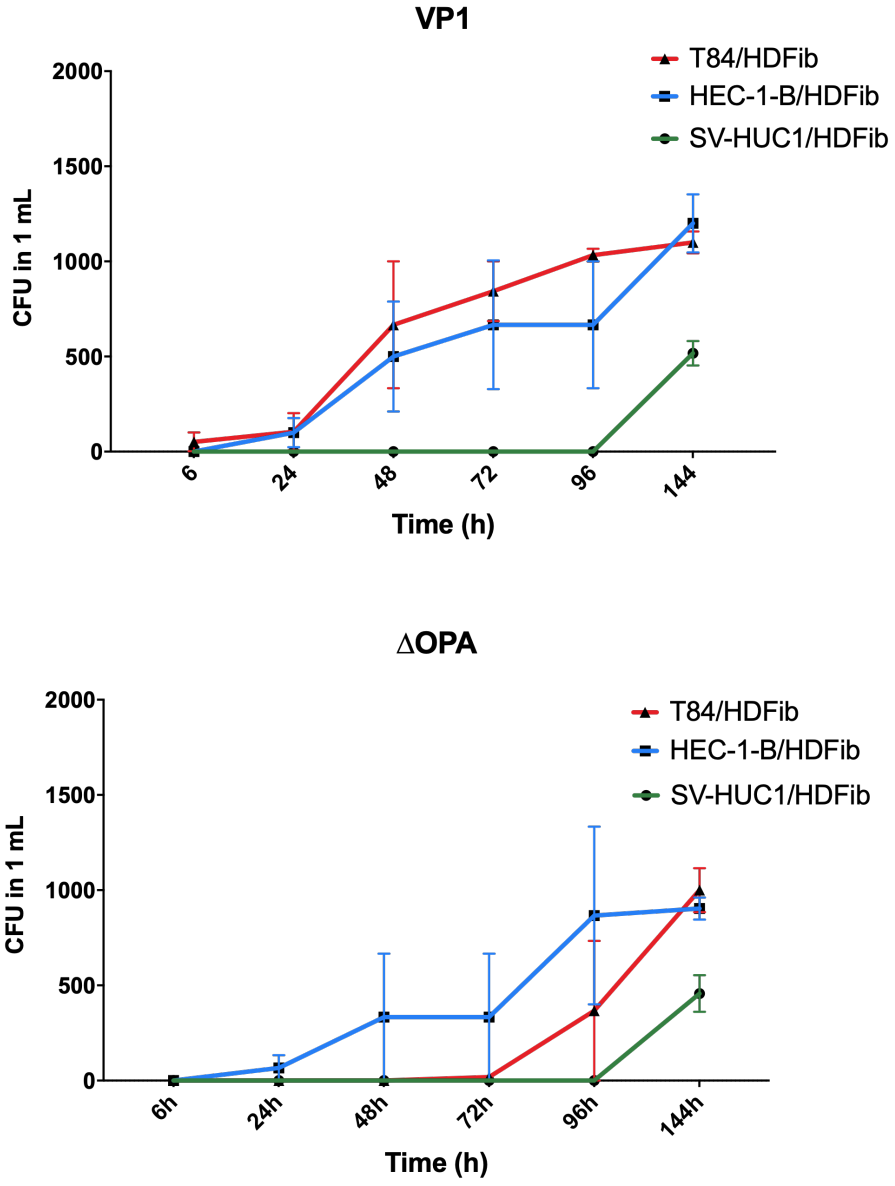

Figure 20. Bacterial transmigration assay (VP1 and MS11/ΔOpa).

3D tissue models based on the SIS scaffold were infected with *N. gonorrhoeae* VP1 and MS11/ΔOpa at MOI 20 and the number of bacteria in the medium from the lower compartment was determined at indicated time points after infection. All graphs represent the mean values ± SD from at least three independent replicates.

Importantly, the differences and delayed transmigration of bacteria through the SIS models were not due to the association of bacteria with the scaffold, because the empty SIS scaffold, as well as the SIS scaffold populated with fibroblasts for 2 days, were not presenting much of a barrier. We collected high numbers of bacteria from the basolateral compartment 30 minutes after infection for all strains and derivatives (Figure 21).

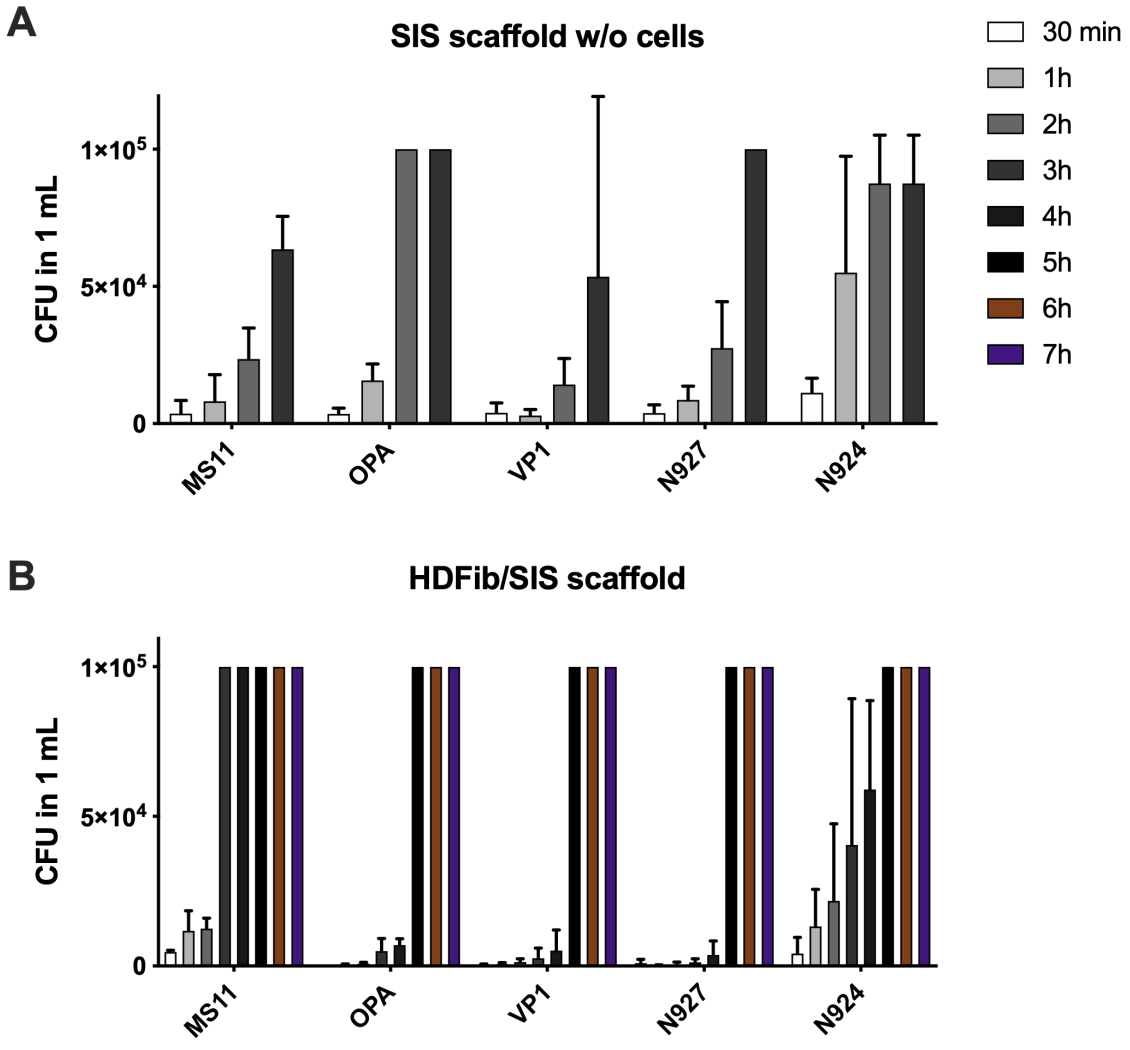

Figure 21. Transmigration of bacteria in the empty and SIS-HDFib scaffold.

(A) Blank SIS scaffold was mounted on Cell Crowns in the cell culture medium. (B) HDFib ($3x10^5$ cell/cm^2) were grown on the SIS scaffold 2 days prior to infection. Infection was performed in the HEPES medium at MOI 20 and was allowed to proceed for 7 h. Samples (25 µL) were collected from the basolateral compartment at indicated time points and plated with serial dilutions on GC agar plates. CFUs were counted up to a maximum of 100,000. The graphs show the mean values ± SD from two independent replicates.

3.5.3 Barrier permeability

We measured the barrier permeability of Transwell® models using FITC-dextran assay (Figure 22). The results showed an increase of permeability to ≈15% after 24 h upon infection for all the three independent co-culture models. In addition, no significant differences observed in barrier permeability of the Transwell® models when infected with different bacterial strains. The outcome of this assay indicated that the barrier permeability of the co-culture Transwell® models was independent of cell type and of bacterial strain.

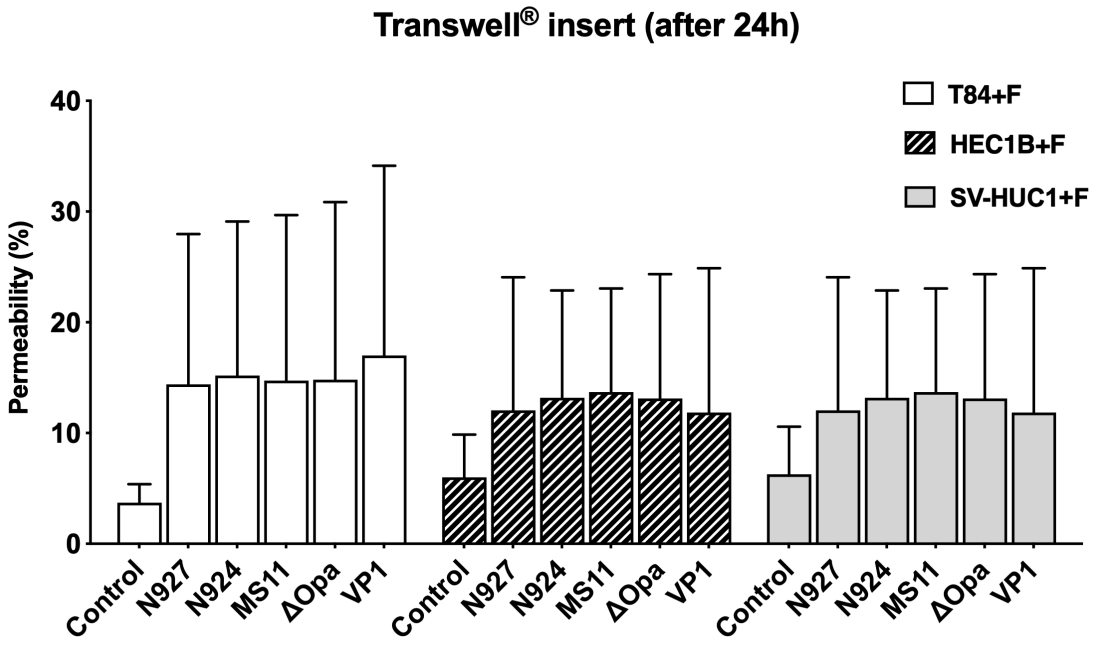

Figure 22. Barrier permeability measurement for Transwell® insert models after infection.
Barrier permeability in Transwell® models after 24 h of infection with *N. gonorrhoeae*. The co-culture tissue models are T84/HDFib, HEC-1-B/HDFib, and SV-HUC-1/HDFib as described in section 2.2.2. The permeability of the models was measured by 4 kDa FITC-dextran assay. The graphs represent the mean values ± SD from at least three independent replicates.

We also measured barrier permeability of the co-culture 3D tissue models on days 1, 2 and 6 after infection (Figure 23). In contrast to the Transwell® model in which the bacteria translocated quickly across the cell models, in 3D tissue models based on SIS scaffold, we could detect bacterial transmigration sometimes only after 144 h of infection.

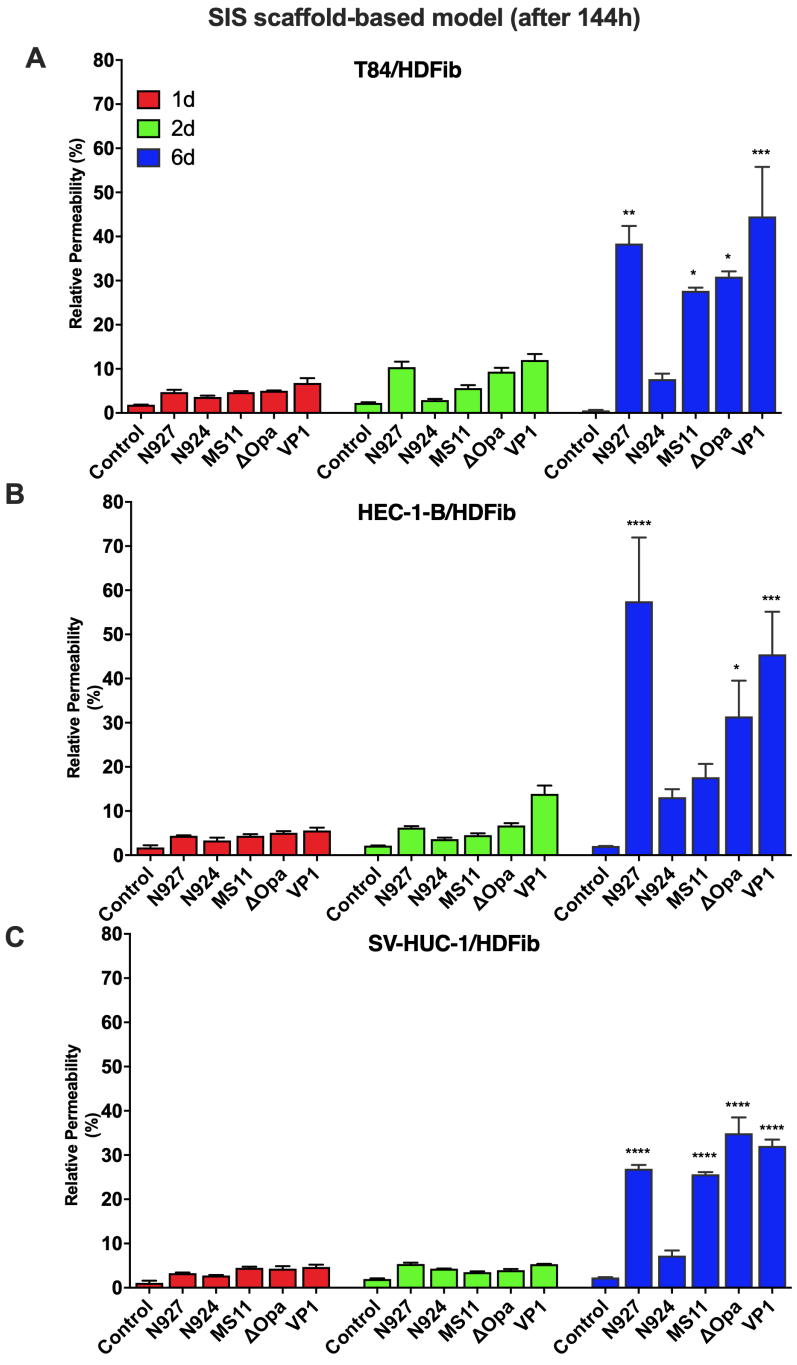

Figure 23. Barrier permeability measurement for the 3D tissue models-based on the SIS scaffold after infection.

Barrier permeability in 3D tissue models (T84/HDFib, HEC-1-B/HDFib, and SV-HUC-1/HDFib) as described in section 2.2.2 and Figure 5 after 144 h of infection with with *N. gonorrhoeae*. The permeability of the models was measured by 4 kDa FITC-dextran assay. The graphs represent the mean values ± SD from at least three independent replicates. Statistical significance of permeability change in comparison to non-infected control was tested by one-way ANOVA: ns – p>0.05, * - p≤0.05, ** - p≤0.01, *** - p≤0.001, **** - p≤0.0001.

The barrier permeability did not rise abruptly after 48 h of infection. Less permeable 3D tissue models allow us to perform a long-term study of the infection. The permeability analysis of the tissue models upon infections showed meaningful differences between cell types and strains, while such differences were not possible to detect in Transwell® models.

After 144 h of infection, the bacteria that increased permeability for co-culture models of T84/HDFib, HEC-1-B/HDFib, and SV-HUC-1/HDFib the most were VP1 (44.52%), N927 (57.52%), and ΔOpa (34.92%), respectively. In addition, the low rate of permeability after 144 h of infection with N924 for all the 3D tissue models (permeability ≈7-13%) showed that the N924 was a less destructive strain. The overall lowest level of permeability was observed in the tissue model of SV-HUC-1/HDFib (≈35%).

3.5.4 Cytotoxicity analysis

We measured the cytotoxicity of the tissue models upon infection by LDH assay (Figure 24). The results showed higher cytotoxicity of VP1 in T84/HDFib (≈82%), N927 and VP1 in HEC-1-B/HDFib (≈70%), and N927 and VP1 in SV-HUC-1/HDFib (≈60%).

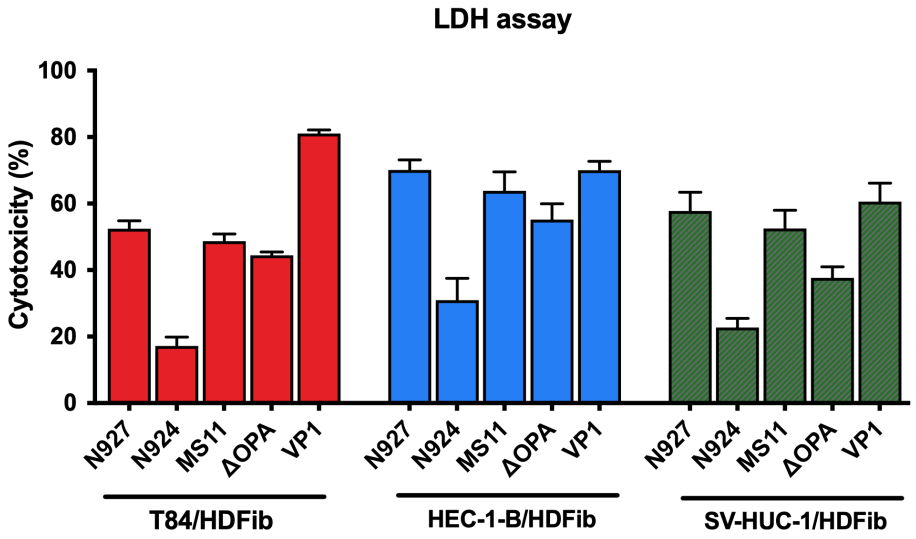

Figure 24. Cytotoxicity measurement of 3D tissue models after infection.

3D tissue models based on SIS scaffold were infected for 144 h as described in section 2.2.2. The cytotoxicity of the different *N. gonorrhoeae* was evaluated using lactate dehydrogenase (LDH) assay. The graphs represent the mean values ± SD from at least three independent replicates.

In addition, infection with N924 was less cytotoxic in all the 3D tissue models (≈17-30%). The destruction of the tissue models upon infection caused an increase in barrier permeability and translocation of bacteria across the tissues (Figure 23). The results indicated that *N. gonorrhoeae* subtype $PorB_{IA}$ (expressed in VP1 and N927 strains) mediates bacterial attachment and tissue destruction, facilitating migration of bacteria across the tissue.

3.5.5 Ultrastructure analysis after infection

SEM analysis indicated a successful adhesion of bacteria to the cell surface and the elongation of microvilli (Figure 25a). Here we can observe the colonization of folds between cells by *N. gonorrhoeae* (N927) and individual microcolonies, which interacted with the adjacent cells (Figure 25b). In addition, we tried to find the precise location of *N. gonorrhoeae* using TEM analysis in the infected tissue models. However, we could only observe the bacteria on the surface of the tissue (Figure 25c).

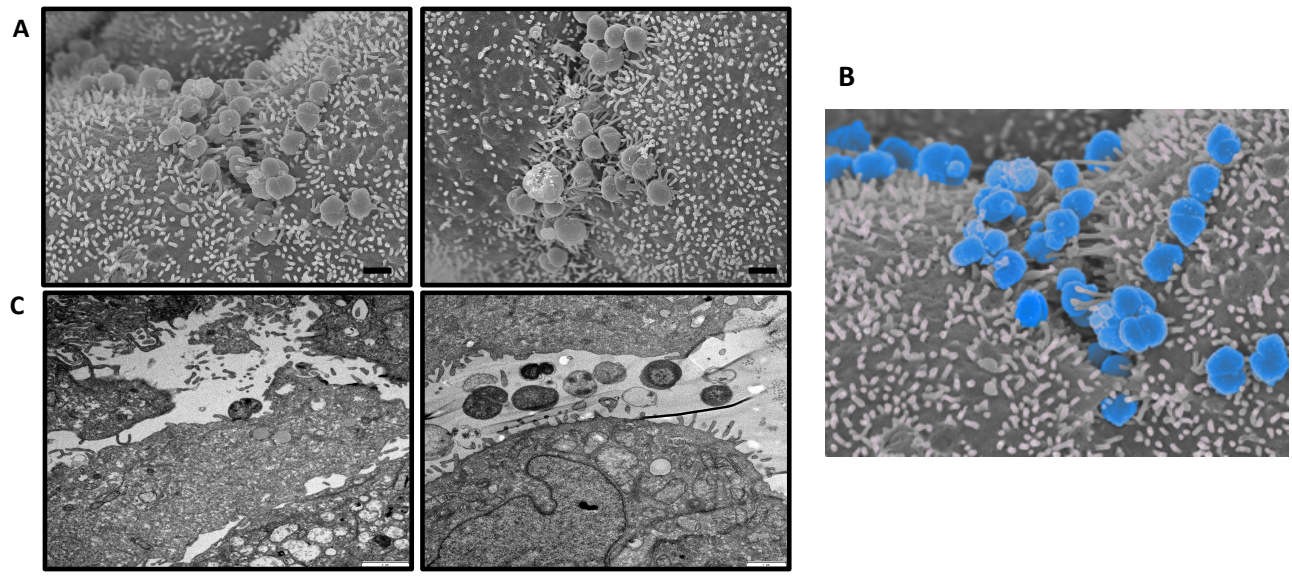

Figure 25. Electron microscopy (SEM and TEM) of the infected HEC-1-B SIS tissue model.
The co-culture model of (HEC-1-B/ HDFib) was infected with *N. gonorrhoeae* (N927) for 24 h. (A) SEM analysis of the infected tissue model (HEC-1-B/ HDFib). (B) *N. gonorrhoeae* (N927) were pseudocolored (blue) using the GNU Image Manipulation Program (GIMP 2.10.8) (http://www.gimp.org/). The colonies of N927 are mostly located in the area of the between cells. Microvilli around the *N. gonorrhoeae* are also elongated. (C) TEM analysis of the infected tissue model (HEC-1-B/ HDFib). The scale bar is 1 µm.

3.5.6 Confocal microscopy and analysis of infected T84/HDFib models

3.5.6.1. Infected T84/HDFib tissue models

After infection with *N. gonorrhoeae*, we performed immunohistochemistry staining of the both infected and non-infected samples. The results showed general morphological changes and loss of cell polarity after the infection with *N. gonorrhoeae* (Figure 26). However, we could not observe the precise location of *N. gonorrhoeae* interacting with epithelial cells. The Figure 26b and Figure 26c show the infected T84/HDFib tissue model with VP1 and N924, respectively. We could not detect the exact location of bacteria in these tissue samples. We, therefore, stained whole tissues in order to analyze the effect of infection on the morphology of the epithelial cells using confocal microscopy.

We analyzed the early and late stages of infection of T84/HDFib tissue models using confocal microscopy, with the least and the most aggressive bacteria, N924 and VP1, respectively. After 24 h, the cell layer and TJs appeared still conserved, whereas at the later stage of infection after 144 h we observed significant cell lysis and destruction of TJs in SIS models infected by VP1, but not so much when N924 gonococci were used. N924 bacteria seemed to be distributed more in the middle of the cells and VP1 localized in the areas of cell-cell contacts. In the orthogonal views of the samples, we observed bacteria only at the surface of the models (Figure 27a). The intensity of ZO-1 TJs was quantified in the 3D tissue models infected with N924 and VP1. The results indicated that after 6 days of infection, VP1 disrupted ZO-1 TJ significantly higher than N924 (Figure 27b). We repeated the experiments to evaluate concurrently the bacteria adherence, invasion, and transmigration (Figure 28). We assessed the number of adherence bacteria by lysing epithelial cells using saponin (1%) (Figure 28a). We detected bacteria after 6 h, 24 h, and 144 h of infection. There is no difference in bacterial adhesion after 6h and 24 for both VP1 and N924. However, after 144 h of infection, great level of VP1 (≥5000 CFU/mL) presented in the site of infection in the T84/HDFib tissue model.

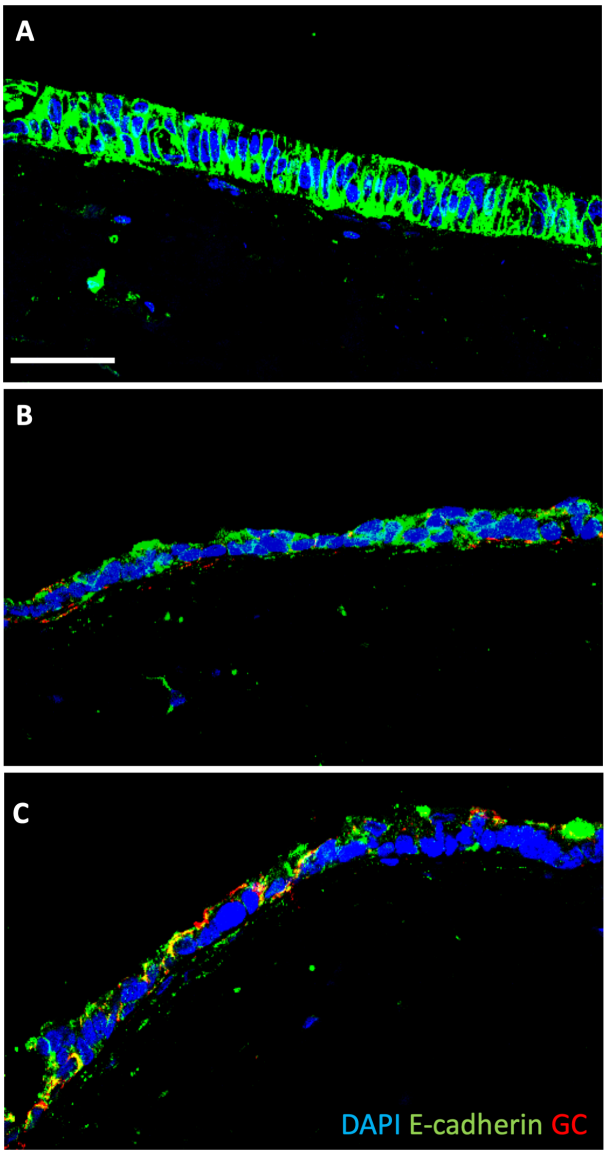

Figure 26. Immunohistochemical analysis of paraffin-embedded tissue.
Immunohistochemistry staining of (A) the non-infected T84/HDFib tissue model, (B) the infected T84/HDFib tissue model with VP1, and (C) the infected T84/HDFib tissue model with N924. Anti-*N. gonorrhoeae* (red), E-Cadherin (green), and DAPI (blue). The scale bar is 50 µm.

The adherence analysis showed that the number of VP1 bacteria associated with the model greatly increased after 144 h of infection, whereas the number of N924 bacteria remained approximately the same. After 6 h, 24 h and 144 h following the infection, the culture media from the basolateral chamber collected and plated on GC agar. The transmigration assay showed that the VP1 strain has a high capacity for transmigration.

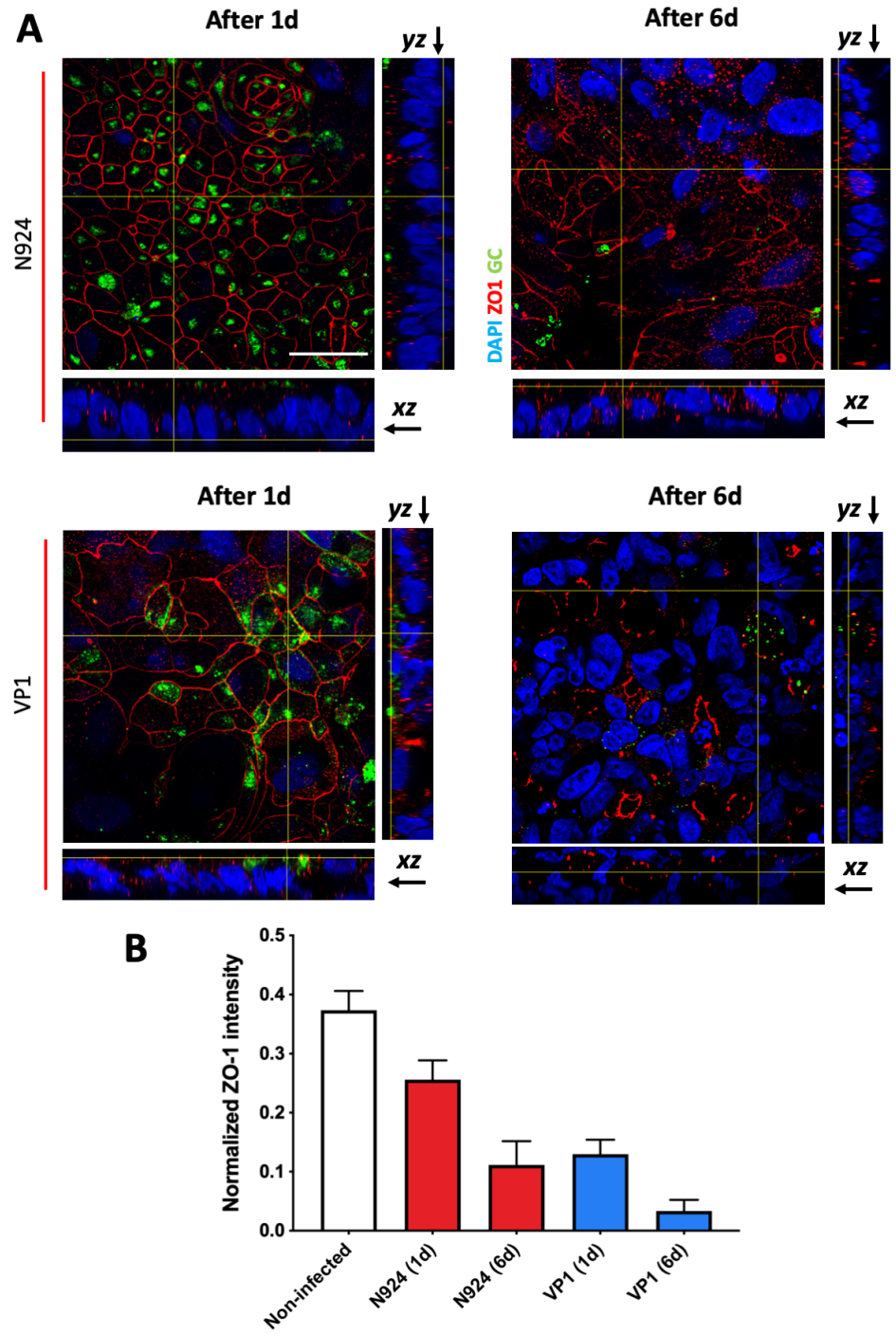

Figure 27. Confocal microscopy and analysis of the infected 3D tissue model of T84/HDFib based on the SIS scaffold.

(A) Tissue models with co-culture of T84/HDFib cells were prepared and infected with N924 or VP1 strains of *N. gonorrhoeae* for 24 h or 144 h, as described in Figure 5. The tissue model was stained with ZO-1 (red), anti- *N. gonorrhoeae* antibody (green), and DAPI (blue). Z-stack images were made using confocal fluorescence microscope beginning at the top of the epithelial layer to the SIS scaffold. Z-stacks were made using confocal fluorescence microscopy and the images were analyzed and reconstructed using FIJI.

Orthogonal view of confocal microscopy (XY) with side views of YZ (right) and XZ (bottom). The scale bar is 25 µm. (B) Quantification of the intensity of ZO-1 TJs of confocal images depicted in A. For quantification, the fluorescence intensity of views was measured (Rectangular tool (Fiji)) and backgrounds were subtracted (3 views per biological replicate). The graphs represent the mean values ± SD.

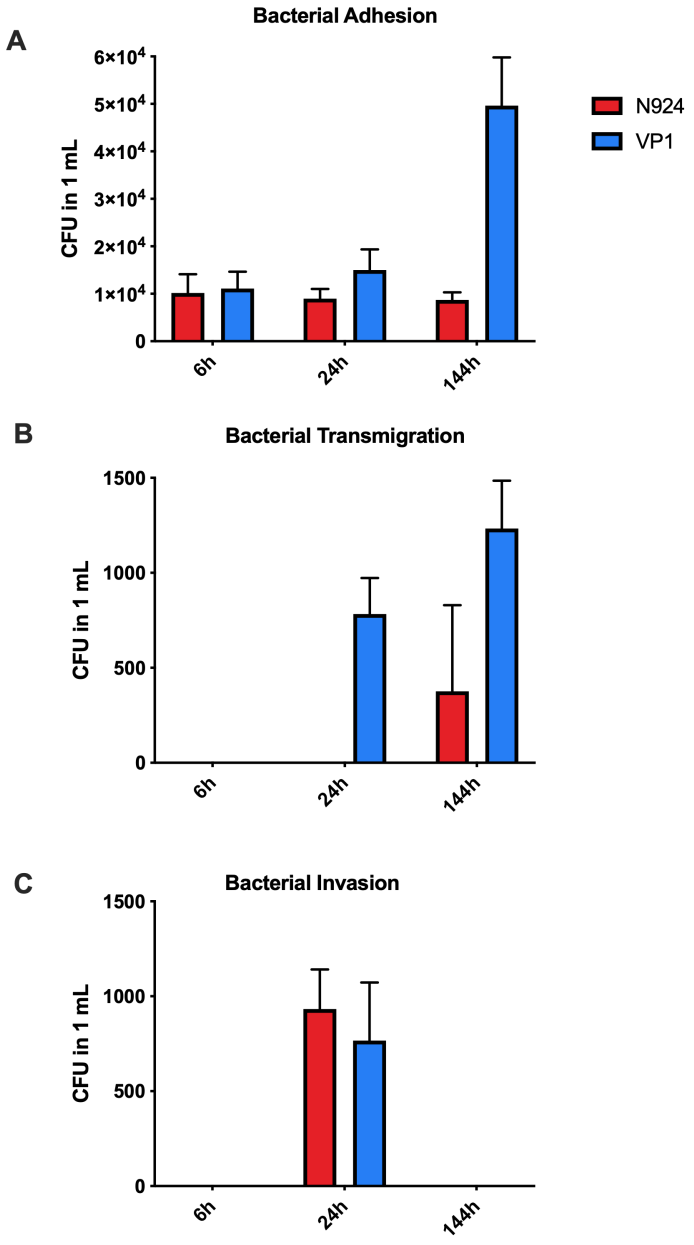

Figure 28. Bacterial adhesion, transmigration, and invasion.

T84/HDFib tissue models were infected with N924 or VP1 strains of *N. gonorrhoeae* for 6 h, 24 h or 144 h. The number of (A) adherent bacteria, (B) transmigrated bacteria, and (C) invaded bacteria were assessed by plating and counting colony forming units (CFU). The graphs represent the mean values ± SD from at least three independent replicates.

The N924 strain transmigrated after 144 h of infection (Figure 28b). We evaluated the bacteria invasion in the T84/HDFib tissue model using gentamicin assay. We treated the infected tissue model with gentamicin from the apical and basolateral side. After 6 h and 144 h of infection, all bacteria were efficiently killed. We detected N924 and VP1 after 24 h of infection (Figure 28c).

3.5.6.1. Infected T84/HDFib Transwell® model

We infected the Transwell® model of T84/HDFib with N924 and VP1. The confocal analysis showed that after 24 h of infection, both strains destructed ZO-1 TJs and transmigrated across the tissue model (Figure 29). Nevertheless, no tangible differences in TJs destruction observed in the Transwell® model of T84/HDFib when infected with N924 and VP1.

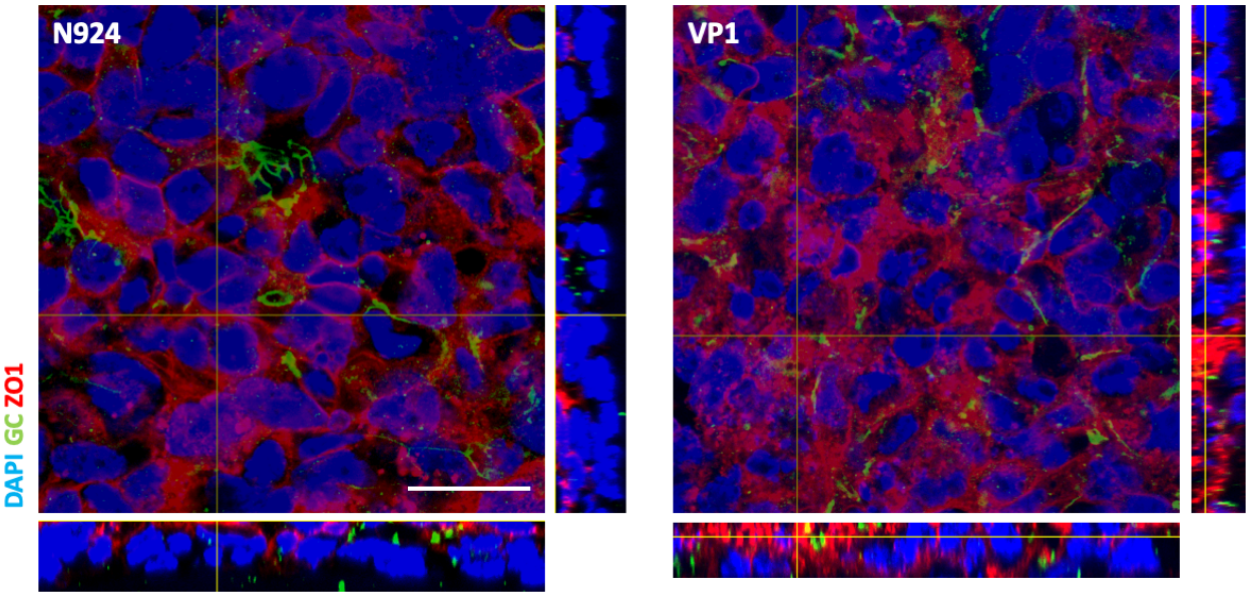

Figure 29. Confocal microscopy and analysis of the infected Transwell® model of T84/HDFib.

The Transwell® model of T84/HDFib was established and infected with N924 and VP1 as described in section 2.2.2. The tissue models then stained with ZO-1 (red), anti- *N. gonorrhoeae* antibody (green), and DAPI (blue). Z-stack images were made using the confocal fluorescence microscope beginning at the top of the epithelial layer to the PC membrane. Z-stacks were made using confocal fluorescence microscopy and the images were analyzed and reconstructed using FIJI. Orthogonal view of confocal microscopy (XY) with side views of YZ (right) and XZ (bottom). The scale bar is 25 µm.

3.5.7 Cytokine measurements in response to infection

After 24 h of infection, we assessed the amount of pro-inflammatory cytokines (IL-6 and TNFα) and chemokine (IL-8) in both Transwell® (Figure 30) and 3D tissue models based on the SIS scaffold (Figure 31). We expected that upon the infection the cytokines release to the apical compartment. The level of IL-6 in the SV-HUC-1/HDFib model are greater than other tissue models upon infection with all the *N. gonorrhoeae* strains (Figure 30). The highest and lowest level of IL-6 in the SV-HUC-1/HDFib model happened when infected with N927 and VP1, which were 6479.22 and 1084.64 pg/mL, respectively. However, the highest level of IL-6, which produced in T84/HDFib when infected with N927 and HEC-1-B/HDFib when infected with VP1 was 404.46 pg/mL and 273.57 pg/mL, respectively. Production of IL-8 in the SV-HUC-1/HDFib model was significantly higher than other models (3575.04 pg/mL ≤ IL-8 ≤ 4180.98 pg/mL) while the IL-8 did not produce well in the T84/HDFib and HEC-1-B/HDFib when cultured in Transwell® insert (Figure 30). The level of TNF-α increased in all the Transwell® models when challenged with VP1. However, the level of VP1 in the Transwell® model of SV-HUC-1/HDFib was greater (48.75 pg/mL) than HEC-1-B/HDFib (26.93 pg/mL) and T84/HDFib (2.58 pg/mL).

The measurement of pro-inflammatory cytokines (IL-6 and TNFα) and chemokine (IL-8) showed that the level of cytokines that are produced in the tissue models is greater than Transwell® models (Figure 31). Production of IL-6 is greater in the male uroepithelial 3D tissue model with SV-HUC-1 cells (SV-HUC-1/HDFib) than other tissue models based on the SIS scaffold. The highest and lowest level of IL-6 happened when SV-HUC-1/HDFib infected with MS11 (10467.24 pg/mL) and N924 (6266.01 pg/mL), respectively. Nevertheless, the level of IL-6 did not significantly increase in T84/HDFib and HEC-1-B/HDFib when challenged with different strains of *N. gonorrhoeae* (Figure 31). The IL-8 production in the tissue model of T84/HDFib, when infected with ΔOpa, showed the highest level (7111.02 pg/mL). Moreover, IL-8 level in SV-HUC-1/HDFib tissue model was high for all the strains (≈4000 pg/mL) while the HEC-1-B/HDFib tissue model produced IL-8 only when challenged with N924 (1389.18 pg/mL). In addition to IL-6 and IL-8, the level of TNF-α increased only in the SV-HUC-1/HDFib tissue model when infected with all the strains except N924.

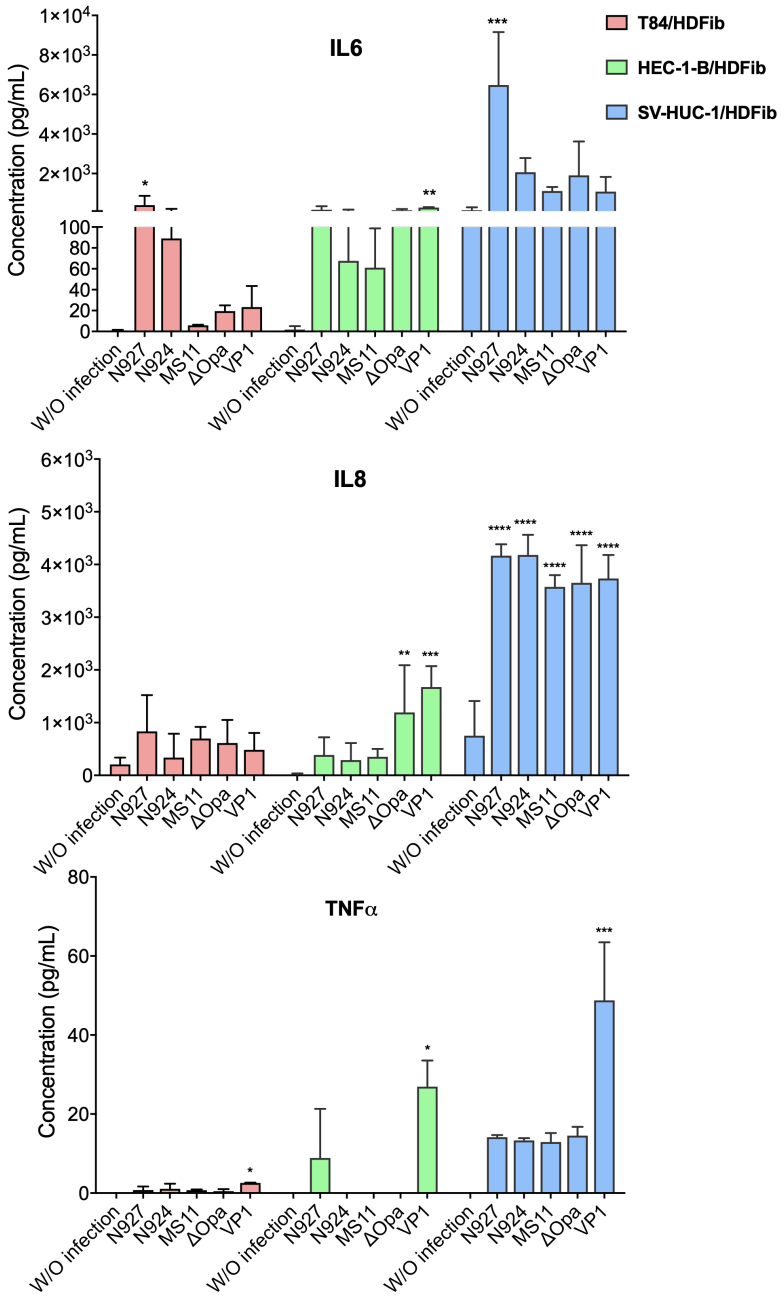

Figure 30. Cytokines measurements (IL-6, IL-8, and TNF α) in response to infection in Transwell® models.

Measurement of the IL6, IL8 and TNFα production in the Transwell® models upon infection with *N. gonorrhoeae*. The medium was collected and the concentration measurement of IL6, IL8, and TNFα was performed using Luminex assay. The graphs represent the mean values ± SD from at least three independent replicates. Statistical significance of the changes in cytokines concentration in comparison to non-infected control was tested by one-way ANOVA: * - p≤0.05, ** - p≤0.01, *** - p≤0.001, **** - p≤0.0001.

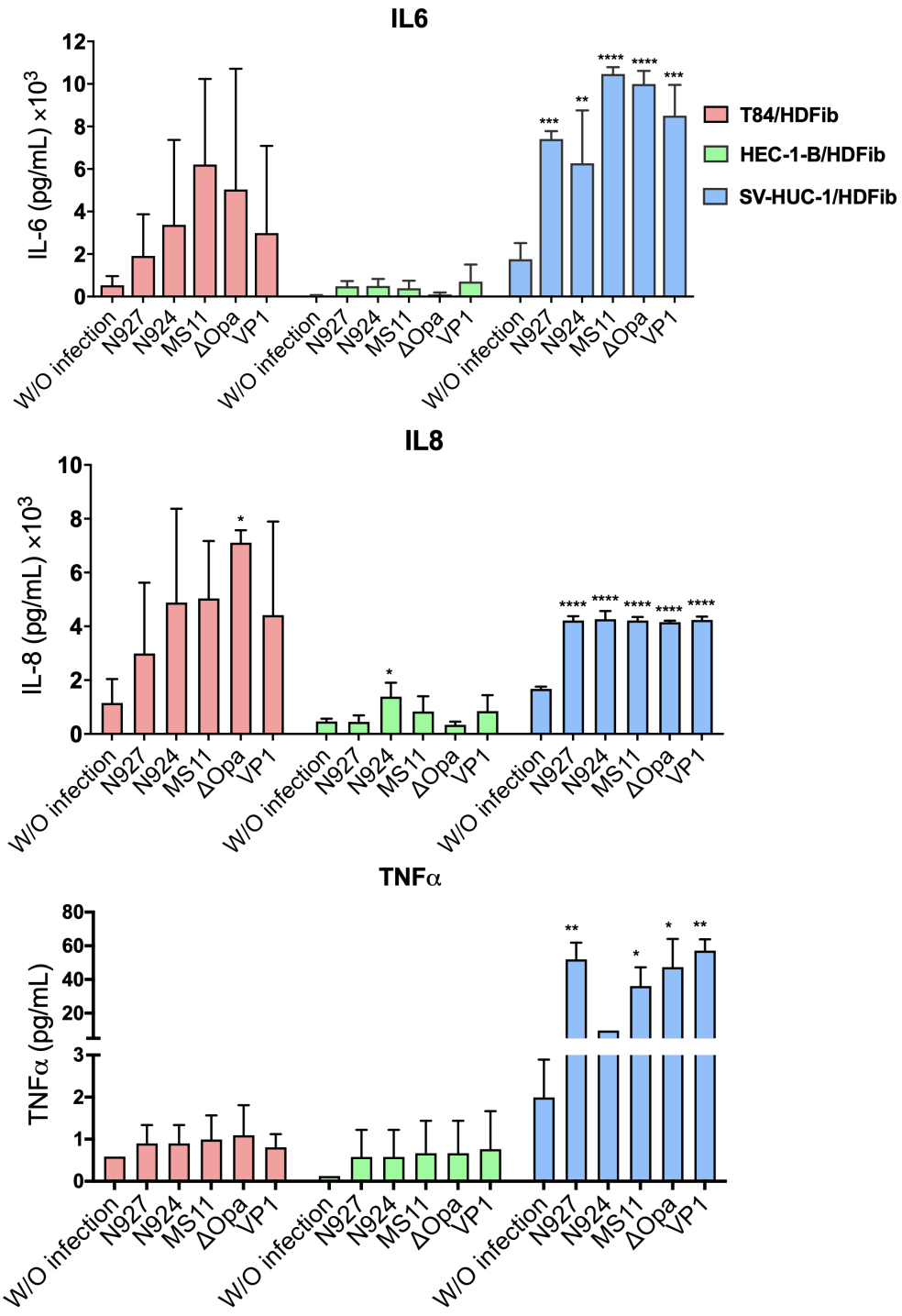

Figure 31. Cytokines measurements (IL-6, IL-8, and TNF α) in response to infection in 3D tissue models based on the SIS scaffold.

Measurement of the IL6, IL8 and TNFα production in the 3D tissue models based on the SIS scaffold, descried in section 2.2.2 after infection with *N. gonorrhoeae*. The medium was collected and the concentration measurement of IL6, IL8, and TNFα was performed using Luminex assay. The graphs represent the mean values ± SD from at least three independent replicates. Statistical significance of the

changes in cytokines concentration in comparison to non-infected control was tested by one-way ANOVA: * - p≤0.05, ** - p≤0.01, *** - p≤0.001, **** - p≤0.0001.

The results showed that among the Transwell® models, male uroepithelial with SV-HUC-1 cells produced a greater level of cytokines compared to the non-infected model while in the established tissue models, the level of IL-6, IL-8, and TNF-α completely depend on the tissue model (epithelial cells) and type of strains.

3.6 Neutrophil transmigration

3.6.1 Triple co-culture model

We modified the already established co-culture 3D tissue model (Section 2.2.2) to investigate neutrophil transmigration to the site of infection. In the modified 3D tissue model, we generated a triple co-culture of HDFib, T84 and HUVEC cells. Histological characterization of the established tissue model after fixation and paraffin embedding of the tissue model showed the presence of polarized epithelial monolayer on apical side, fibroblast in the middle and flat endothelial monolayer on the basal side of the tissue model (Figure 32a). The paraffin embedded tissues were also stained with E-cadherin and mucin 1 (Muc1) antibodies from the apical side in order to observe the cell-cell contacts and mucus production (Figure 32b). The samples were also stained by VE- Cadherin and CD31 antibody to specifically observe the endothelial cells from the basal side (Figure 32c-d). The results of immunohistochemistry and immunofluorescence staining of the tissue model revealed that the flat monolayer of endothelial cells is located on the basal side of the scaffold (Figure 32e).

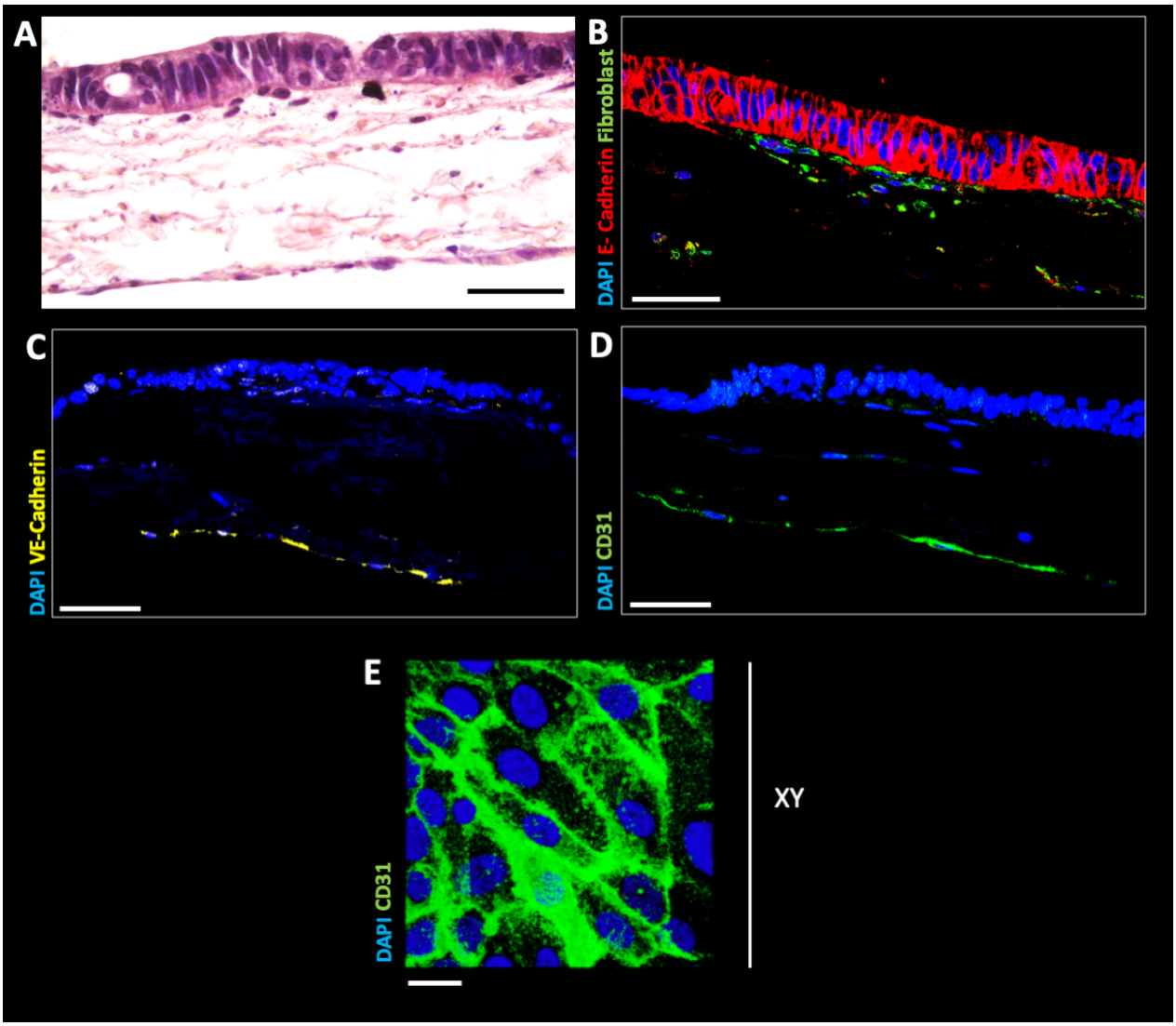

Figure 32. Histological and immunofluorescence analysis of triple co-culture model.
(A) H&E staining of the triple co-culture 3D tissue model as described in section 2.2.14 showing three layers of cells including epithelial (T84, top layer), fibroblasts (HDFib, middle layer), and endothelial (HUVEC, basal layer) cells. (B-D) The tissue model was stained with anti-E-cadherin (red), anti-fibroblast (green), anti-VE-cadherin (yellow), anti-CD31 (green), and DAPI (blue). The images showed the formation of an epithelial (stained by E-cadherin) and endothelial (stained by VE-cadherin and CD31) monolayer and the presence of connective tissue (stained by anti-fibroblast). The scale bars are 50 µm. (E) XY view of Immunofluorescence staining of the 3D tissue model with anti CD31 (green) and DAPI (blue). The scale bar is 5 µm.

3.6.2 Functional analysis

We measured TEER and permeability of the triple co-culture tissue model (Figure 33). The TEER values for the triple co-culture model of T84/HDFib/HUVECs showed a slight increase (≈400 Ω*cm^2) in comparison to the co-culture model of T84/HDFib (≈320 Ω*cm^2) after12 days of cultivation (Figure 33a). The permeability of the model was also tested on day 12 using the FITC-dextran permeability assay. The results indicated that the triple co-culture model is less permeable (permeability ≈ 0.5%) than the co-culture model (permeability ≈ 1%) (Figure 33b).

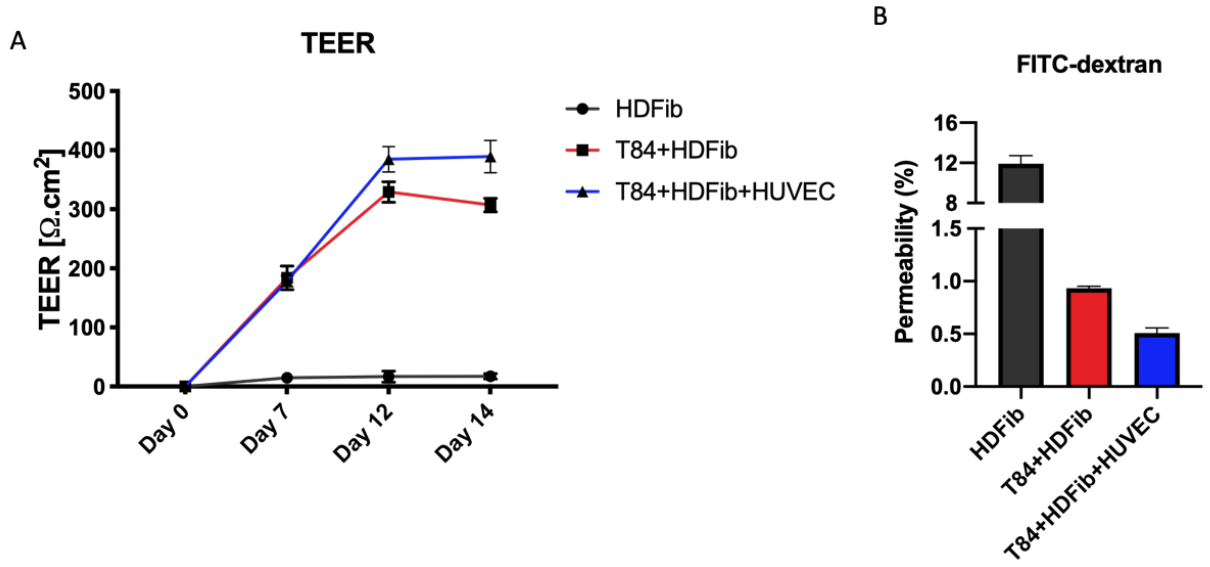

Figure 33. Functional analysis of the triple co-culture model (T84/HDFib/HUVECs).
(A) TEER measurement of HDFib, co-culture (T84/HDFib) and triple co-culture (T84/HDFib/HUVECs) 3D tissue model on the SIS scaffold on day 0, 7, 12 and 14. (B) Barrier permeability assessment using FITC-dextran (4 kDa) of HDFib, co-culture (T84/HDFib) and triple co-culture (T84/HDFib/HUVECs) model on the SIS scaffold on day 12. The graphs represent the mean values ± SD from at least three independent replicates.

3.6.3 Neutrophil characterization

We stained the isolated cells with anti-human neutrophil cytosolic factor 2 (NCF2), which is specific for human neutrophils. In addition, the segmented shape of neutrophils nuclei was visualized by DAPI staining (Figure 34a-b). We also characterized the isolated neutrophils from the healthy blood donor with the CD66b marker, which is a member of the immunoglobulin

superfamily and expressed on granulocytes. The results demonstrated that the isolated cells largely expressed CD66b (more than 90%) (Figure 34c). After confirmation of the purity of isolated neutrophils, we administered them to the tissue model (section 2.2.14).

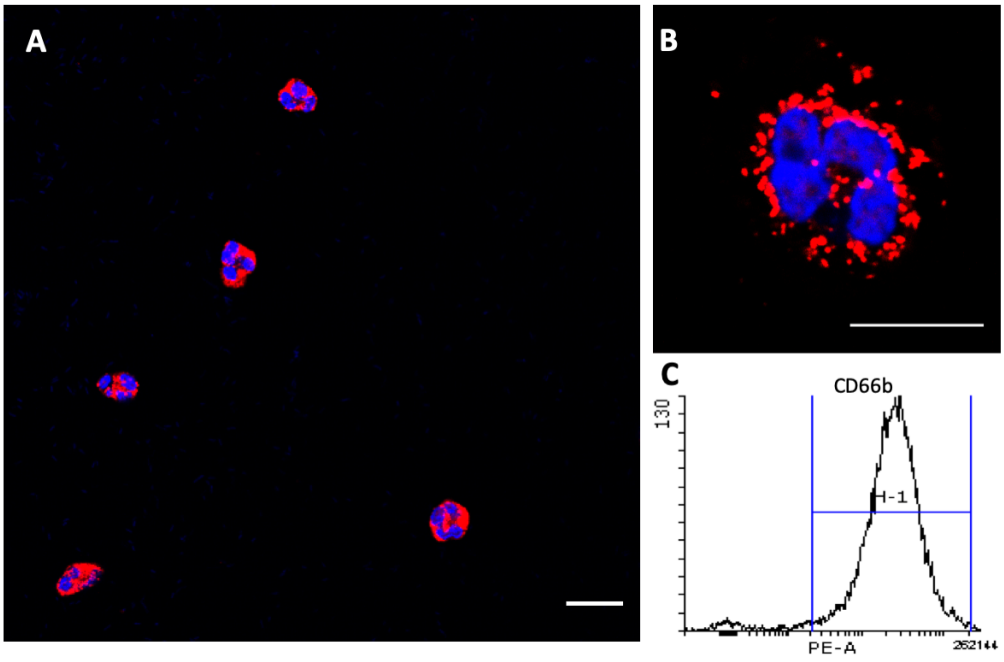

Figure 34. Characterization of neutrophils isolated from the healthy blood donor.
(A-B) Immunofluorescence staining of isolated neutrophils. DAPI (blue) and anti-human neutrophil cytosolic factor 2 (NCF2, red). The scale bar is 10 µm. (C) FACS analysis of isolated neutrophils from the healthy blood donor with CD66b marker.

3.6.4 Neutrophil activation status

Isolated neutrophils from the human blood were administered to the endothelial cells thorugh the basal chamber of the biorecator via perfusion for 2 h (Figure 7). Neutrophil activation (expression of CD11b) was measured for only neutrophils without circulation (control), neutrophils with circulation through the non-infected 3D tissue model, and neutrophils with circulation through the infected 3D tissue model with *N. gonorrhoeae* in the bioreactor system. The results showed that the level of expression of CD11b increased up to 90% in presence of *N. gonorrhoeae* while the circulation might not affect neutrophil activation (≈20% for both control and non-infected) (Figure 35).

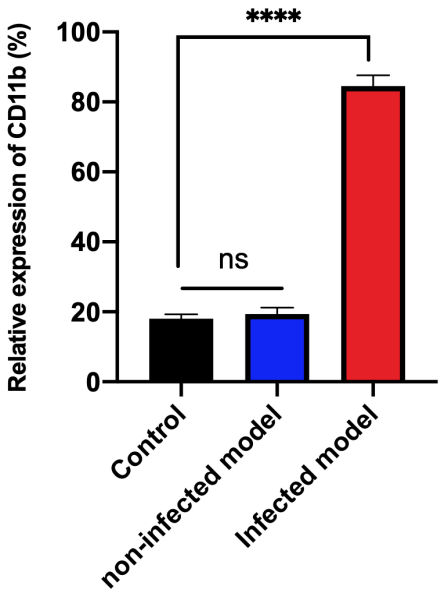

Figure 35. Neutrophil activation evaluated by expression of CD11b.
Expression of CD11b (in percentage) for control (neutrophils without circulation), circulation of neutrophils through the non-infected tissue model, and circulation of neutrophils in an infected tissue model in the perfusion-based bioreactor system after 2h. The data represent the mean values ± SD from at least three independent replicates. **** - p≤0.0001 by one-way ANOVA with Dunnett test.

3.6.5 Neutrophil transmigration

We did an immunofluorescence analysis of the triple co-culture 3D tissue model infected with *N. gonorrhoeae* after 2 hours of perfusion in the bioreactor. It is challenging to do a complete microscopy in the z-direction of the tissue model due to the thickness of the tissue model (in total is ≈150 µm). We cut the tissue into two pieces and stained both apical and basal parts of the tissue separately to visualize both of the endothelial and epithelial sides. Confocal images demonstrated the ZO-1 junctions on the epithelial side (top layer, Figure 36a) and CD31 on the endothelial side (basal layer, Figure 36b) remained intact showing that the perfusion did not disturb the junctions. In addition, immunofluorescence analysis revealed the transmigration of the neutrophils across the 3D tissue models and phagocytosis of *N. gonorrhoeae* on the surface of the model (Figure 36 c-d). Deformation of the neutrophils also depicted the crawling neutrophils (Henry et al. 2013; Salvermoser et al. 2018) passing along the 3D tissue model (Figure 36c).

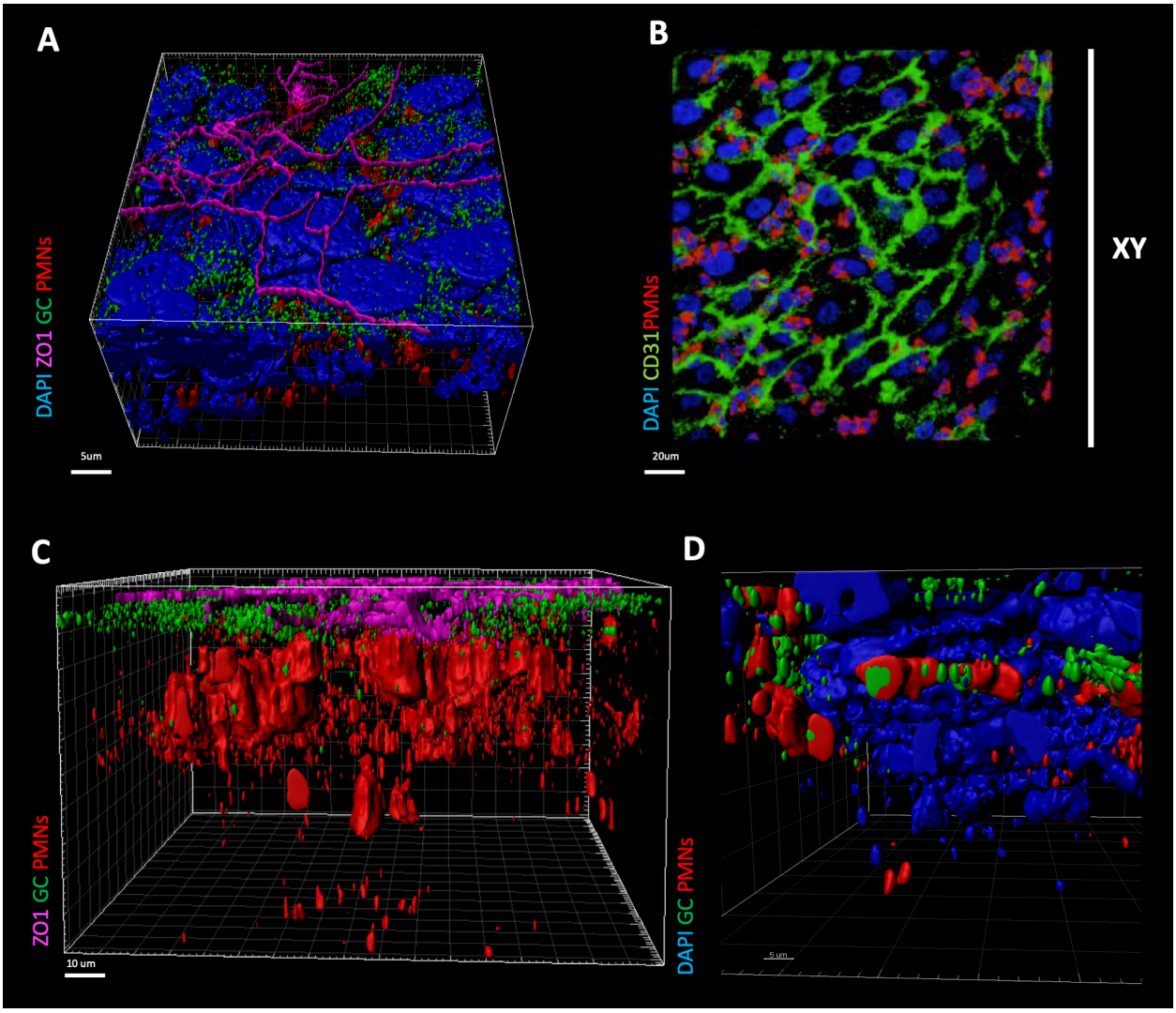

Figure 36. Confocal microscopy of triple co-culture 3D tissue model infected with *N. gonorrhoeae* under dynamic conditions.

A triple co-culture 3D tissue model of HDFib, T84, and HUVEC cells was developed as described in section 2.2.2. (A) The perspective view from the top side of the tissue. The z-stack images were made using confocal fluorescence microscope beginning at the top of the epithelial layer to the SIS scaffold. The tissue model stained with ZO1 (magenta), anti-*N. gonorrhoeae* antibody (green), NCF2 (red) and DAPI (blue). The confocal image of the whole 3D tissue model was surfaced rendered by IMARIS. The scale bar is 5 µm. (B) XY projection from the basal side of the tissue. The tissue model stained with CD31 (green), NCF2 (red) and DAPI (blue). The images were analyzed and reconstructed using FIJI. The scale bar is 20 µm. (C) Higher magnification of the surfaced rendered image of the perspective view of the tissue from the top side. ZO1 (magenta), anti-*N. gonorrhoeae* antibody (green), and NCF2 (red). The alteration in the shape of neutrophils shows the crawling neutrophils. The scale bar is 20 µm. (D) The surfaced rendered image of the perspective view of the tissue from the top side. NCF2 (red), anti-*N. gonorrhoeae* antibody (green), and DAPI (blue). Co-localization of the red and green signals indicates the phagocytosis of *N. gonorrhoeae* by neutrophils. The scale bar is 5 µm.

We also evaluated the neutrophil migration using LSFM (Figure 37). The neutrophils circuited through the infected tissue T84/HDFib/HUVECs model in the bioreactor for 2h. The infected tissue model contacting neutrophils then fixed and stained with antibodies. The tissues then cleared for LSFM analysis. LSFM revealed the distribution of neutrophils through all the tissue model based on the SIS scaffold. We could not observe the GFP expressing N927 due to the limit of resolution of the LSFM. In addition, unspecific background signals were detected, which might impact on the visibility of GFP expressing N927.

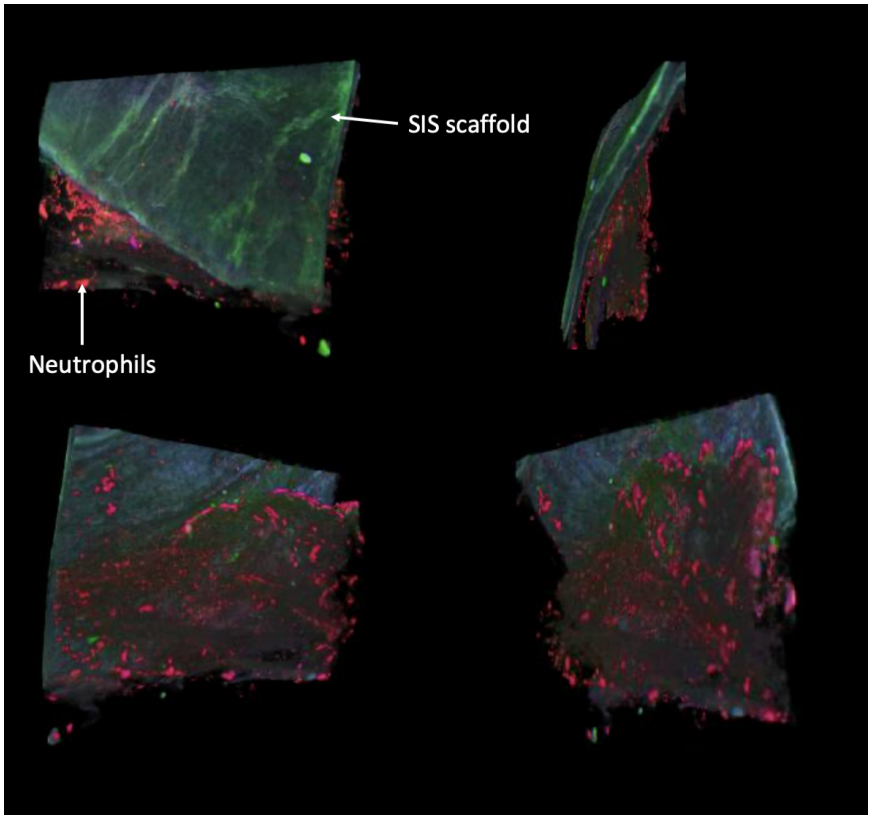

Figure 37. LSFM analysis of the infected T84/HDFib/HUVECs tissue model

The T84/HDFib/HUVECs tissue model was infected with the GFP expressing N927 (green) and the human isolated neutrophils administrated to the tissue in the bioreactor system for 2 h. The tissue first fixed and then stained with NCF2 for neutrophils (red). The tissues were then cleared using BABB protocol for LSFM analysis.

3.6.6 Analysis of neutrophil sub-population

We analyzed the neutrophils population using FACS after 2 hours of circulation in the bioreactor. The infection was performed with GFP-expressing N927 ($PorB_{IA}$, $Pili^-$, Opa^-) and infected neutrophils were detected using the GFP signal. The gating strategy for identifying and sorting the neutrophil population was based on FITC divided into three categories including uninfected, mixed and infected populations. Figure 38a shows the fresh neutrophil population isolated from human blood. After 2h of circulation neutrophils on the non-infected tissue model, the flow cytometry histogram shifted to the right indicating growth in GFP signal. This population was then plated on GC agar and no bacteria were detected (Figure 38a-b). The GPF signal increased in the population of neutrophils after circulation through the infected models (Figure 38c).

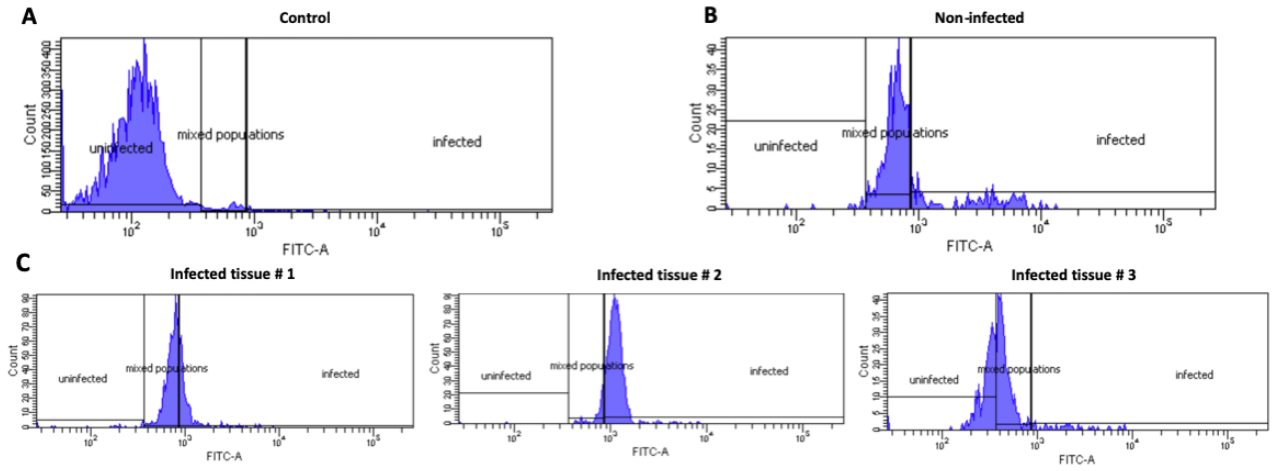

Figure 38. FACS analysis of the neutrophil population.
(A) Neutrophils after isolation from the blood. (B) Neutrophils circulated through the non-infected tissue for 2 h (C) Neutrophils circulate through the infected tissue models (n=3) with GFP N927, MOI 20, 24 h of infection.

FACS-sorted cells were stained with DAPI and Phalloidin and then visualized using confocal microscopy (Figure 39). The results presented that there is no green signal in the non-infected population showing they do not contain any *N. gonorrhoeae*. The permeabilized neutrophils plated on GC agar and no bacteria detected. The mixed population of neutrophils contained a number of infected and no-infected neutrophils. However, in infected populations, we observed plenty of highly infected neutrophils (strong signal) and some with a mediate signal, which is hard to mention whether they are infected or not.

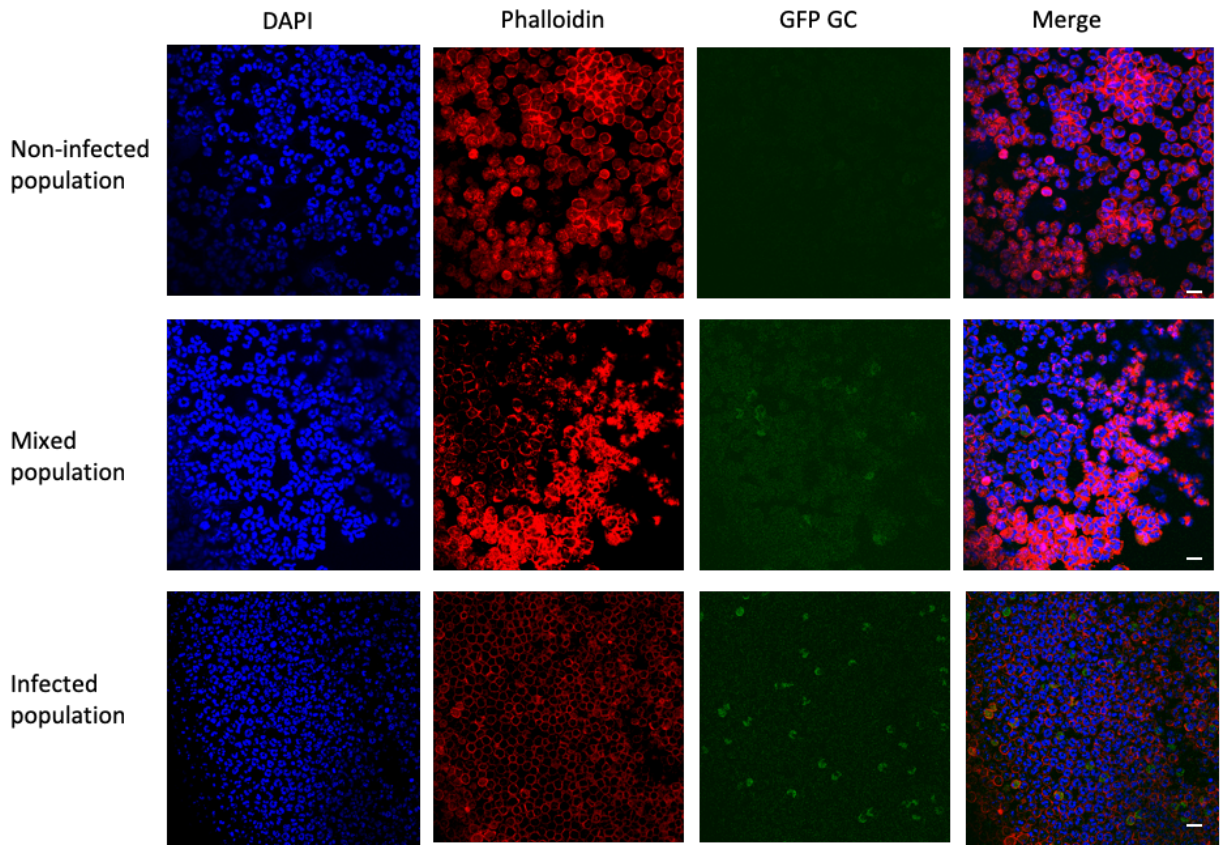

Figure 39. Immunofluorescence analysis of FACS-sorted neutrophils after infection study.
FACS-sorted neutrophils cells were stained with Phalloidin (red) and DAPI (blue) and visualized using confocal fluorescence microscopy. The green signal is GFP from the GFP expressing by *N. gonorrhoeae.* No green signal was detected in the infected population (first row). The mixed population includes both infected and no-infected neutrophils (second row). Considerable numbers of GFP positive neutrophils were observed in infected neutrophils (third row). The scale bar is 25 µm.

3.7 Tissue model based on primary cell

Following primary cell isolation, endometrium organoids expanded in Matrigel®. The culture media for endometrium organoids contains advanced DMEM/F12, N2 supplement, B27 supplement, N-Acetyl-L-cysteine, L-glutamine, ALK inhibitor, nicotinamide, and recombinant human EGF, Noggin, R-spondin-1, FGF-10, and HGF. The culture media for the proliferation of cervix organoids contain advanced DMEM/F12, N2 supplement, B27 supplement, ALK inhibitor, nicotinamide, and recombinant human EGF, Noggin, R-spondin-1, FGF-10, and WNT. The

endometrium organoid expanded while cervix organoids could not successfully expand after 10 days, as it shows in Figure 10.

Two independent primary 3D tissue models were then established by seeding $4x10^5$ cells from endometrium and cervix organoids on the SIS scaffold that was previously populated with $1x10^5$ fibroblast isolated from the same biopsy. The primary tissue models were cultured for 20 days under submerged and static culture conditions.

Histological characterization using H&E staining of the established tissue models after 20 days showed an overview of architecture in each model (Figure 40a-b). Primary cells in both tissue models grew as a confluent monolayer. In the cervix tissue model, the epithelial cells grew as simple cuboidal while the epithelial cells in the endometrium tissue models formed a flat and simple squamous epithelial cell layer (Figure 40a-b).

We also performed a histological analysis of the cervix and endometrium biopsies derived from the patient. The H&E staining of the cervix tissue showed cuboidal epithelial cells in the basal layer, flatten cells in the intermediate layer, and superficial squamous layers of the epithelium. In addition, the stroma tissue presents beneath epithelial layers (Figure 40e). The endometrium tissue showed tall and columnar epithelial cells (glandular cells), which surrounded by endometrial stroma (Figure 40f).

The immunofluorescence staining of both cervix and endometrium tissue models presented the expression of fibroblast (anti-fibroblast antibody) and secretory (anti-PAX8 antibody) cells.

However, the nuclear presence of PAX8 in the endometrium tissue model showed a higher signal.

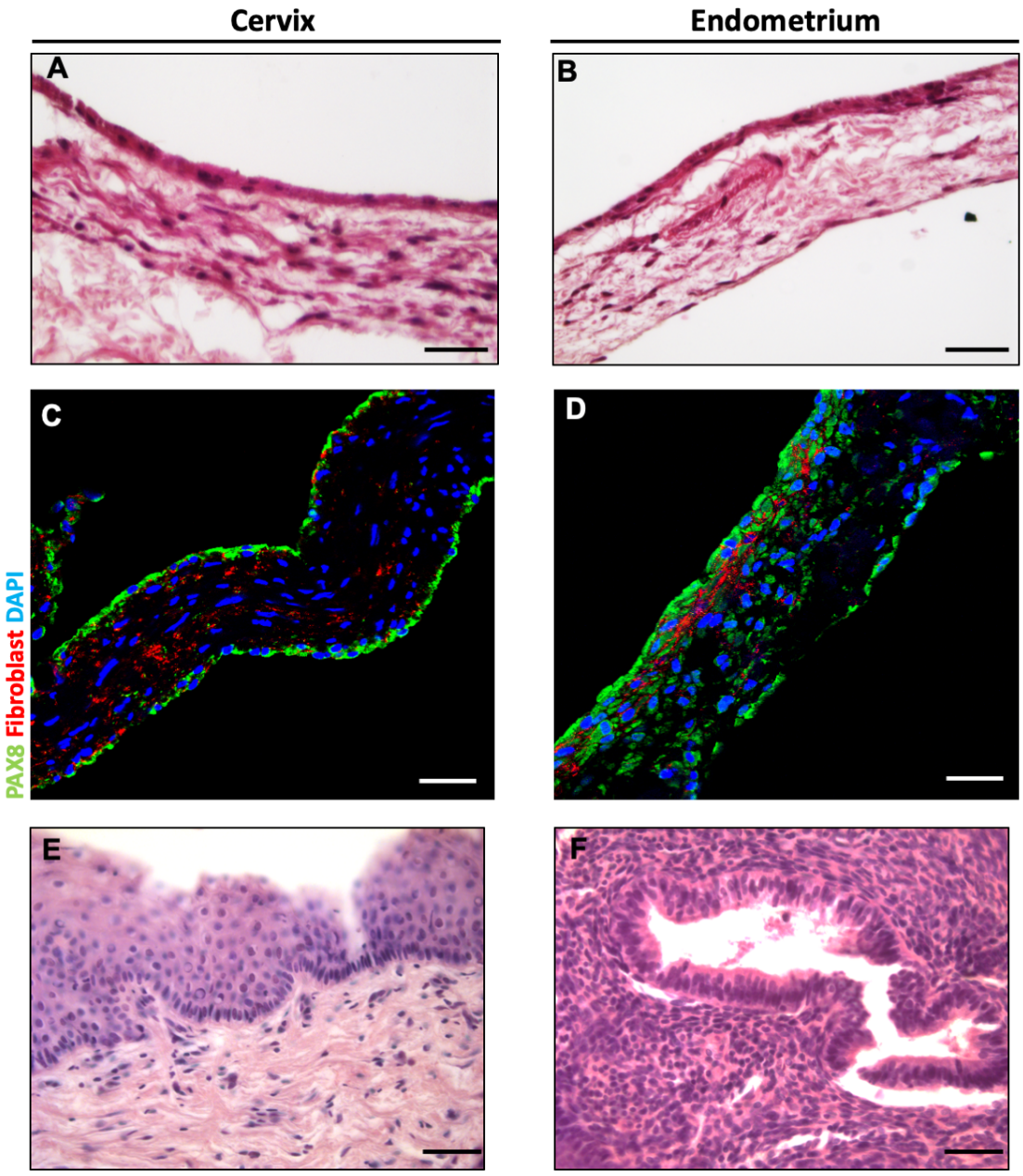

Figure 40. Histological and immunofluorescence analysis of co-culture 3D tissue model of primary cells.

Primary cells were isolated from the endometrium and the cervix of a biopsy tissue taken from a patient. Cells proliferated in the form of organoids for 2 weeks and then seeded on the SIS scaffold/primary fibroblast from the same patient for 20 days. The Histological characterization of co-culture tissue models using primary cells derived from (A) cervix and (B) endometrium. Immunofluorescence analysis of co-culture tissue models using primary cells derived from (C) cervix and (D) endometrium. XY snapshot Image was acquired by confocal fluorescence microscopy. PAX 8 antibody (green), anti-fibroblast antibody (red) and DAPI (blue). Histological characterization of (E) cervix and (F) endometrium of the same biopsy tissue used for cell isolation. The scale bar is 50 μm.

Chapter 4 Discussion

N. gonorrhoeae is a human-specific diplococcus bacterium causing gonorrhea disease which is the second most common sexually transmitted infection worldwide. Upon the infection, *N. gonorrhoeae* colonizes the mucosal surface of the female reproductive tract and the male urethra, anorectal, pharyngeal, and conjunctival areas. There are some partial treatments for this disease such as antibiotic treatment including penicillin, ceftriaxone, tetracycline, and cephalosporins. Nevertheless, *N. gonorrhoeae* is a superbug and its complete treatment has not yet been achieved. In this study, we aimed to establish a realistic *in vitro* 3D tissue culture model for a comprehensive study of *N. gonorrhoeae* including bacteria adhesion, invasion and transmigration in different tissue layers. In addition, host cell- *N. gonorrhoeae* interaction was investigated in different models from mono-culture to triple co-culture 3D tissue model mimicking the site of infection.

4.1 Establishment of a 3D tissue model for long-term study of *N. gonorrhoeae* Infection

In this study, we established biomimetic 3D *in vitro* tissue models in order to study the site of infection of *N. gonorrhoeae*. A suitable *in vitro* tissue model enables us to simultaneously explore various aspects of infection including bacterial attachment and transmigration to tissue layers, invasion of the epithelial barrier, and stimulation of inflammatory responses.

The in vitro models developed up to now are based on the commercial porous membranes, which are mainly made out of polycarbonate (such as Transwell® inserts). The Transwell® are normally used to create the epithelial cell models in order to investigate gonococcal infection (Stein et al. 2015; L. C. Wang et al. 2017). In spite of the advantage of commercial Transwell® inserts such as air-liquid interface (ALI) culture, these cell culture models are suffering from the lack of complexity of the site of infection. Cell functions highly rely on the their 3D environment mechanical factors such as matrix stiffness, matrix-binding factors, fiber strength and pore size (Griffith and Swartz 2006). In addition to the biophysical properties of the substrate, cell-cell and cell-matrix interaction are necessary for mimicking normal physiological function of the cells (Bardsley et al. 2017). Moreover, cervix ECM consisting of fibrillar collagen, proteoglycans, and

glycoproteins, plays a pivotal role in structural function of the tissue and regulates intercellular communication and dynamic behavior of cells (Yao et al. 2016; Yoshida et al. 2019)

The most prevalent site of infection in gonorrhea disease is urogenital tract in female and urethra in male. However, other parts including anorectal, conjunctival, pharyngeal, and uterine could be also infected (Miller 2006). The available *in vitro* models are mainly monoculture of the epithelial cells such as T84 cells (Hopper, Wilbur, et al. 2000; Wang et al. 2008) while fibroblasts, immune cells and endothelial cells are presence as well in the site of infection (Figure 2 and Figure 40e-f). It has also been shown that the presence of fibroblasts has a positive effect on epithelial cell growth and polarization due to the secretion of different components, which are important for the basal membrane formation (Arnold et al. 2001; Steinke et al. 2014). Fibroblasts have receptors for different enzymes and cytokines can control the mechanical properties of the tissue. In addition, fibroblasts are active keys player of the immune system, which can modulate immune cell behaviors (Griffith and Swartz 2006; Van Linthout, Miteva, and Tschope 2014).

In this study, we used porcine small intestinal scaffold (SIS), which keeps ECM characteristics of the native organ and provides suitable conditions for cell proliferation and differentiation. The SIS scaffolds represents an acellular biological ECM and widely uses in many studies in order to establish a human tissue model. This natural-based scaffold contains collagen, fibronectin, laminin, elastin, glycosaminoglycans, proteoglycans, and growth factors, which can mimic the main mechanical and physical properties of the ECM in the site of infection (Shi et al. 2013). The pore size of the SIS scaffold ranges from 20 to 30 µm, which are interconnected (Figure 17) and facilitate the cell signaling while the pores in Transwell® membranes are not connected.

We also developed co-culture models of epithelial and fibroblast cells in order to recreate a more realistic *in vitro* model. Co-culturing of fibroblast and epithelial cells, showed the formation of the basement stroma, which played a supportive role for the epithelial monolayer both physically and chemically.

In this research, we established three independent co-culture 3D tissue models based on the SIS scaffold in order to study the gonococcal infection.

I) A tight epithelial barrier model with highly polarized cells based on the colon carcinoma cell line (T84), which co-cultured with fibroblasts (HDFib).

II) II) An epithelial model representing female reproductive tract mucosal tissue using endometrial adenocarcinoma cell line (HEC-1-B), which co-cultured with fibroblasts (HDFib).

III) III) A model for the male urogenital tissue consisting of the immortalized uroepithelial cell line (SV-HUC-1), which co-cultured with fibroblasts (HDFib).

4.1.1 Morphological characterization of the established tissue models

One of the main advantages of our biomimetic epithelial tissue models is the polarization of epithelial cells and the formation of TJs. The polarized epithelial cell layer is the first physical barrier against *N. gonorrhoeae*. When *N. gonorrhoeae* faces the cell barrier, the bacteria either enter the cells or transmigrate across the cell-cell junctions (Stein et al. 2015).

The TJs are the apical structure of the intercellular junctional complex, which form tight seals between epithelial cells and separates the apical and basolateral membranes. The formation of TJ creates a selectively permeable membrane and hinders mixing the components of two membranes (Wang and Margolis 2007). In polarized epithelial cells, the proteins are segregated to the apical and basolateral membranes. Figure 14a-c clearly showed that epithelial cells in our tissue models form a polarized monolayer. The confocal analysis also showed that epithelial cells in the T84/HDFib tissue model are polarized well compared to the HEC-1-B/HDFib and SV-HUC-1/HDFib tissue models (Figure 14a). Immunofluorescence analysis also showed ZO-1 TJs expressed well in the T84/HDFib tissue model while the formation of ZO-1 TJs in the HEC-1-B/HDFib and SV-HUC-1/HDFib tissue models were not as intense as the T84/HDFib tissue model (Figure 14a-c). The higher formation of ZO-1, which we observed at the top of the cell layer in T84/HDFib tissue model, has been already reported in another study on Transwell® models of T84 epithelial cells (Navabi et al. 2013).

We also characterized the morphology of the 3D tissue models. TEM micrograph (Figure 17) showed the formation of tight appositions of neighboring epithelial cells, which is the indicator of TJs. In addition, SEM analysis revealed the presence of microvilli on the surface of the epithelial layer (Figure 17).

E-cadherin is a transmembrane glycoprotein, which is a key structural component of the adherens junctions. E-cadherins mediate the cell-cell adhesion and initiate the translocation of junctional proteins (Mendonsa, Na, and Gumbiner 2018; Wong et al. 2018). As immunofluorescence staining of our 3D tissue models showed, the E-cadherins were expressed in all the tissue models (Figure 13), which can be considered as a sign of cell polarization and the formation of epithelial barrier (Rübsam et al. 2017). The previous study on Transwell® models of T84 and HEC-1-B epithelial cells indicated that E-cadherins are produced after formation of epithelial layer, which translocate from apical junctions to the cytoplasmic vesicles upon infection with *N. gonorrhoeae* (Edwards et al. 2013). We also observed the deformation of the E-cadherin in our T84/HDFib tissue model upon challenging with *N. gonorrhoeae* (Figure 26).

Earlier investigations revelaed that the E-cadherins were strongly epressed in 2D culture of SV-HUC-1 epithelial cells (Ding et al. 2014; Yu et al. 2017). We developed a 3D SV-HUC-1/HDFib tissue model based on the SIS scaffold, which showed a higher resilience to bacterial translocation (Figure 19b). The aggressive clinical isolate VP1 can trasmigrate across the SV-HUC-1/HDFib tissue model only after 144 h of infection, which indicates the suitability of the developed tissue model for long-term study.

Mucus lining and epithelial cells act as a physical barrier against *N. gonorrhoeae* (Rodríguez-Tirado et al. 2012). As Figure 13 shows, a uniform and relatively thin mucus layer formed on the top of the epithelial cells in our established 3D tissue models. It has been shown that the mucosal layer is involved in adherence and invasion of *N. gonorrhoeae* to epithelial cells (Jarvis, Li, and Swanson 1999).

4.1.2 Functional characterization of the established models

In addition to morphological characterization, we assessed the barrier function of epithelial cells in the established tissue models. We used the TEER measurement as a quantitative technique, which is normally used to monitor barrier integrity and the formation of TJs of epithelial and endothelial cells monolayer (Srinivasan et al. 2015). We evaluated the barrier integrity using TEER measurements for two goals. First, the state of maturation of the tissue model can be determined by TEER measurement. The TEER values showed that we need 12 days to obtain a proper and

mature tissue model of T84/HDFib and SV-HUC-1/HDFib while this duration is 14 days for HEC-1-B/HDFib tissue model. However, in Transwell® models, all the models need approximately 10 days to become mature enough. In addition to the determination of whether the tissue models are mature enough, we found that T84/HDFib (TEER≈340 $\Omega*cm^2$) formed a tighter barrier compared to the HEC-1-B/HDFib (TEER≈180 $\Omega*cm^2$) and SV-HUC-1/HDFib (TEER≈135 $\Omega*cm^2$) tissue models (Figure 15). The results are in line with the TEER values that have already been reported (Navabi et al. 2013).

Shaken cell culture has been shown to influence the morphology of the tissue models (Massie et al. 2017). We evaluated the effect of shaking on the maturation of the 3D tissue models via measuring TEER values (Figure 15b). We found that culturing cells on the orbital shaker could not considerably affect tissue maturation and barrier formation, which was measured by the TEER values. Thus, we decided to do our experiments under static conditions.

We also measured the barrier integrity of the tissue models after maturation using FITC-dextran permeability assays. The permeability of monoculture of HDFib cells when cultured on the SIS scaffold and Transwell® insert is ≈12% and ≈40%, respectively (Figures 16). The permeability of the co-culture tissue models based on the SIS scaffold is slightly less than Transwell® models, which shows a tighter barrier formation. These results revealed the importance of the SIS scaffold, which provides interconnected pores for fibroblasts to grow and form connective tissues. However, there are no significant differences between the TEER values of Transwell® models and 3D tissue models. Among the established 3D tissue models, the T84/HDFib tissue model formed strong TJs (Figures 14 and 17), which resulted in higher barrier integrity (TEER ≈320 $\Omega*cm^2$) (Figure 15). The secretion of TJs in HEC-1-B/HDFib and SV-HUC-1/HDFib tissue models was not as intense as the T84/HDFib tissue model, which is confirmed by TEER and permeability analysis (Figures 14-16).

Morphological characterization of the established tissue models revealed that epithelial cells were polarized in our tissue models. However, consideration of TEER and permeability data, we conclude that T84/HDFib develops better barrier function (higher TEER and lower permeability).

4.2 Infection study

N. gonorrhoeae express a different set of virulence factors that make the bacteria capable of attachment, invasion, and transmigration (Figure 1). Pili enable the attachment of bacteria to human epithelial cells (Maier and Wong 2015). Opa proteins are also essential for efficient host cell invasion (van Putten 1993). PorB mediates the invasion independent of pili and Opa (Rechner et al. 2007). After establishing the 3D tissue models, we studied different pathogenicity factors in *N. gonorrhoeae*. We used 5 different strains and derivatives of *N. gonorrhoeae*: N927 ($PorB_{IA}$, Opa^-, $Pili^-$), N924 ($PorB_{IB}$, Opa^-, $Pili^-$), MS11 ($PorB_{IB}$, Opa^+, $Pili^+$), MS11 ΔOpa ($PorB_{IB}$, Opa^-, $Pili^+$), and VP1 clinical strain ($PorB_{IA}$, Opa^-, $Pili^-$). We could study the role of various virulence factors in adhesion, invasion, and transmigration of *N. gonorrhoeae* on different host-cells.

The results showed that the *N. gonorrhoeae* can easily transmigrate across the cell barrier in all the established Transwell® models after 6 h of infection while N927, N924 and MS11 can transmigrate after 6 days of infection in the 3D tissue models based on the SIS scaffold.

We performed infection studies in the SIS scaffold (without cells) and monoculture of HDFib on the SIS scaffold (Figure 21). The results showed that all the strains can transmigrate across the SIS scaffold and HDFib/SIS scaffold after 1 h of infection. Therefore, the connective tissue layer beneath the epithelial cells and the SIS scaffold did not act as a physical barrier against *N. gonorrhoeae.*

Although the established 3D tissue models can provide a long-term infection study, highly invasive strains of *N. gonorrhoeae* such as VP1 and ΔOpa translocated after 6 h and 72 h of infection, respectively, in the T84/HDFib tissue model. The transmigration of VP1 and ΔOpa also took 24 h after infection in HEC-1-B/HDFib. VP1 is a clinical isolate strain of *N. gonorrhoeae* derived from a patient with disseminated gonococcal disease (van Putten 1993; Roth et al. 2013), which has been reported to be a highly invasive strain (Makino et al. 1991).

We also measured the permeability of the tissue models upon infection. The results showed that the higher level of permeability observed in tissue models when challenged with VP1, ΔOpa and N927. VP1 expresses $PorB_{IA}$, which promotes host cell invasion under low-phosphate conditions (Rechner et al. 2007). We performed all the infection studies in the HEPES culture media, which provides a low phosphate environment, in order to investigate the effect of $PorB_{IA}$. LDH analysis

of the infected tissue models showed that VP1 and N927, containing $PorB_{IA}$, induce higher cell cytotoxicity compared to the other strains (Figure 24).

ΔOpa has been already reported to have fast transmigration through the epithelial cell monolayer (T84 epithelial cells) because of the absence of Opa proteins (Stein et al. 2015).

We also analyzed Opa phenotype of the strains, before and after the infection (data not shown). We observed loss of Opa protein expression in VP1 strain upon infection in the 3D tissue model based on the SIS scaffold, which might explain the high transmigration efficiency. However, MS11, N927, and N924 switched to Opa^+ phenotypes following the infection showing other factors apart from Opa might be involved.

In addition to pili, Opa, and PorB, other virulence factors such as phase variable LOS are playing a key role in both bacterial invasion and immune resistance. For instance, it has been shown that VP1 strain efficiently invades Chang cells in presence of serum while MS11 fails to invade epithelial cells due to the differentiall level of sialylation in LOS (van Putten 1993). We also analyzed the pili phenotype of the strains, before and after the infection. In the infection study, we chose the $pili^+$ phenotype (MS11 and ΔOpa). However, the results of western blots showed that the seleced bacteria could not express pilin (data not shown). As a result, It is diffiuclt to discuss about the role of pili in in adherence and transmigration of *N. gonorrhoeae* across the tissue models.

Infection study indicated that the 3D tissue models based on the SIS scaffold have better endurance to bacterial transmigration offering robust tissue models for investigating the *N. gonorrhoeae* infection over the course of several days.

4.2.1 Bacteria-host interaction

In this research, we decided to develop independent tissue models in order to not only study the role of virulence factors in gonococcal infection but also investigate the effect of type of epithelial cells on bacteria-host interaction. The established 3D tissue models in this study allow us to investigate different mechanism of *N. gonorrhoeae*-host interaction in various sites of infections. *N. gonorrhoeae* employs the different mechanisms in order to interact and translocate the epithelium including adhesion to the surface, exocytosis of *N. gonorrhoeae*, intracellular

penetration, exfoliation of cells, cellular destruction and invasion of deeper epithelial cells (Mosleh et al. 1997). These functions are regulated via the interaction of bacteria virulence factors with host cell receptors. Colonization of *N. gonorrhoeae* intrigues at the apical surface of epithelial cells leading to multiple stages of the adhesion cascades (Merz and So 2000). The first step of the adhesion cascades during initial infection is the attachment of *N. gonorrhoeae* via type IV pili following by formation of microcolonies and biofilms (Quillin and Seifert 2018).

We decided to find the location of *N. gonorrhoeae* using gentamicin assay. Gentamicin targets the extracellular pathogens (Shaw and Falkow 1988). We treated the infected T84/HDFib tissue model with gentamicin from the apical and basolateral side 6 h, 24 h, and 144 h after infection (Figure 28). The results showed that all bacteria were efficiently killed in 6 h and 144 h infected models, meaning that the bacteria could not migrate via the transcellular channel. It might be the bacteria mostly transmigrate through the junction between adjacent cells. However, after 24 h of infection, we could recover bacteria from the infected tissue models with N924 and VP1. The confocal microscopy analysis of the infected tissue models (Figure 27a) showed many microcolonies after 24 h of infection on the cell surface. Some bacteria might be protected inside the microcolonies aggregations when treated with gentamicin. The gentamicin assay is normally used in the 2D culture system. We think that this assay should be adjusted for application in 3D tissue models.

In our tissue models, the SV-HUC-1/HDFib had the lowest bacteria transmigration. In the SV-HUC-1 cells, adjacent cells are overlapped causing the TJs are not easily accessible to the bacteria. In addition, the low level of bacteria transmigration might be due to the lack of microvilli on the surface of these cells. The microvilli could be necessary for the engulfment of *N. gonorrhoeae* (Griffiss et al. 1999). We observed the elongation of microvilli during the infection of the HEC-1-B/HDFib tissue model, engaging with the *N. gonorrhoeae* (Figure 25b).

N. gonorrhoeae induces the disruption of epithelial cell junction complexes (Maisey et al. 2012). We assessed the barrier permeability of the tissue models following the infection using FITC-dextran assay. In Transwell® models, we could observe a relatively uniform change in permeability, independently from the bacterial strains or derivative, which are in agreement with previously reported data (Stein et al. 2015). We measured barrier permeability of the 3D tissue

models on days 1, 2 and 6 after infection (Figure 23). We observed that the barrier permeability did not rise abruptly after 48 h of infection. However, after 144 h of infection, the tissue models showed meaningful differences between cell types and strains. After 144 h of infection, N924 showed a less destructive effect on all the 3D models with a lower permeability effect. After the same infection time, VP1, N927, and ΔOpa indicated the highest barrier permeability on T84/HDFib, HEC-1-B/HDFib, and SV-HUC-1/HDFib models, respectively.

Furthermore, we observed the destruction of ZO-1 TJs in the infected T84/HDFib tissue model by VP1 after 6 days (≥85% as quantified by the fluorescence intensity of ZO-1) while the TJs were not fully destroyed when N924 gonococci were used (≈55%) (Figure 27b).

The results of permeability assay upon infection showed that long-term infection study is essential for investigating differences between derivatives and strains of bacteria.

It would be difficult to fully understand the bacterial invasion into the cells and translocation of bacteria through the tissue barrier via transcytosis. We used TEM to find out the accurate location of *N. gonorrhoeae*. We could only observe the bacteria on the cell surface (Figure 25c). This might be due to the preparation sample for TEM such as a proper cutting angle that needs to be adjusted in order to locate the penetrated pathogens into a deeper layer.

We also performed immunohistochemical staining of paraffin-embedded infected tissues (Figure 26). We observed the loss of polarization of epithelial cells upon infection; however, we could not detect the location of *N. gonorrhoeae* either inside the host cell or in the adjacent epithelial cells by this method. The thickness of each slice is ca. 6 µm that would not be proper for covering a complex of the bacteria-host cell. Thus, we decided to carry out the whole tissue staining for visualization of the infected tissue models using confocal microscopy (Figure 27a). The confocal microscopy showed the bacteria attachment to the cell surface and transepithelial migration through the tissue, while we could not detect the uptake of gonococci into the cells. Detection of bacteria only at the surface of the tissue models might be due to the staining protocol causing the dyes and antibodies not to diffuse to the deeper layer of the tissue.

N. gonorrhoeae is a sensitive pathogen is prone to autolysis under different environmental conditions such as pH, temperature, and ions supply (Hebeler and Young 1976). When *N. gonorrhoeae* is cultured on GC agar plates or in a liquid medium, they are likely to autolyse

(Garcia and Dillard 2006). Our results of the Transwell® model based on different epithelial cell lines showed that we can study the infection in these models only for a few hours (≤ 6 h), which is in agreement with the already published data of Transwell® model (Stein et al. 2015). However, we could collect viable bacteria even after 6 days of infection in our tissue models, indicating that we can study *N. gonorrhoeae* infection in longer period of time in the 3D tissue models based on the SIS scaffold. *N. gonorrhoeae* cannot survive outside the host, withstand dehydration, and non-physiological temperatures. It has been shown that *N. gonorrhoeae* requires complex media for proliferation such as glucose, glutamine, thiamine, phosphate, iron and carbon dioxide (Quillin and Seifert 2018). When we infected our tissue models with *N. gonorrhoeae*, we think that the bacteria meet the nutritional requirements necessary for growth in more closely physiological conditions such as superior bacteria-host interaction, suitable temperature, and wet environment.

4.2.2 Inflammatory responses

The level of inflammatory cytokines IL-6, IL-8, and TNF-α increases in the site of infection imidiately upon the gonorrhoea infection before initiation of the gonococcal disease (Ramsey et al. 1995). The results of the cytokine measurement showed that in Transwell® model, the co-culture of SV-HUC-1/HDFib produced greater level of IL-6, IL-8, and TNF-α upon challenging with *N. gonorrhoeae* strains. Previously reported data showed that regardless of the strain or derivative of *N. gonorrhoeae* used or the state of invasion, the presence of *N. gonorrhoeae* itself can induce the level of cytokines in the epithelial cells (Christodoulides et al. 2000; Fichorova et al. 2001). However, in our tissue models based on the SIS scaffold, the type of epithelial cells and *N. gonorrhoeae* have effect on the production of IL-6, IL-8, and TNF-α upon infection.

Łaniewski et al. showed that the expression levels of cytokines IL-8 and TNF-α levels in spheroid model of HEC-1-B epithelial cells were significantly induced in a dose-dependent manner (Łaniewski et al. 2017). They also showed that wild-type *N. gonorrhoeae* influenced the expression of IL-8 significantly higher than the ΔpilT mutant. Our results of immune response upon infection with *N. gonorrhoeae* indicated that the established 3D tissue models in this study are capable of secreting greater level of IL-6, IL-8, and TNFα in comparison to the Transwell®

models (Figures 30 and 31). The higher production of the immune response in the 3D tissue models might be due to the 3D porous construction of the SIS scaffold, which facilitates the formation of the connective tissue. It has been shown that the fibroblast cells have a key role in inflammation regulation and synthesis of different chemokines and cytokines (Buckley et al. 2001; Silzle et al. 2004; Smith et al. 1997).

In both the tissue and Transwell® models, the immune response in SV-HUC-1/HDFib, male uroepithelial cell line, was greater than T84/HDFib and HEC-1-B/HDFib tissue models (except IL-8 for T84/HDFib tissue model), which can indicate the importance of the type of epithelial cells on inflammatory responses. Gonorrhea disease has different symptoms in male and female so that more than 50% of women infected with *N. gonorrhoeae* do not show the symptoms. In addition, females and males do not have the same inflammatory responses (Edwards and Apicella 2004; Hedges et al. 1998; Jerse et al. 2014). Therefore, studying the gender difference in immune response and cytokine production in response to *N. gonorrhoeae* could reveal the reason of more asymptomatic cases in females than males.

As we discussed earlier, our tissue models not only can mimic more closely clinical pathology, but also allow *N. gonorrhoeae* to interact with the host cells for extended period of time (6 days). Long-term infection study might provide biomimetic conditions, which is not possible by the current in vitro cell culture models based on Transwell® insert.

4.3 Triple co-culture model for studying neutrophil transmigration

One of the hallmarks of gonorrhea infection is a robust neutrophil influx to the site of infection (Stevens and Criss 2018). All the neutrophils, however, do not undergo apoptosis initially. It has been shown that a sub-population of *N. gonorrhoeae* may escape from the neutrophil phagosome and replicate within the neutrophils (Simons et al. 2005). It has been suggested that a population of neutrophils might turn back to the blood vessels and somehow contribute to the inflammation distribution (De Oliveira, Rosowski, and Huttenlocher 2016). Therefore, we decided to improve the established 3D tissue model by introducing endothelial cells to the basal side of co-culture models in order to mimic the blood vessel barriers.

In the triple co-culture model of T84/ HDFib/ HUVECs on the SIS scaffold, a polarized monolayer of epithelial cells formed on the apical side, which is supported by fibroblast in the middle layer. In addition, a flat monolayer of endothelial is located on the basal side of the tissue model (Figure 32). We also evaluated the barrier integrity of the triple co-culture model by TEER measurement and permeability assay (Figure 33). The modified tissue model showed a tighter barrier formation (TEER≈400 $\Omega*cm^2$) and lower permeability (permeability ≈ 0.5%) after 12 days of cultivation compared to the co-culture model of T84/HDFib on the SIS scaffold.

For studying neutrophils transmigration upon infection in a biomimetc tissue model, a perfusion-based bioreactor system was used to mimic the blood flow (in endothelial side) and apply a shear stress to the cells. Many cell types respond to mechanical forces such as shear stress which is induced by blood circulation in the body. Shear stress is playing a crucial role in the cell proliferation and function of the endothelial cells (Sakamoto et al. 2010). The used bioreactor system in this study can circulate the culture media through the tissue model and apply shear stress (0.005 Dyn/cm^2) to the cells, which offers a dynamic cell culture model. This dynamic cell culture model also resembles the floating neutrophils in the blood vessel.

After establishing the triple co-culture model, the isolated human neutrophils administrated to the tissue models using the bioreactor system. We first infected the tissue model of T84/ HDFib/ HUVECs with GFP expressing N927 for 24 h in static conditions. The infected tissue model then transferred to the bioreactor system for administrating the neutrophils, which perfused to the main chamber of the bioreactor system from the basal compartment (endothelial side) (Figure 8). After 2 h of neutrophils circulation, we analyzed the neutrophils characteristic and activation upon challenging with GFP expressing N927.

CD11b is a receptor on the neutrophil surface crucial for neutrophil migration to the site of infection. The overexpression of CD11b occurs because of the inflammatory responses (e.g. IL-8) to the infection (Detmers 1990). In this study, after the administration of neutrophils into the endothelial side of the infected 3D tissue model via perfusion, over 90% of neutrophils presented an activated phenotype ($CD11b^+$) while in absence of infection, the activation level of neutrophils is less than 15% (Figure 35). The results showed that the expression level of CD11b plays a major role in the transepithelial migration of neutrophils, which agrees with other studies on the

Transwell® model of T84 epithelial cells (Blake et al. 2004; Parkos et al. 1991). Parkos et al. showed that lack of CD11b surface expression leads to failure in neutrophils migration across the T84 monolayer (Parkos et al. 1991). In addition, another study showed the increasing level of CD11b expression on neutrophils that transmigrated across the alveolar epithelial cells (A549 cell line) in response to the respiratory syncytial virus (Deng et al. 2018).

The expression of CD11b is also required for transendothelial migration of neutrophils through vascular endothelial cells (Filippi 2019). The CD11b expression upregulates immediately after the adherence of neutrophils to the endothelial cells to mediate the adhesion process (Filippi 2019). We observed an increase in the level of CD11b expression on neutrophils upon challenging with *N. gonorrhoeae* compared to the non-infected model (Figure 35).

Flow cytometry analysis of neutrophils population after 2 h of circulation in the bioreactor showed an increase in GFP signal of neutrophils in the infected tissue model (Figure 33). The GFP signal slightly increased when neutrophils passed through a non-infected model which might be because of the autofluorescence of the SIS scaffold which contains ECM proteins.

The confocal microscopy analysis demonstrated that *N. gonorrhoeae* can recruit the neutrophils from the basal compartment (endothelial layer) and tracking them to the apical side (epithelial layer). It also depicted that the neutrophils are present in the layers of the whole tissue model showing the neutrophils transmigration (Figure 36c). The bacteria phagocytosis (co-localization of signal in neutrophils and bacteria) could be observed mainly on the surface of the tissue model (Figure 36d). The process of neutrophils recruitment to the infected tissue contains different steps. First of all, the inflammatory responses cause an increase of adhesive molecules on the endothelial cells and trigger the floating neutrophils reaching the endothelial cells. After initial attachment to endothelial cells, the neutrophils transmigrate across the endothelial barrier by crawling between cells, as we observed when neutrophils administrated to the triple co-culture tissue model (Figure 32c).

The modified 3D triple co-culture tissue model provides us the opportunity to study transmigration of neutrophil across the endothelium through the SIS scaffold, reaching the epithelial layer. It has been shown that epithelial cells are also playing a role in neutrophil migration to *N. gonorrhoeae* (Stevens et al. 2018). Stevens et al. developed a Transwell® model

of endocervical epithelial cells to investigate *in vitro* neutrophil transepithelial migration. They revealed that the *N. gonorrhoeae* infection provokes endocervical cell singnaling pathways causing 12-R-lipoxygenase activation and subsequently neutrophil transepithelial migration. They also showed that epithelial protein kinase C, cytosolic phospholipase A2, and eLOX3 hepoxilin synthase were essential for neutrophil transmigration to *N. gonorrhoeae* (Stevens et al. 2018).

LSFM is a useful method for studying whole organs in three dimensions. We studied neutrophils moving up across the endothelial barrier using LSFM analysis. Recruitment of neutrophils to the site of infection is detected by LSFM. However, we could not detect directly colocalization of bacteria and neutrophils, which could be due to the not sufficient resolution of light sheet microscopy for visualization of individual bacteria. We also detected the autofluorescence background of the SIS scaffold, which is challenging for the visualization of bacteria with the green signal.

Another microscopy method so-called micro-optical coherence tomography has been recently developed to show the time-profile of neutrophil migration across the Transwell® model of T84 epithelial cells (Chu et al. 2017). In this model, neutrophils transmigrated after 30 min in response to chemoattractant N-formylmethionyl-leucyl-phenylalanine (fMLP). This type of 3D time-lapse can quantitatively evaluate the migration of neutrophils. The similar method was used in primary human airway basal stem cells on Transwell® model in order to study the transepithelial migration of neutrophils in response to *Pseudomonas aeruginosa* infection (Yonker et al. 2017).

The piliation is crucial for bacterial survival inside human neutrophils (Stohl et al. 2013). We developed a triple co-culture SV-HUC-1/HDFib/HUVECs tissue model to study the role of piliation (data not shown). We used the bioreactor system containing two separate inputs for *N. gonorrhoeae* and neutrophils, which can be circulated through the 3D tissue model. Our primary data showed that the challenging the tissue model with E1RECA (pili^{+}) *N. gonorrhoeae* for 2 h activated a higher level of CD11b expression on the neutrophil surface compared to the N924 (pili^{-}) *N. gonorrhoeae* infection. This might be due to the role of pili, which mediates the adherence to the host cell leading neutrophil transmigration (Söderholm et al. 2011; Stohl et al.

2013). However, further investigations are required for understanding the role of pilus in the interaction with neutrophils.

To our knowledge, this is the first report on establishing a 3D tissue model including co-culturing of epithelial and fibroblast cells and triple co-culture of epithelial, fibroblast and endothelial cells to study neisserial infection and immune response. Our model provides physiologically relevant conditions containing both the connective tissue and polarized epithelial cell monolayer, representing a significant advance in modeling of *N. gonorrhoeae* infection.

4.4 Primary cell models

Organoids technology has provided a useful tool for studying the host-pathogen physiology in infection disease (Engevik et al. 2018; Kessler et al. 2012). Several investigations employed micro-injection to introduce pathogen to the organoids for providing a direct contact of the pathogen with the apical side of the cells (Forbester et al. 2015, 2016; Schumacher et al. 2015). We decided to develop a 3D tissue model based on the primary cells, facilitating the pathogen-host contact during the infection. We planned to add connective tissue as a supportive layer of epithelial cells, which is not available in the organoid models. As discussed earlier, the fibroblasts are playing an essential role in proliferation of epithelial cells and mediation of the inflammatory responses. We isolated primary cells from the cervix and endometrium derived from the patient in order to generate the endometrium and cervix organoids. We could expand the proper amount of endometrium organoids after 10 days of cultivation while we could obtain only a few numbers of organoids for cervix at the same time of culturing. Separation of the endocervix and ectocervix parts in the cervix biopsy is necessary (Chumduri et al. 2018). Ectocervix required inhibition of the Wnt signaling pathway while endocervix is driven by the Wnt signaling pathway, showing that cells in these regions may require the specific culture media for proliferation (Chumduri et al. 2018). We used culture media contains Wnt signaling proteins for the cervix organoids, which might induce the proliferation of the only endocervical cells.

After proliferation of the organoids from the isolated cells, we seeded the primary cells on the SIS scaffold to develop primary tissue models. H&E staining of the established tissue models showed that primary cells in both tissue models formed a confluent monolayer (Figure 40a-b).

However, they are not as polarized as the columnar epithelial cells in the endometrium and cervix of the tissue from the same patient (Figure 40e-f). In this study, we used the basal media for proliferation of organoids. It has been shown that the differentiation medium contains the hormones such as estradiol, progesterone, and cyclic adenosine monophosphate (cAMP) influences the differentiation of endometrium stem cells and polarization of the epithelial cells (Turco et al. 2017). We think that the lack of hormones in our culture media impacts on the polarization of the epithelial cells.

In addition, the fibroblasts in the natural tissue from the patient are denser compared to what we observed in the established 3D tissue models. The fibroblast proliferation might be solved by increasing the cultivation time and the initial seeding number of fibroblasts.

The immunohistochemical analysis of primary tissue models showed the expression of fibroblast and secretory cells (PAX8) (Figure 40c-d). PAX8 is normally produced in proliferative and secretary endometrium (Kessler et al. 2015; Turco et al. 2017). In the endometrium tissue model, cells showed a positive PAX8, which is the characteristic of endometrial glands. In the cervix tissue models, a week signal of PAX8 was detected, presenting the absence of secretory cells.

The establishment of the primary tissue models showed promising results, providing biomimetic conditions for infection studies. However, further experiments are required for the development of tissue models to enhance the proliferation and differentiation of the epithelial cells on the SIS scaffold. In addition, optimization of the culture media supplemented with the essential hormones may improve the polarization of the isolated cells. Another effective parameter would be the adjustment of the culture conditions. As we discussed in the triple co-culture models, a dynamic cell culture system creates a more realistic environment crucial step towards a physiological model.

Chapter 5 Conclusions and future perspective

In this project, we developed several culture models based on the SIS scaffold and Transwell® insert in order to study the *N. gonorrhoeae* infection including adhesion, invasion, transmigration, and inflammatory responses (Table 20). We established monoculture, co-culture, and triple co-culture tissue models to mimic the site of infection and study the different strains of *N. gonorrhoeae* for long-term infection.

First, we established three independent 3D tissue models based on the SIS scaffold by co-culturing of epithelial (T84, HEC-1-B, and SV-HUC-1) and fibroblast (HDFib) cells. We also developed the same co-culture models based on the Transwell® insert. The 3D tissue and Transwell® models then characterized by histological, immunohistochemical, ultrastructural, and functional analysis. The tissue models showed the formation of TJs, microvilli and connective tissue in addition to mucus production. The modified 3D tissue models have a permeability of ≈1-2% (FITC-dextran, 4 kDa) which is less permeable than the counterpart i.e. Transwell® model (≈3-5%).

We then infected the established 3D tissue models with different *N. gonorrhoeae* strains and derivatives presenting various phenotypes regarding adhesion and invasion. The results showed the disruption of TJs by *N. gonorrhoeae.* Among the different strains, VP1 showed a higher destructive effect on the ZO-1 TJs (≥85%). In addition, MS11 derivative N924, lacking three major virulence factors ($Pili^-$, Opa^- and $PorB_{IB}$) had a milder effect on tissue barrier integrity than the clinical isolate VP1. Taken together, the findings demonstrated that the disruption of TJs and immune response are dependent on the type of bacteria strains and cell lines.

Furthermore, the transmigration efficacy results showed the *N. gonorrhoeae* can transmigrate across the epithelial cell barrier in Transwell® models after 6 h of infection. However, the 3D tissue models based on the SIS scaffold created a more closely physiologic environment, providing suitable conditions for studying infection up to 6 days.

We showed that in the infection study using our tissue models based on the SIS scaffold, the type of epithelial cells and *N. gonorrhoeae* strains are effective on the production of IL-6, IL-8, and TNF-α upon infection while the previously reported data indicated that the presence of *N. gonorrhoeae* itself can induce the production of cytokines in the epithelial cells regardless of the strains and the state of the invasion.

Table 20. Summary of the established tissue models in this present study.

The complexity of tissue model

Tissue model	Scaffold	Static/ dynamic	*N. gonorrhoeae* strain	Key remark
Co-culture of HEC-1-B /HDFib	Transwell®	Static	N927, N924, MS11, MS11/ΔOpa, VP1	An *in vitro* model of the female reproductive tract tissue
Co-culture of SV-HUC-1 /HDFib	Transwell®	Static	N927, N924, MS11, MS11/ΔOpa, VP1	An *in vitro* model of the male urogenital tissue
Co-culture of T84/HDFib	Transwell®	Static	N927, N924, MS11, MS11/ΔOpa, VP1	An *in vitro* model of colon epithelial cells with a tight epithelial barrier
Co-culture of HEC-1-B/ HDFib	SIS	Static/ dynamic	N927, N924, MS11, MS11/ΔOpa, VP1	-A 3D tissue mucosal model resembling female reproductive tract tissue -Long-term infection study
Co-culture of SV-HUC-1/HDFib	SIS	Static/ dynamic	N927, N924, MS11, MS11/ΔOpa, VP1	-A 3D tissue model mimicking the male urogenital tissue with a squamous epithelial layer -A model with a strong immune response
Co-culture of T84/HDFib	SIS	Static/ dynamic	N927, N924, MS11, MS11/ΔOpa, VP1	-A 3D biomimetic tissue model with a tight epithelial barrier and highly polarized cells -long-term infection study
Co-culture of primary cervix cells/ primary fibroblast	SIS	Static	Not studied	A biomimetic tissue model that retains the morphological and functional characteristics of the tissue of origin (cervix).
Co-culture of primary endometrium cells/primary fibroblast	SIS	Static	Not studied	A biomimetic tissue model that retains the morphological and functional characteristics of the tissue of origin (endometrium).
Triple co-culture of T84/HDFib/ HUVEC	SIS	Static/ dynamic	N927- GFP	A 3D tissue model for studying the role of neutrophils upon infection

We conclude that the T84/HDFib tissue model, with higher TEER and lower permeability, produces better barrier function.

Furthermore, we modified one of the co-culture models of the previous step by triple co-culturing of T84/ HDFib /HUVECs in order to study the transmigration of neutrophils isolated from human blood to the site of infection. We investigated the neutrophils activation upon infection using a perfusion-based bioreactor system. During the experiment, neutrophils are perfused to the tissue model from the side of endothelial mimicking the *in vivo* conditions. At the same time, GFP-expressing N927 was circulated from the epithelial side of the tissue model. The outcome of this experiment showed the deformation shape of neutrophils and the crawling of neutrophils along with the tissue layers. Nevertheless, transcriptome analysis of the special population i.e infected and non-infected neutrophils using single-cell sequencing is highly recommended.

Multiple investigations examined the effect of dynamic culture conditions on the cellular mechanisms and the interaction between cell and pathogens. To our knowledge, this is the first 3D tissue triple co-culture model for studying infection and neutrophils transmigration under *in vitro* dynamic conditions.

Furthermore, there are a couple of important aspects to be considered for further improvement of the 3D tissue models based on the SIS scaffold.

In this work, primary cells have been used and the results were promising. One perspective work would be the differentiation of primary cells including the hormone responsiveness of the tissue model. The role of the stromal cells is also of significance, especially for endometrial tissue where stromal cells contribute to the growth of epithelial cells as well as to the tissue response to hormones (Arnold et al. 2001; Bläuer et al. 2005). Such improvement of the models would enable us to study the relationship between the hormonal status of the host and the infection. Moreover, the availability of primary epithelial cells from the urogenital tract by the usage of organoid technology (Boretto et al. 2017; Kessler et al. 2015) is a useful tool for studying the infection.

In addition, the pH of the site of infection is an effective parameter on *N. gonorrhoeae* growth and metabolism (Morse and Hebeler 1978; St Amant, Valentin-Bon, and Jerse 2002). It is recommended that further experiments could be designed in order to study the role of pH on

the property of mucus and the efficacy of infection (Gorodeski 1996; Heckels et al. 1976; Zheng, Alcorn, and Cohen 1994).

One of the challenging issues in the field of *N. gonorrhoeae* is to understand the role of pilus in the infection process. Further experiments should be performed to find out more information about the mechanism of the pilus in the infection.

Another effective factor on infection study would be microbiota. Microbiota in various parts of the human female reproductive system is not identical. It has also been reported that there is a relation between microbiota and menstrual cycle and immune responses of the genital tract (Chen et al. 2017; Forsgren-brusk 2006; Mirmonsef et al. 2011). Exploring host-microbiome interactions during the infection would help us to understand the protective role of microbiota against the infection.

The majority of the studies in neisserial infection have been done under static culture conditions. One potential work would be employing the bioreactor systems in order to provide well-controlled culture conditions such as applying shear stress to the cells. It is suggested that the bioreactor system can be implemented in the infection studies in order to investigate various facets of *N. gonorrhoeae* infection.

In this study, we established biomimetic tissue models based on the SIS scaffold for studying *N. gonorrhoeae* infection. According to the literature, most of the studies relied on the mono-culture of epithelial cells on the Transwell® insert. Here, we introduced co-culture and triple co-culture models mimicking the site of infection. The results showed that our tissue models provide suitable conditions for long-term infection study, which is not possible in the Transwell® models. Furthermore, we attempted to establish primary tissue models based on the SIS scaffold. The preliminary data were encouraging. However, further investigations are required to develop a more physiological model based on the primary cells.

References

Amich, Jorge, Zeinab Mokhtari, Marlene Strobel, Elena Vialetto, Natarajaswamy Kalleda, Katja J. Jarick, Christian Brede, Ana-Laura Jordán-Garrote, Sina Thusek, Katharina Schmiedgen, Berkan Arslan, Jürgen Pinnecker, Christopher R. Thornton, Matthias Gunzer, Sven Krappmann, Hermann Einsele, Katrin G. Heinze, and Andreas Beilhack. 2019. "3D Light Sheet Fluorescence Microscopy of Lungs to Dissect Local Host Immune - Aspergillus Fumigatus Interactions." *BioRxiv* 661157.

Anahtar, Melis N., Elizabeth H. Byrne, Kathleen E. Doherty, Brittany A. Bowman, Hidemi S. Yamamoto, Magali Soumillon, Nikita Padavattan, Nasreen Ismail, Amber Moodley, Mary E. Sabatini, Musie S. Ghebremichael, Chad Nusbaum, Curtis Huttenhower, Herbert W. Virgin, Thumbi Ndung'u, Krista L. Dong, Bruce D. Walker, Raina N. Fichorova, and Douglas S. Kwon. 2015. "Cervicovaginal Bacteria Are a Major Modulator of Host Inflammatory Responses in the Female Genital Tract." *Immunity* 42(5):965–76.

Anderson, Deborah, Joseph A. Politch, and Jeffrey Pudney. 2011. "HIV Infection and Immune Defense of the Penis." *American Journal of Reproductive Immunology* 65(3):220–29.

Arko, R. J. 1972. "Neisseria Gonorrhoeae: Experimental Infection of Laboratory Animals." *Science* 177(4055):1200–1201.

Arko, R. J. 1974. "An Immunologic Model in Laboratory Animals for the Study of Neisseria Gonorrhoeae." *Journal of Infectious Diseases* 129(4):451–55.

Arko, R. J. 1989. "Animal Models for Pathogenic Neisseria Species." *Clinical Microbiology Reviews* 2(Suppl):S56–59.

Arnold, Julia T., David G. Kaufman, Markku Seppälä, and Bruce A. Lessey. 2001. "Endometrial Stromal Cells Regulate Epithelial Cell Growth in Vitro: A New Co-Culture Model." *Human Reproduction* 16(5):836–45.

Badylak, Stephen F. 2007. "The Extracellular Matrix as a Biologic Scaffold Material." *Biomaterials* 28(25):3587–93.

Bancroft, Gregory N., Vassilios I. Sikavitsas, and Antonios G. Mikos. 2003. "Technical Note: Design of a Flow Perfusion Bioreactor System for Bone Tissue-Engineering Applications." *Tissue Engineering* 9(3):549–54.

Bardsley, Katie, Anthony J. Deegan, Alicia El Haj, and Ying Yang. 2017. "Current State-of-the-Art 3D Tissue Models and Their Compatibility with Live Cell Imaging." Pp. 3–18 in *Advances in Experimental Medicine and Biology*.

Bauer, Frank J., Thomas Rudel, Markus Stein, and Thomas F. Meyer. 1999. "Mutagenesis of the Neisseria Gonorrhoeae Porin Reduces Invasion in Epithelial Cells and Enhances Phagocyte Responsiveness." *Molecular Microbiology* 31(3):903–13.

Bhat, K. S., C. P. Gibbs, O. Barrera, S. G. Morrison, F. Jähnig, A. Stern, E. M. Kupsch, T. F. Meyer, and J. Swanson. 1991. "The Opacity Proteins of Neisseria Gonorrhoeae Strain MS11 Are Encoded by a Family of 11 Complete Genes." *Molecular Microbiology* 5(8):1889–1901.

Blake, K. M., S. O. Carrigon, A. C. IssekutzZ, and A. W. Stadynk. 2004. "Neutrophils Migrate across Intestinal Epithelium Using Beta2 Integrin (CD11b/CD18)-Independent Mechanisms." *Clinical and Experimental Immunology* 136(2):262–68.

Bläuer, Merja, P. K. Heinonen, P. M. Martikainen, E. Tomás, and T. Ylikomi. 2005. "A Novel Organotypic Culture Model for Normal Human Endometrium: Regulation of Epithelial Cell Proliferation by Estradiol and Medroxyprogesterone Acetate." *Human Reproduction* 20(4):864–71.

Boretto, Matteo, Benoit Cox, Manuel Noben, Nikolai Hendriks, Amelie Fassbender, Heleen Roose, Frédéric Amant, Dirk Timmerman, Carla Tomassetti, Arne Vanhie, Christel Meuleman, Marc Ferrante, and Hugo Vankelecom. 2017. "Development of Organoids from Mouse and Human Endometrium Showing Endometrial Epithelium Physiology and Long-Term Expandability." *Development* 144(10):1775–86.

Borregaard, Niels. 2010. "Review Neutrophils , from Marrow to Microbes." *Immunity* 33(5):657–70.

Brede, Christian, Mike Friedrich, Ana-Laura Jordán-Garrote, Simone S. Riedel, Carina A. Bäuerlein, Katrin G. Heinze, Tobias Bopp, Stephan Schulz, Anja Mottok, Carolin Kiesel, Katharina Mattenheimer, Miriam Ritz, Viktoria von Krosigk, Andreas Rosenwald, Hermann Einsele, Robert S. Negrin, Gregory S. Harms, and Andreas Beilhack. 2012. "Mapping Immune Processes in Intact Tissues at Cellular Resolution." *Journal of Clinical Investigation* 122(12):4439–46.

Buckley, Christopher D., Darrell Pilling, Janet M. Lord, Arne N. Akbar, Dagmar Scheel-Toellner, and Mike Salmon. 2001. "Fibroblasts Regulate the Switch from Acute Resolving to Chronic Persistent Inflammation." *Trends in Immunology* 22(4):199–204.

Cannon, J. G., T. M. Buchanan, and P. F. Sparling. 1983. "Confirmation of Association of Protein I Serotype of Neisseria Gonorrhoeae with Ability to Cause Disseminated Infection." *Infection and Immunity* 40(2):816–19.

Château, Alice and H. Steven Seifert. 2016. "Neisseria Gonorrhoeae Survives within and Modulates Apoptosis and Inflammatory Cytokine Production of Human Macrophages." 18(October 2015):546–60.

Chen, Adrienne and H. Steven Seifert. 2013. "Structure-Function Studies of the Neisseria Gonorrhoeae Major Outer Membrane Porin." *Infection and Immunity* 81(12):4383–91.

Chen, Chen, Xiaolei Song, Weixia Wei, Huanzi Zhong, Juanjuan Dai, Zhou Lan, Fei Li, Xinlei Yu, Qiang Feng, Zirong Wang, Hailiang Xie, Xiaomin Chen, Chunwei Zeng, Bo Wen, Liping Zeng, Hui Du, Huiru Tang, Changlu Xu, Yan Xia, Huihua Xia, Huanming Yang, Jian Wang, Jun Wang, Lise Madsen, Susanne Brix, Karsten Kristiansen, Xun Xu, Junhua Li, Ruifang Wu, and Huijue Jia. 2017. "The Microbiota Continuum along the Female Reproductive Tract and Its Relation to Uterine-Related Diseases." *Nature Communications* 8(1):875.

Christodoulides, Myron, J. Sylvia Everson, Bin L. Liu, Paul R. Lambden, Peter J. Watt, Eric J. Thomas, and John E. Heckels. 2000. "Interaction of Primary Human Endometrial Cells with Neisseria Gonorrhoeae Expressing Green Fluorescent Protein." *Molecular Microbiology* 35(1):32–43.

Chu, Kengyeh K., Mark E. Kusek, Linbo Liu, Avira Som, Lael M. Yonker, Huimin Leung, Dongyao Cui, Jinhyeob Ryu, Alexander D. Eaton, Guillermo J. Tearney, and Bryan P. Hurley. 2017. "Illuminating Dynamic Neutrophil Trans-Epithelial Migration with Micro-Optical Coherence Tomography." *Scientific Reports* 7(1):45789.

Chumduri, Cindrilla, Rajendra Kumar Gurumurthy, Hilmar Berger, Stefanie Koster, Volker Brinkmann, Uwe Klemm, Hans-Joachim Mollenkopf, Hermann Herbst, Mandy Mangler, and

Thomas F. Meyer. 2018. “Transition of Wnt Signaling Microenvironment Delineates the Squamo-Columnar Junction and Emergence of Squamous Metaplasia of the Cervix.” 2–41.

Craig, Lisa and Juliana Li. 2008. “Type IV Pili: Paradoxes in Form and Function.” *Current Opinion in Structural Biology* 18(2):267–77.

Delves, Peter, Ivan Roitt. 1999. “Encyclopedia of Immunology.” *Choice Reviews Online* 36(07):36-3668-36–3668.

Deng, Yu, Jenny A. Herbert, Claire M. Smith, and Rosalind L. Smyth. 2018. “An in Vitro Transepithelial Migration Assay to Evaluate the Role of Neutrophils in Respiratory Syncytial Virus (RSV) Induced Epithelial Damage.” *Scientific Reports* 8(1):6777.

Deo, Pankaj, Seong H. Chow, Iain D. Hay, Oded Kleifeld, Adam Costin, Kirstin D. Elgass, Jhih-Hang Jiang, Georg Ramm, Kipros Gabriel, Gordon Dougan, Trevor Lithgow, Eva Heinz, and Thomas Naderer. 2018. “Outer Membrane Vesicles from Neisseria Gonorrhoeae Target PorB to Mitochondria and Induce Apoptosis” edited by T. Kubori. *PLOS Pathogens* 14(3):e1006945.

Detmers, Patricia A. 1990. “Neutrophil-Activating Protein 1/Interleukin 8 Stimulates the Binding Activity of the Leukocyte Adhesion Receptor CD11b/CD18 on Human Neutrophils.” *Journal of Experimental Medicine* 171(4):1155–62.

Ding, X., Y. Wang, X. Ma, H. Guo, X. Yan, Q. Chi, J. Li, Y. Hou, and C. Wang. 2014. “Expression of HMGA2 in Bladder Cancer and Its Association with Epithelial-to-Mesenchymal Transition.” *Cell Proliferation* 47(2):146–51.

Doyle, R. J., F. Nedjat-Haiem, K. F. Keller, and C. E. Frasch. 1984. “Diagnostic Value of Interactions between Members of the Family Neisseriaceae and Lectins.” *Journal of Clinical Microbiology* 19(3):383–87.

Draper, C. F., K. Duisters, B. Weger, A. Chakrabarti, A. C. Harms, L. Brennan, T. Hankemeier, L. Goulet, T. Konz, F. P. Martin, S. Moco, and J. van der Greef. 2018. “Menstrual Cycle Rhythmicity: Metabolic Patterns in Healthy Women.” *Scientific Reports* 8(1):14568.

Drury, Jeanie L. and David J. Mooney. 2003. “Hydrogels for Tissue Engineering: Scaffold Design Variables and Applications.” *Biomaterials* 24(24):4337–51.

Edwards, Jennifer L. and Michael a Apicella. 2004. “The Molecular Mechanisms Used by Neisseria Gonorrhoeae To Initiate Infection Differ between Men and Women The Molecular Mechanisms Used by Neisseria Gonorrhoeae To Initiate Infection Differ between Men and Women.” *Clinical Microbiology Reviews* 17(4):965–81.

Edwards, Vonetta L., Liang Chun Wang, Valerie Dawson, Daniel C. Stein, and Wenxia Song. 2013. “Neisseria Gonorrhoeae Breaches the Apical Junction of Polarized Epithelial Cells for Transmigration by Activating EGFR.” *Cellular Microbiology* 15(6):1042–57.

Engevik, Kristen A., Andrea L. Matthis, Marshall H. Montrose, and Eitaro Aihara. 2018. “Organoids as a Model to Study Infectious Disease.” *Methods in Molecular Biology* 1734:71–81.

Faulstich, Michaela, Franziska Hagen, Elita Avota, Vera Kozjak-Pavlovic, Ann Cathrin Winkler, Yibo Xian, Sibylle Schneider-Schaulies, and Thomas Rudel. 2015. “Neutral Sphingomyelinase 2 Is a Key Factor for PorB-Dependent Invasion of Neisseria Gonorrhoeae.” *Cellular Microbiology* 17(2):241–53.

Fichorova, Raina Nakova, Pragnya Jasvantrai Desai, F. C. Gibson, and Caroline Attardo Genco. 2001. “Distinct Proinflammatory Host Responses to Neisseria Gonorrhoeae Infection in Immortalized Human Cervical and Vaginal Epithelial Cells.” *Infection and Immunity* 69(9):5840–48.

Fielding, Ceri A., Rachel M. McLoughlin, Louise McLeod, Chantal S. Colmont, Meri Najdovska, Dianne Grail, Matthias Ernst, Simon A. Jones, Nicholas Topley, and Brendan J. Jenkins. 2008. "IL-6 Regulates Neutrophil Trafficking during Acute Inflammation via STAT3." *The Journal of Immunology* 181(3):2189–95.

Filippi, Marie-Dominique. 2019. "Neutrophil Transendothelial Migration: Updates and New Perspectives." *Blood* 133(20):2149–58.

Forbester, Jessica L., David Goulding, Ludovic Vallier, Nicholas Hannan, Christine Hale, Derek Pickard, Subhankar Mukhopadhyay, and Gordon Dougan. 2015. "Interaction of Salmonella Enterica Serovar Typhimurium with Intestinal Organoids Derived from Human Induced Pluripotent Stem Cells." *Infection and Immunity* 83(7):2926–34.

Forbester, Jessica L., Nicholas Hannan, Ludovic Vallier, and Gordon Dougan. 2016. "Derivation of Intestinal Organoids from Human Induced Pluripotent Stem Cells for Use as an Infection System." Pp. 157–69 in *Methods in molecular biology (Clifton, N.J.)*. Vol. 1283.

Forsgren-brusk, Ulla Birgitta. 2006. "Lactobacilli in the Female Genital Tract in Relation to Other Genital Microbes and Vaginal PH." (December 2005).

Francis, Ian P., Epshita A. Islam, Adam C. Gower, Yazdani B. Shaik-Dasthagirisaheb, Scott D. Gray-Owen, and Lee M. Wetzler. 2018. "Murine Host Response to Neisseria Gonorrhoeae Upper Genital Tract Infection Reveals a Common Transcriptional Signature, plus Distinct Inflammatory Responses That Vary between Reproductive Cycle Phases." *BMC Genomics* 19(1):1–19.

Freitag, Nancy E., H. Steven Seifert, and Michael Koomey. 1995. "Characterization of the PilF?PilD Pilus-Assembly Locus of Neisseria Gonorrhoeae." *Molecular Microbiology* 16(3):575–86.

Fussenegger, Martin, Thomas Rudel, Roland Barten, Roland Ryll, and Thomas F. Meyer. 1997. "Transformation Competence and Type-4 Pilus Biogenesis in Neisseria Gonorrhoeae – a Review 1." 192:125–34.

Fyfe, J. A., C. S. Carrick, and J. K. Davies. 1995. "The PilE Gene of Neisseria Gonorrhoeae MS11 Is Transcribed from a Sigma 70 Promoter during Growth in Vitro." *Journal of Bacteriology* 177(13):3781–87.

Garcia, Daniel L. and Joseph P. Dillard. 2006. "AmiC Functions as an N-Acetylmuramyl-L-Alanine Amidase Necessary for Cell Separation and Can Promote Autolysis in Neisseria Gonorrhoeae." *Journal of Bacteriology* 188(20):7211–21.

Ghosh, D. and J. Sengupta. 1995. "Morphological Characteristics of Human Endometrial Epithelial Cells Cultured on Rat-Tail Collagen Matrix." *Human Reproduction* 10(4):785–90.

Giardina, P. C., R. Williams, D. Lubaroff, and M. A. Apicella. 1998. "Neisseria Gonorrhoeae Induces Focal Polymerization of Actin in Primary Human Urethral Epithelium." *Infection and Immunity* 66(7):3416–19.

Gilbert, Thomas W., Tiffany L. Sellaro, and Stephen F. Badylak. 2006. "Decellularization of Tissues and Organs." *Biomaterials* 27(19):3675–83.

Gipson, Ilene K. 2001. "The Amount of MUC5B Mucin in Cervical Mucus Peaks at Midcycle." *Journal of Clinical Endocrinology & Metabolism* 86(2):594–600.

Gordon, Siamon and Philip R. Taylor. 2005. "Monocyte and Macrophage Heterogeneity." *Nature Reviews Immunology* 5(12):953–64.

Gorodeski, George I. 1996. "The Cultured Human Cervical Epithelium: A New Model for Studying Paracellular Transport." *Journal of the Society for Gynecologic Investigation* 3(5):267–80.

Grassmé, H. U., Robin M. Ireland, and J. P. van Putten. 1996. "Gonococcal Opacity Protein Promotes Bacterial Entry-Associated Rearrangements of the Epithelial Cell Actin Cytoskeleton." *Infection and Immunity* 64(5):1621–30.

Graver, Michelle A. and Jeremy J. Wade. 2011. "The Role of Acidification in the Inhibition of Neisseria Gonorrhoeae by Vaginal Lactobacilli during Anaerobic Growth." *Annals of Clinical Microbiology and Antimicrobials* 10:1–5.

Griffiss, J. M., H. Schneider, R. E. Mandrell, R. Yamasaki, G. A. Jarvis, J. J. Kim, B. W. Gibson, R. Hamadeh, and M. A. Apicella. 1988. "Lipooligosaccharides: The Principal Glycolipids of the Neisserial Outer Membrane." *Clinical Infectious Diseases* 10(Supplement 2):S287–95.

Griffiss, J. McLeod, Claudia J. Lammel, Jun Wang, Nusi P. Dekker, and G. F. Brooks. 1999. "Neisseria Gonorrhoeae Coordinately Uses Pili and Opa to Activate HEC-1- B Cell Microvilli, Which Causes Engulfment of the Gonococci." *Infection and Immunity* 67(7):3469–80.

Griffith, Linda G. and Melody A. Swartz. 2006. "Capturing Complex 3D Tissue Physiology in Vitro." *Nature Reviews Molecular Cell Biology* 7(3):211–24.

Gu, Angel, Zhifang Zhang, Nan Zhang, Walter Tsark, and John E. Shively. 2010. "Generation of Human CEACAM1 Transgenic Mice and Binding of Neisseria Opa Protein to Their Neutrophils" edited by A. J. Ratner. *PLoS ONE* 5(4):e10067.

Hansen, Lea K., Naja Becher, Sara Bastholm, Julie Glavind, Mette Ramsing, Chong J. Kim, Roberto Romero, Jørgen S. Jensen, and Niels Uldbjerg. 2014. "The Cervical Mucus Plug Inhibits, but Does Not Block, the Passage of Ascending Bacteria from the Vagina during Pregnancy." *Acta Obstetricia et Gynecologica Scandinavica* 93(1):102–8.

Harvey, Hillery A., Deborah M. B. Post, and Michael A. Apicella. 2002. "Immortalization of Human Urethral Epithelial Cells : A Model for the Study of the Pathogenesis of and the Inflammatory Cytokine Response to Neisseria Gonorrhoeae Infection." 70(10):5808–15.

Hebeler, B. H. and F. E. Young. 1976. "Mechanism of Autolysis of Neisseria Gonorrhoeae." *Journal of Bacteriology* 126(3):1186–93.

Heckels, J. E., B. Blackett, J. S. Everson, and M. E. Ward. 1976. "The Influence of Surface Charge on the Attachment of Neisseria Gonorrhoeae to Human Cells." *Journal of General Microbiology* 96(2):359–64.

Hedges, Spencer R., Don A. Sibley, Matthew S. Mayo, Edward W. Hook III, and Michael W. Russell. 1998. "Cytokine and Antibody Responses in Women Infected with *Neisseria Gonorrhoeae:* Effects of Concomitant Infections." *The Journal of Infectious Diseases* 178(3):742–51.

Henry, Katherine M., Luke Pase, Carlos Fernando Ramos-Lopez, Graham J. Lieschke, Stephen A. Renshaw, and Constantino Carlos Reyes-Aldasoro. 2013. "PhagoSight: An Open-Source MATLAB® Package for the Analysis of Fluorescent Neutrophil and Macrophage Migration in a Zebrafish Model" edited by J. Z. Rappoport. *PLoS ONE* 8(8):e72636.

Hickey, D. K., M. V. Patel, J. V. Fahey, and C. R. Wira. 2011. "Innate and Adaptive Immunity at Mucosal Surfaces of the Female Reproductive Tract: Stratification and Integration of Immune Protection against the Transmission of Sexually Transmitted Infections." *Journal of Reproductive Immunology* 88(2):185–94.

Holz, Claudia, Dirk Opitz, Lilo Greune, Rainer Kurre, Michael Koomey, M. Alexander Schmidt, and Berenike Maier. 2010. "Multiple Pilus Motors Cooperate for Persistent Bacterial Movement in Two Dimensions." *Physical Review Letters* 104(17):178104.

Hook, Edward W. 2012. "Gender Differences in Risk for Sexually Transmitted Diseases." *The*

American Journal of the Medical Sciences 343(1):10–11.

Hopper, Sylvia, Brandi Vasquez, Alex Merz, Susan Clary, J. Scott Wilbur, and Magdalene So. 2000. "Effects of the Immunoglobulin A1 Protease on Neisseria Gonorrhoeae Trafficking across Polarized T84 Epithelial Monolayers." *Infection and Immunity* 68(2):906–11.

Hopper, Sylvia, J. Scott Wilbur, Brandi L. Vasquez, Jason Larson, Susan Clary, Ian J. Mehr, H. S. Seifert, and Magdalene So. 2000. "Isolation of Neisseria Gonorrhoeae Mutants That Show Enhanced Trafficking across Polarized T84 Epithelial Monolayers." *Infection and Immunity* 68(2):896–905.

Idriss, Haitham T. and James H. Naismith. 2000. "TNFα and the TNF Receptor Superfamily: Structure-Function Relationship(S)." *Microscopy Research and Technique* 50(3):184–95.

Irwin, Juan C., David Kirk, Roger J. B. King, Martin M. Quigley, and Ralph B. L. Gwatkin. 1989. "Hormonal Regulation of Human Endometrial Stromal Cells in Culture: An in Vitro Model for Decidualization." *Fertility and Sterility* 52(5):761–68.

James-Holmquest, A. N., J. Swanson, T. M. Buchanan, R. D. Wende, and R. P. Williams. 1974. "Differential Attachment by Piliated and Nonpiliated Neisseria Gonorrhoeae to Human Sperm." *Infection and Immunity* 9(5):897–902.

Jarvis, Gary A., Jing Li, and Karen V. Swanson. 1999. "Invasion of Human Mucosal Epithelial Cells by Neisseria Gonorrhoeae Upregulates Expression of Intercellular Adhesion Molecule 1 (ICAM-1)." *Infection and Immunity* 67(3):1149–56.

Jerse, Ann E., Margaret C. Bash, and Michael W. Russell. 2014. "Vaccines against Gonorrhea : Current Status and Future Challenges." *Vaccine* 32(14):1579–87.

Jerse, Ann E., Hong Wu, Mathanraj Packiam, Rachel A. Vonck, Afrin A. Begum, and Lotisha E. Garvin. 2011. "Estradiol-Treated Female Mice as Surrogate Hosts for Neisseria Gonorrhoeae Genital Tract Infections." *Frontiers in Microbiology* 2(JULY):1–13.

Johnson, A. P., D. Taylor-Robinson, and Z. A. McGee. 1977. "Species Specificity of Attachment and Damage to Oviduct Mucosa by Neisseria Gonorrhoeae." *Infection and Immunity* 18(3):833–39.

Kerle, K. K., J. R. Mascola, and T. A. Miller. 1992. "Disseminated Gonococcal Infection." *American Family Physician* 45(1):209–14.

Kessler, Mirjana, Karen Hoffmann, Volker Brinkmann, Oliver Thieck, Susan Jackisch, Benjamin Toelle, Hilmar Berger, Hans-Joachim Mollenkopf, Mandy Mangler, Jalid Sehouli, Christina Fotopoulou, and Thomas F. Meyer. 2015. "The Notch and Wnt Pathways Regulate Stemness and Differentiation in Human Fallopian Tube Organoids." *Nature Communications* 6(1):8989.

Kessler, Mirjana, Julia Zielecki, Oliver Thieck, Hans-Joachim Mollenkopf, Christina Fotopoulou, and Thomas F. Meyer. 2012. "Chlamydia Trachomatis Disturbs Epithelial Tissue Homeostasis in Fallopian Tubes via Paracrine Wnt Signaling." *The American Journal of Pathology* 180(1):186–98.

Kim, Minsoo, Hiroshi Ashida, Michinaga Ogawa, Yuko Yoshikawa, Hitomi Mimuro, and Chihiro Sasakawa. 2010. "Bacterial Interactions with the Host Epithelium." *Cell Host and Microbe* 8(1):20–35.

Kim, Won Jong, Dustin Higashi, Maira Goytia, Maria A. Rendón, Michelle Pilligua-Lucas, Matthew Bronnimann, Jeanine A. McLean, Joseph Duncan, David Trees, Ann E. Jerse, and Magdalene So. 2019. "Commensal Neisseria Kill Neisseria Gonorrhoeae through a DNA-Dependent

Mechanism." *Cell Host & Microbe* 26(2):228-239.e8.
Kishimoto, T. 1989. "The Biology of Interleukin-6." *Blood* 74(1):1–10.
Kloppot, Peggy, Martina Selle, Christian Kohler, Sebastian Stentzel, Stephan Fuchs, Volkmar Liebscher, Elke Müller, Devika Kale, Knut Ohlsen, Barbara M. Bröker, Peter F. Zipfel, Barbara C. Kahl, Ralf Ehricht, Michael Hecker, and Susanne Engelmann. 2015. "Microarray-Based Identification of Human Antibodies against Staphylococcus Aureus Antigens." *Proteomics. Clinical Applications* 9(11–12):1003–11.
Knapp, J. S. and K. K. Holmes. 1975. "Disseminated Gonococcal Infections Caused by Neisseria Gonorrhoeae with Unique Nutritional Requirements." *J Infect Dis* 132(2):204–8.
Knapp, Joan S. and Virginia L. Clark. 1984. "Anaerobic Growth of Neisseria Gonorrhoeae Coupled to Nitrite Reduction." 46(1):176–81.
Kozjak-Pavlovic, Vera, Elke A. Dian-Lothrop, Michael Meinecke, Oliver Kepp, Katharina Ross, Krishnaraj Rajalingam, Anke Harsman, Eva Hauf, Volker Brinkmann, Dirk Günther, Ines Herrmann, Robert Hurwitz, Joachim Rassow, Richard Wagner, and Thomas Rudel. 2009. "Bacterial Porin Disrupts Mitochondrial Membrane Potential and Sensitizes Host Cells to Apoptosis" edited by H. S. Seifert. *PLoS Pathogens* 5(10):e1000629.
Kuhlewein, C., Cindy Rechner, Thomas F. Meyer, and Thomas Rudel. 2006. "Low-Phosphate-Dependent Invasion Resembles a General Way for Neisseria Gonorrhoeae To Enter Host Cells." *Infection and Immunity* 74(7):4266–73.
Kumar, V. and A. Sharma. 2010. "International Immunopharmacology Neutrophils : Cinderella of Innate Immune System." *International Immunopharmacology* 10(11):1325–34.
Kupsch, E. M., B. Knepper, T. Kuroki, I. Heuer, and T. F. Meyer. 1993. "Variable Opacity (Opa) Outer Membrane Proteins Account for the Cell Tropisms Displayed by Neisseria Gonorrhoeae for Human Leukocytes and Epithelial Cells." *The EMBO Journal* 12(2):641–50.
Kurita, Takeshi. 2011. "Normal and Abnormal Epithelial Differentiation in the Female Reproductive Tract." *Differentiation* 82(3):117–26.
Langer, R. and J. Vacanti. 1993. "Tissue Engineering." *Science* 260(5110):920–26.
Łaniewski, Paweł, Adriana Gomez, Geoffrey Hire, Magdalene So, and Melissa M. Herbst-Kralovetz. 2017. "Human Three-Dimensional Endometrial Epithelial Cell Model To Study Host Interactions with Vaginal Bacteria and Neisseria Gonorrhoeae" edited by A. J. Bäumler. *Infection and Immunity* 85(3):1–15.
Le, Anh D. and Jimmy James Brown. 2012. "Wound Healing." Pp. 6–10 in *Current Therapy In Oral and Maxillofacial Surgery*. Elsevier.
Leuzzi, Rosanna, Laura Serino, Maria Scarselli, Silvana Savino, Maria Rita Fontana, Elisabetta Monaci, Annarita Taddei, and Gunter Fischer. 2005. "Ng-MIP , a Surface-Exposed Lipoprotein of Neisseria Gonorrhoeae , Has a Peptidyl-Prolyl Cis / Trans Isomerase (PPIase) Activity and Is Involved in Persistence in Macrophages." 58:669–81.
Li, C. X. and Mark J. Poznansky. 1990. "Characterization of the ZO-1 Protein in Endothelial and Other Cell Lines." *Journal of Cell Science* 97:231–37.
Li, Guocai, Hongmei Jiao, Hua Yan, Jinsong Wang, Xiaohong Wang, and Mingchun Ji. 2011. "Establishment of a Human CEACAM1 Transgenic Mouse Model for the Study of Gonococcal Infections." *Journal of Microbiological Methods* 87(3):350–54.
Li, Wan-Ju, Rabie M. Shanti, and Rocky S. Tuan. 2007. "Electrospinning Technology for Nanofibrous Scaffolds in Tissue Engineering." in *Nanotechnologies for the Life Sciences*. Vol.

9. Weinheim, Germany: Wiley-VCH Verlag GmbH & Co. KGaA.

Ligon, B. Lee. 2005. “Albert Ludwig Sigesmund Neisser: Discoverer of the Cause of Gonorrhea.” *Seminars in Pediatric Infectious Diseases* 16(4):336–41.

Van Linthout, Sophie, Kapka Miteva, and C. Tschope. 2014. “Crosstalk between Fibroblasts and Inflammatory Cells.” *Cardiovascular Research* 102(2):258–69.

Liu, Guangyu, Christoph M. Tang, and Rachel M. Exley. 2015. “Non-Pathogenic Neisseria: Members of an Abundant, Multi-Habitat, Diverse Genus.” *Microbiology* 161(7):1297–1312.

Liu, Yingru, Nejat K. Egilmez, and Michael W. Russell. 2013. “Enhancement of Adaptive Immunity to Neisseria Gonorrhoeae by Local Intravaginal Administration of Microencapsulated Interleukin 12.” 208:1821–29.

Lu, Ping, Shuyi Wang, Yan Lu, Dante Neculai, Qiming Sun, and Stijn van der Veen. 2018. “A Subpopulation of Intracellular Neisseria Gonorrhoeae Escapes Autophagy-Mediated Killing Inside Epithelial Cells.” *The Journal of Infectious Diseases* 219(1):133–44.

Lucas, Charles T. 1971. “Transfer of Gonococcal Urethritis From Man to Chimpanzee.” *JAMA* 216(10):1612.

Lucas, Charles T., Francis Chandler, John E. Martin, and John D. Schmale. 1971. “Transfer of Gonococcal Urethritis From Man to Chimpanzee: An Animal Model for Gonorrhea.” *JAMA: The Journal of the American Medical Association* 216(10):1612–14.

Lysko, P. G. and S. A. Morse. 1980. “Effects of Steroid Hormones on Neisseria Gonorrhoeae.” *Antimicrobial Agents and Chemotherapy* 18(2):281–88.

Maier, Berenike and Gerard C. L. Wong. 2015. “How Bacteria Use Type IV Pili Machinery on Surfaces.” *Trends in Microbiology* 23(12):775–88.

Maisey, Kevin, Felipe E. Rodrı, Carolina Rodrı, and Felipe E. Reyes-lo. 2012. “Neisseria Gonorrhoeae Induced Disruption of Cell Junction Complexes in Epithelial Cells of the Human Genital Tract.” 14:290–300.

Makino, S., J. P. van Putten, and T. F. Meyer. 1991. “Phase Variation of the Opacity Outer Membrane Protein Controls Invasion by Neisseria Gonorrhoeae into Human Epithelial Cells.” *The EMBO Journal* 10(6):1307–15.

Martin, Jennifer N., Louise M. Ball, Tsega L. Solomon, Alison H. Dewald, Alison K. Criss, and Linda Columbus. 2016. “Neisserial Opa Protein–CEACAM Interactions: Competition for Receptors as a Means of Bacterial Invasion and Pathogenesis.” *Biochemistry* 55(31):4286–94.

Massie, Isobel, Kristina Spaniol, Andreas Barbian, Gereon Poschmann, Kai Stühler, Gerd Geerling, Marco Metzger, Sonja Mertsch, and Stefan Schrader. 2017. “Evaluation of Decellularized Porcine Jejunum as a Matrix for Lacrimal Gland Reconstruction in Vitro for Treatment of Dry Eye Syndrome.” *Investigative Ophthalmology and Visual Science* 58(12):5564–74.

Mendonsa, Alisha M., Tae-Young Na, and Barry M. Gumbiner. 2018. “E-Cadherin in Contact Inhibition and Cancer.” *Oncogene* 37(35):4769–80.

Merz, Alexey J. and Magdalene So. 2000. “Interactions of Pathogenic Neisseriae with Epithelial Cell Membranes.” *Annual Review of Cell and Developmental Biology* 16(1):423–57.

Meseguer, M., A. Pellicer, and C. Simo. 1998. “MUC1 and Endometrial Receptivity.” 4(12):1089–98.

Mickelsen, Patricia A., Eleanore Blackman, and P. Frederick Sparlingl. 1982. “Ability of Neisseria Gonorrhoeae , Neisseria Meningitidis , and Commensal Neisseria Species to Obtain Iron From Lactoferrin.” 35(3):915–20.

Mihm, M., S. Gangooly, and S. Muttukrishna. 2011. “The Normal Menstrual Cycle in Women.” *Animal Reproduction Science* 124(3–4):229–36.

Miller, Karl E. 2006. “Diagnosis and Treatment of Neisseria Gonorrhoeae Infections.” *American Family Physician* 73(10).

Mills, Melody and Mary K. Estes. 2016. “Physiologically Relevant Human Tissue Models for Infectious Diseases.” *Drug Discovery Today* 21(9):1540–52.

Mirmonsef, Paria, Douglas Gilbert, Mohammad R. Zariffard, Bruce R. Hamaker, Amandeep Kaur, Alan L. Landay, and Greg T. Spear. 2011. “The Effects of Commensal Bacteria on Innate Immune Responses in the Female Genital Tract.” *American Journal of Reproductive Immunology* 65(3):190–95.

Moran, Anthony P., Martina M. Prendergast, and Ben J. Appelmelk. 1996. “Molecular Mimicry of Host Structures by Bacterial Lipopolysaccharides and Its Contribution to Disease.” *FEMS Immunology & Medical Microbiology* 16(2):105–15.

Morse, S. A. and B. H. Hebeler. 1978. “Effect of PH on the Growth and Glucose Metabolism of Neisseria Gonorrhoeae.” *Infection and Immunity* 21(1):87–95.

Mosleh, Ibrahim M., Hans Jürgen Boxberger, Michael J. Sessler, and Thomas F. Meyer. 1997. “Experimental Infection of Native Human Ureteral Tissue with Neisseria Gonorrhoeae: Adhesion, Invasion, Intracellular Fate, Exocytosis, and Passage through a Stratified Epithelium.” *Infection and Immunity* 65(8):3391–98.

Muench, Dawn F., David J. Kuch, Hong Wu, Afrin A. Begum, Sandra J. Veit, Marie-Eve Pelletier, Ángel A. Soler-García, and Ann E. Jerse. 2009. “Hydrogen Peroxide–Producing Lactobacilli Inhibit Gonococci In Vitro but Not during Experimental Genital Tract Infection.” *The Journal of Infectious Diseases* 199(9):1369–78.

Navabi, Nazanin, Michael A. McGuckin, and Sara K. Lindén. 2013. “Gastrointestinal Cell Lines Form Polarized Epithelia with an Adherent Mucus Layer When Cultured in Semi-Wet Interfaces with Mechanical Stimulation” edited by B. Foligne. *PLoS ONE* 8(7):e68761.

Nguyen, Philip V., Jessica K. Kafka, Victor H. Ferreira, Kristy Roth, and Charu Kaushic. 2014. “Innate and Adaptive Immune Responses in Male and Female Reproductive Tracts in Homeostasis and Following HIV Infection.” *Cellular & Molecular Immunology* 11(5):410–27.

Noguchi, Kazuhiro, Kiyoshi Tsukumi, and Toru Urano. 2003. “Qualitative and Quantitative Differences in Normal Vaginal Flora of Conventionally Reared Mice, Rats, Hamsters, Rabbits, and Dogs.” *Comparative Medicine* 53(4):404–12.

Ohnishi, Makoto, Daniel Golparian, Ken Shimuta, Takeshi Saika, Shinji Hoshina, Kazuhiro Iwasaku, Shu-ichi Nakayama, Jo Kitawaki, and Magnus Unemo. 2011. “Is Neisseria Gonorrhoeae Initiating a Future Era of Untreatable Gonorrhea?: Detailed Characterization of the First Strain with High-Level Resistance to Ceftriaxone.” *Antimicrobial Agents and Chemotherapy* 55(7):3538–45.

De Oliveira, Sofia, Emily E. Rosowski, and Anna Huttenlocher. 2016. “Neutrophil Migration in Infection and Wound Repair: Going Forward in Reverse.” *Nature Reviews Immunology* 16(6):378–91.

Ott, C., K. Ross, S. Straub, B. Thiede, M. Gotz, C. Goosmann, M. Krischke, M. J. Mueller, G. Krohne, T. Rudel, and V. Kozjak-Pavlovic. 2012. “Sam50 Functions in Mitochondrial Intermembrane Space Bridging and Biogenesis of Respiratory Complexes.” *Molecular and Cellular Biology* 32(6):1173–88.

Parkos, Charles A., Charlene Delp, M. A. Arnaout, and James L. Madara. 1991. "Neutrophil Migration across a Cultured Intestinal Epithelium. Dependence on a CD11b/CD18-Mediated Event and Enhanced Efficiency in Physiological Direction." *Journal of Clinical Investigation* 88(5):1605–12.

Pioli, P. A., E. Amiel, T. M. Schaefer, J. E. Connolly, C. R. Wira, and P. M. Guyre. 2004. "Differential Expression of Toll-Like Receptors 2 and 4 in Tissues of the Human Female Reproductive Tract." *Infection and Immunity* 72(10):5799–5806.

Plaut, A. G., J. V Gilbert, M. S. Artenstein, and J. D. Capra. 1975. "Neisseria Gonorrhoeae and Neisseria Meningitidis: Extracellular Enzyme Cleaves Human Immunoglobulin A." *Science (New York, N.Y.)* 190(4219):1103–5.

Pudlas, Marieke, Steffen Koch, Carsten Bolwien, Sibylle Thude, Nele Jenne, Thomas Hirth, Heike Walles, and Katja Schenke-Layland. 2011. "Raman Spectroscopy: A Noninvasive Analysis Tool for the Discrimination of Human Skin Cells." *Tissue Engineering Part C: Methods* 17(10):1027–40.

Pudney, Jeffrey and Deborah Anderson. 2011. "Innate and Acquired Immunity in the Human Penile Urethra." *Journal of Reproductive Immunology* 88(2):219–27.

Punsalang, A. P. and W. D. Sawyer. 1973. "Role of Pili in the Virulence of Neisseria Gonorrhoeae." *Infection and Immunity* 8(2):255–63.

van Putten, J. P. 1993. "Phase Variation of Lipopolysaccharide Directs Interconversion of Invasive and Immuno-Resistant Phenotypes of Neisseria Gonorrhoeae." *The EMBO Journal* 12(11):4043–51.

Quillin, Sarah Jane and H. Steven Seifert. 2018. "Neisseria Gonorrhoeae Host Adaptation and Pathogenesis." *Nature Reviews Microbiology* 16(4):226–40.

Rahme, L., E. Stevens, S. Wolfort, Jing Shao, R. Tompkins, and F. Ausubel. 1995. "Common Virulence Factors for Bacterial Pathogenicity in Plants and Animals." *Science* 268(5219):1899–1902.

Rampersaud, Ryan, Tara M. Randis, and Adam J. Ratner. 2012. "Seminars in Fetal & Neonatal Medicine Microbiota of the Upper and Lower Genital Tract." *Seminars in Fetal and Neonatal Medicine* 17(1):51–57.

Ramsey, Kyle H., Herman Schneider, Alan S. Cross, John W. Boslego, David L. Hoover, Terri L. Staley, Robert A. Kuschner, and Carolyn D. Deal. 1995. "Inflammatory Cytokines Produced in Response to Experimental Human Gonorrhea." *Journal of Infectious Diseases* 172(1):186–91.

Rechner, Cindy, Christiane Kühlewein, Anne Müller, Hansjörg Schild, and Thomas Rudel. 2007. "Host Glycoprotein Gp96 and Scavenger Receptor SREC Interact with PorB of Disseminating Neisseria Gonorrhoeae in an Epithelial Invasion Pathway." *Cell Host and Microbe* 2(6):393–403.

Rees, E., I. A. Tait, D. Hobson, R. E. Byng, and F. W. Johnson. 1977. "Neonatal Conjunctivitis Caused by Neisseria Gonorrhoeae and Chlamydia Trachomatis." *The British Journal of Venereal Diseases* 53(3):173–79.

Reimer, Anastasija, Florian Seufert, Matthias Weiwad, Jutta Ebert, Nicole M. Bzdyl, Charlene M. Kahler, Mitali Sarkar-Tyson, Ulrike Holzgrabe, Thomas Rudel, and Vera Kozjak-Pavlovic. 2016. "Inhibitors of Macrophage Infectivity Potentiator-like PPIases Affect Neisserial and Chlamydial Pathogenicity." *International Journal of Antimicrobial Agents* 48(4):401–8.

Rodríguez-Tirado, Carolina, Kevin Maisey, Felipe E. Rodríguez, Sebastián Reyes-Cerpa, Felipe E. Reyes-López, and Mónica Imarai. 2012. "Neisseria Gonorrhoeae Induced Disruption of Cell Junction Complexes in Epithelial Cells of the Human Genital Tract." *Microbes and Infection* 14(3):290–300.

Rosales, Carlos. 2018. "Neutrophil: A Cell with Many Roles in Inflammation or Several Cell Types?" *Frontiers in Physiology* 9(FEB):1–17.

Roth, Alexandra, Corinna Mattheis, Petra Muenzner, Magnus Unemo, and Christof R. Hauck. 2013. "Innate Recognition by Neutrophil Granulocytes Differs between Neisseria Gonorrhoeae Strains Causing Local or Disseminating Infections" edited by B. A. McCormick. *Infection and Immunity* 81(7):2358–70.

Rübsam, Matthias, Aaron F. Mertz, Akiharu Kubo, Susanna Marg, Christian Jüngst, Gladiola Goranci-Buzhala, Astrid C. Schauss, Valerie Horsley, Eric R. Dufresne, Markus Moser, Wolfgang Ziegler, Masayuki Amagai, Sara A. Wickström, and Carien M. Niessen. 2017. "E-Cadherin Integrates Mechanotransduction and EGFR Signaling to Control Junctional Tissue Polarization and Tight Junction Positioning." *Nature Communications* 8(1):1250.

Rudel, Thomas, Dirk Facius, Roland Barten, I. Scheuerpflug, Edgar Nonnenmacher, and Thomas F. Meyer. 1995. "Role of Pili and the Phase-Variable PilC Protein in Natural Competence for Transformation of Neisseria Gonorrhoeae." *Proceedings of the National Academy of Sciences* 92(17):7986–90.

Rudel, Thomas, Oliver Kepp, and Vera Kozjak-Pavlovic. 2010. "Interactions between Bacterial Pathogens and Mitochondrial Cell Death Pathways." *Nature Reviews. Microbiology* 8(10):693–705.

Rudel, Thomas, Jos P. M. Putten, Carol P. Gibbs, Rainer Haas, and Thomas F. Meyer. 1992. "Interaction of Two Variable Proteins (PilE and PilC) Required for Pilus-Mediated Adherence of Neisseria Gonorrhoeae to Human Epithelial Cells." *Molecular Microbiology* 6(22):3439–50.

Sakamoto, Naoya, Naoki Saito, Xiaobo Han, Toshiro Ohashi, and Masaaki Sato. 2010. "Effect of Spatial Gradient in Fluid Shear Stress on Morphological Changes in Endothelial Cells in Response to Flow." *Biochemical and Biophysical Research Communications* 395(2):264–69.

Salvermoser, Melanie, Daniela Begandt, Ronen Alon, and Barbara Walzog. 2018. "Nuclear Deformation During Neutrophil Migration at Sites of Inflammation." *Frontiers in Immunology* 9(NOV):2680.

Schindelin, Johannes, Curtis T. Rueden, Mark C. Hiner, and Kevin W. Eliceiri. 2017. "The ImageJ Ecosystem: An Open Platform for Biomedical Image Analysis." 82(608):518–29.

Schmid, Benjamin, Johannes Schindelin, Albert Cardona, Mark Longair, and Martin Heisenberg. 2010. "A High-Level 3D Visualization API for Java and ImageJ." *BMC Bioinformatics* 11(1):274.

Schumacher, Michael A., Rui Feng, Eitaro Aihara, Amy C. Engevik, Marshall H. Montrose, Karen M. Ottemann, and Yana Zavros. 2015. "Helicobacter Pylori -Induced Sonic Hedgehog Expression Is Regulated by NFκB Pathway Activation: The Use of a Novel In Vitro Model to Study Epithelial Response to Infection." *Helicobacter* 20(1):19–28.

Schweinlin, Matthias, Angela Rossi, Nina Lodes, Christian Lotz, Stephan Hackenberg, Maria Steinke, Heike Walles, and Florian Groeber. 2017. "Human Barrier Models for the in Vitro Assessment of Drug Delivery." *Drug Delivery and Translational Research* 7(2):217–27.

Schweinlin, Matthias, Sabine Wilhelm, and Ivo Schwedhelm. 2016. “Development of an Advanced Primary Human In Vitro Model of the Small Intestine.” 22(9):873–83.

Shaw, J. H. and S. Falkow. 1988. “Model for Invasion of Human Tissue Culture Cells by Neisseria Gonorrhoeae.” *Infect Immun* 56(6):1625–32.

Shi, Lei, Vincent Ronfard, Shi L., and Ronfard V. 2013. “Biochemical and Biomechanical Characterization of Porcine Small Intestinal Submucosa (SIS): A Mini Review.” *International Journal of Burns and Trauma* 3(4):173–79.

Shukla, Vasudha, Victoria Barnhouse, William E. Ackerman, Taryn L. Summerfield, Heather M. Powell, Jennifer L. Leight, Douglas A. Kniss, and Samir N. Ghadiali. 2018. “Cellular Mechanics of Primary Human Cervical Fibroblasts: Influence of Progesterone and a Pro-Inflammatory Cytokine.” *Annals of Biomedical Engineering* 46(1):197–207.

Sikora, Aleksandra E., Igor H. Wierzbicki, Ryszard A. Zielke, Rachael F. Ryner, Konstantin V Korotkov, Susan K. Buchanan, and Nicholas Noinaj. 2018. “Structural and Functional Insights into the Role of BamD and BamE within the β-Barrel Assembly Machinery in Neisseria Gonorrhoeae.” *Journal of Biological Chemistry* 293(4):1106–19.

Silzle, Tobias, Gwendalyn J. Randolph, Marina Kreutz, and Leoni A. Kunz-Schughart. 2004. “The Fibroblast: Sentinel Cell and Local Immune Modulator in Tumor Tissue.” *International Journal of Cancer* 108(2):173–80.

Simon, Carlos. 2018. “Introduction: Do Microbes in the Female Reproductive Function Matter?” *Fertility and Sterility* 110(3):325–26.

Simons, Mark P., William M. Nauseef, Michael A. Apicella, and I. Nfect I. Mmun. 2005. “Interactions of Neisseria Gonorrhoeae with Adherent Polymorphonuclear Leukocytes.” 73(4):1971–77.

Smith, R. S., T. J. Smith, T. M. Blieden, and R. P. Phipps. 1997. “Fibroblasts as Sentinel Cells. Synthesis of Chemokines and Regulation of Inflammation.” *The American Journal of Pathology* 151(2):317–22.

Smith, W. B., J. R. Gamble, I. Clark-Lewis, and M. A. Vadas. 1991. “Interleukin-8 Induces Neutrophil Transendothelial Migration.” *Immunology* 72(1):65–72.

Söderholm, Niklas, Katarina Vielfort, Kjell Hultenby, and Helena Aro. 2011. “Pathogenic Neisseria Hitchhike on the Uropod of Human Neutrophils.” *PLoS ONE* 6(9):1–12.

Spiliotis, Markus, Sabrina Lechner, Dennis Tappe, Carsten Scheller, Georg Krohne, and Klaus Brehm. 2008. “Transient Transfection of Echinococcus Multilocularis Primary Cells and Complete in Vitro Regeneration of Metacestode Vesicles.” *International Journal for Parasitology* 38(8–9):1025–39.

Spurbeck, Rachel R. and Cindy Grove Arvidson. 2010. “Lactobacillus Jensenii Surface-Associated Proteins Inhibit Neisseria Gonorrhoeae Adherence to Epithelial Cells.” *Infection and Immunity* 78(7):3103–11.

Srinivasan, Balaji, Aditya Reddy Kolli, Mandy Brigitte Esch, Hasan Erbil Abaci, Michael L. Shuler, and James J. Hickman. 2015. “TEER Measurement Techniques for In Vitro Barrier Model Systems.” *Journal of Laboratory Automation* 20(2):107–26.

St Amant, D. C., Iris E. Valentin-Bon, and Ann E. Jerse. 2002. “Inhibition of Neisseria Gonorrhoeae by Lactobacillus Species That Are Commonly Isolated from the Female Genital Tract.” *Infection and Immunity* 70(12):7169–71.

Stavreus-Evers, Anneli, George Nikas, Lena Sahlin, Håkan Eriksson, and Britt-Marie Landgren.

2001. “Formation of Pinopodes in Human Endometrium Is Associated with the Concentrations of Progesterone and Progesterone Receptors.” *Fertility and Sterility* 76(4):782–91.

Stein, Daniel C., Adriana Levan, Britney Hardy, Liang Chun Wang, Lindsey Zimmerman, and Wenxia Song. 2015. “Expression of Opacity Proteins Interferes with the Transmigration of Neisseria Gonorrhoeae across Polarized Epithelial Cells.” *PLoS ONE* 10(8):1–15.

Steinke, Maria, Roy Gross, Heike Walles, Rainer Gangnus, Karin Schütze, and Thorsten Walles. 2014. “An Engineered 3D Human Airway Mucosa Model Based on an SIS Scaffold.” *Biomaterials* 35(26):7355–62.

Stevens, Jacqueline S. and Alison K. Criss. 2018. “Pathogenesis of Neisseria Gonorrhoeae in the Female Reproductive Tract: Neutrophilic Host Response, Sustained Infection, and Clinical Sequelae.” *Current Opinion in Hematology* 25(1):13–21.

Stevens, Jacqueline S., Mary C. Gray, Christophe Morisseau, and Alison K. Criss. 2018. “Endocervical and Neutrophil Lipoxygenases Coordinate Neutrophil Transepithelial Migration to Neisseria Gonorrhoeae.” *The Journal of Infectious Diseases* 218(10):1663–74.

Stohl, Elizabeth A., Erin M. Dale, Alison K. Criss, and H. Steven Seifert. 2013. “Neisseria Gonorrhoeae Metalloprotease NGO1686 Is Required for Full Piliation, and Piliation Is Required for Resistance to H2O2- and Neutrophil-Mediated Killing” edited by S. J. Norris. *MBio* 4(4):1–9.

Strom, M. S., D. N. Nunn, and S. Lory. 1993. “A Single Bifunctional Enzyme, PilD, Catalyzes Cleavage and N-Methylation of Proteins Belonging to the Type IV Pilin Family.” *Proceedings of the National Academy of Sciences* 90(6):2404–8.

Turco, Margherita Y., Lucy Gardner, Jasmine Hughes, Tereza Cindrova-Davies, Maria J. Gomez, Lydia Farrell, Michael Hollinshead, Steven G. E. Marsh, Jan J. Brosens, Hilary O. Critchley, Benjamin D. Simons, Myriam Hemberger, Bon-Kyoung Koo, Ashley Moffett, and Graham J. Burton. 2017. “Long-Term, Hormone-Responsive Organoid Cultures of Human Endometrium in a Chemically Defined Medium.” *Nature Cell Biology* 19(5):568–77.

Unemo, Magnus and William M. Shafer. 2014. “Antimicrobial Resistance in Neisseria Gonorrhoeae in the 21st Century: Past, Evolution, and Future.” *Clinical Microbiology Reviews* 27(3):587–613.

Wada-Hiraike, Osamu, Haruko Hiraike, Hiroko Okinaga, Otabek Imamov, R. P. A. Barros, Andrea Morani, Yoko Omoto, Margaret Warner, and J. A. Gustafsson. 2006. “Role of Estrogen Receptor Beta in Uterine Stroma and Epithelium: Insights from Estrogen Receptor Beta-/- Mice.” *Proceedings of the National Academy of Sciences* 103(48):18350–55.

Wang, Dan, Xiaoming Ding, Wujun Xue, Jin Zheng, Xiaohui Tian, Yang Li, Xiaohong Wang, Huanjin Song, Hua Liu, and Xiaohui Luo. 2017. “A New Scaffold Containing Small Intestinal Submucosa and Mesenchymal Stem Cells Improves Pancreatic Islet Function and Survival in Vitro and in Vivo.” *2.341International Journal of Molecular Medicine* 39(1):167–73.

Wang, Jun A., Thomas F. Meyer, and Thomas Rudel. 2008. “Cytoskeleton and Motor Proteins Are Required for the Transcytosis of Neisseria Gonorrhoeae through Polarized Epithelial Cells.” *International Journal of Medical Microbiology* 298(3–4):209–21.

Wang, Jun, Scott D. Gray-Owen, Alexander Knorre, Thomas F. Meyer, and Christoph Dehio. 1998. “Opa Binding to Cellular CD66 Receptors Mediates the Transcellular Traversal of Neisseria Gonorrhoeae across Polarized T84 Epithelial Cell Monolayers.” *Molecular Microbiology*

30(3):657–71.

Wang, Liang Chun, Qian Yu, Vonetta Edwards, Brian Lin, Jessica Qiu, Jerrold R. Turner, Daniel C. Stein, and Wenxia Song. 2017. "Neisseria Gonorrhoeae Infects the Human Endocervix by Activating Non-Muscle Myosin II-Mediated Epithelial Exfoliation." *PLoS Pathogens* 13(4):1–28.

Wang, Q. and B. Margolis. 2007. "Apical Junctional Complexes and Cell Polarity." *Kidney International* 72(12):1448–58.

Wessels, Jocelyn M., Allison M. Felker, Haley A. Dupont, and Charu Kaushic. 2018. "The Relationship between Sex Hormones, the Vaginal Microbiome and Immunity in HIV-1 Susceptibility in Women." *Disease Models & Mechanisms* 11(9):dmm035147.

Who. 2012. "Global Action Plan to Control the Spread and Impact of Antimicrobial Resistance in Neisseria Gonorrhoeae." *World Health Organization* 40.

Wira, Charles R., Katherine S. Grant-Tschudy, and Margaret A. Crane-Godreau. 2005. "Epithelial Cells in the Female Reproductive Tract: A Central Role as Sentinels of Immune Protection." *American Journal of Reproductive Immunology* 53(2):65–76.

Wira, Charles R., Marta Rodriguez-Garcia, and Mickey V. Patel. 2015. "The Role of Sex Hormones in Immune Protection of the Female Reproductive Tract." *Nature Reviews Immunology* 15(4):217–30.

Wong, Sonia How Ming, Chee Mun Fang, Lay-Hong Chuah, Chee Onn Leong, and Siew Ching Ngai. 2018. "E-Cadherin: Its Dysregulation in Carcinogenesis and Clinical Implications." *Critical Reviews in Oncology/Hematology* 121(35):11–22.

Woods, Charles R. 2005. "Gonococcal Infections in Neonates and Young Children." *Semin Pediatr Infect Dis* 16(4):258–70.

Workowski, Kimberly A. and Gail A. Bolan. 2015. "Sexually Transmitted Diseases Treatment Guidelines, 2015." *MMWR. Recommendations and Reports : Morbidity and Mortality Weekly Report. Recommendations and Reports* 64(RR-03):1–137.

Yamasaki, R., D. E. Kerwood, H. Schneider, K. P. Quinn, J. M. Griffiss, and R. E. Mandrell. 1994. "The Structure of Lipooligosaccharide Produced by Neisseria Gonorrhoeae, Strain 15253, Isolated from a Patient with Disseminated Infection. Evidence for a New Glycosylation Pathway of the Gonococcal Lipooligosaccharide." *The Journal of Biological Chemistry* 269(48):30345–51.

Yang, Shoufeng, Kah-Fai Leong, Zhaohui Du, and Chee-kai Chua. 2001. "The Design of Scaffolds for Use in Tissue Engineering. Part I. Traditional Factors." *Tissue Engineering* 7(6):679–89.

Yao, Wang, Yu Gan, Kristin M. Myers, Joy Y. Vink, Ronald J. Wapner, and Christine P. Hendon. 2016. "Collagen Fiber Orientation and Dispersion in the Upper Cervix of Non-Pregnant and Pregnant Women" edited by R. G. Haverkamp. *PLOS ONE* 11(11):e0166709.

Yarbrough, Victoria L., Sean Winkle, and Melissa M. Herbst-Kralovetz. 2015. "Antimicrobial Peptides in the Female Reproductive Tract: A Critical Component of the Mucosal Immune Barrier with Physiological and Clinical Implications." *Human Reproduction Update* 21(3):353–77.

Yonker, Lael M., Hongmei Mou, Kengyeh K. Chu, Michael A. Pazos, Huimin Leung, Dongyao Cui, Jinhyeob Ryu, Rhianna M. Hibbler, Alexander D. Eaton, Tim N. Ford, J. R. Falck, T. Bernard Kinane, Guillermo J. Tearney, Jayaraj Rajagopal, and Bryan P. Hurley. 2017. "Development of a Primary Human Co-Culture Model of Inflamed Airway Mucosa." *Scientific Reports*

7(1):1–12.
Yoshida, Kyoko, Charles Jayyosi, Nicole Lee, Mala Mahendroo, and Kristin M. Myers. 2019. “Mechanics of Cervical Remodelling: Insights from Rodent Models of Pregnancy.” *Interface Focus* 9(5):20190026.
Young, Steven L. 2013. “Oestrogen and Progesterone Action on Endometrium: A Translational Approach to Understanding Endometrial Receptivity.” *Reproductive BioMedicine Online* 27(5):497–505.
Yu, Dexin, Hao Geng, Zhiqi Liu, Li Zhao, Zhaofeng Liang, Zhiqiang Zhang, Dongdong Xie, Yi Wang, Tao Zhang, Jie Min, and Caiyun Zhong. 2017. “Cigarette Smoke Induced Urocystic Epithelial Mesenchymal Transition via MAPK Pathways.” *Oncotarget* 8(5):8791–8800.
Zeth, Kornelius, Vera Kozjak-Pavlovic, Michaela Faulstich, Martin Fraunholz, Robert Hurwitz, Oliver Kepp, and Thomas Rudel. 2013. “Structure and Function of the PorB Porin from Disseminating Neisseria Gonorrhoeae.” *Biochemical Journal* 449(3):631–42.
Zheng, H. Y., Timothy M. Alcorn, and Myron S. Cohen. 1994. “Effects Of H2 O2-Producing Lactobacilli On Neisseria Gonorrhoeae Growth and Activity.” 1209–15.

List of Abbreviations

Abbreviation	Full form
%	Percent
Ω	Ohm
®	Registered
°C	Degrees centigrade
µg	Microgram
µl	Microliter
µm	Micrometer
2D	Two-dimensional
3D	Three-dimensional
BSA	Bovine serum albumin
CEACAM	Carcinoembryonic ntigen cellular adhesion molecule
CFU	Colony Forming Unit
Cm^2	Square centimeter
DAPI	4',6-Diamidino-2-phenylindole
DGI	Disseminated Gonococcal Infections
dH_2O	distilled water
DMEM	Dulbecco's modified Eagle medium
DMSO	Dimethyl sulfoxide
ECM	Extracellular matrix
EDTA	Ethylenediaminetetraacetic acid
EGF	epidermal growth factor
FCS	Fetal Calf Serum
FGF	Fibroblast growth factor

FITC	Fluorescein-isocyanate
GC	*Neisseria gonorrhoeae*, gonococcus
h	hours
H&E	Hematoxylin and Eosin
HBSS	Hanks' Balanced Salt Solution
HGF	Hepatocyte growth factor
IF	Immunofluorescence staining
kDa	kilodalton
kGy	kilo Gray
LOS	Lipooligosaccharide
LPS	Lipopolysaccharide
MOI	Multiplicity of infection
M	Molar
mL	Milliliter
min	minutes
OD	Optical Density
OMV	Outer Membrane Vesicle
Opa	Opacity-associated proteins
PBMC	Peripheral blood mononuclear cell
PBS	Phosphate-buffered saline
Pen/Strep	Penicillin/Streptomycin
PET	Polyethylenterephthalat
PFA	Paraformaldehyd
PID	Pelvic Inflammatory Disease
PMN	Polymorphonuclear leukocyte
PorB	Outer membrane porin protein B
$PorB_{IA}$	PorB serotype A

$PorB_{IB}$	PorB serotype B
Porin	Pore-forming proteins
PPM	Proteose peptone medium
rbc	Red blood cell
rpm	Revolutions er minute
RT	Room Temperature
SD	Standard Deviation
SDS	Sodium Dodecyl Sulphate
SEM	Scanning Electron Microscopy
STI	Sexually Transmitted Infection
TEER	Transepithelial resistance
TEM	Transmission Electron Microscopy
TEMED	Tetramethylethylenediamine
Tfp	Type IV pili
TJ	Tight Junction
UV	Ultra Violet
w/v	Weight per volume
WB	Western blotting
WHO	World Health Organization

Publications and Presentations

1. **Heydarian Motaharehsadat**, Tao Yang, Matthias Schweinlin, Maria Steinke, Heike Walles, Thomas Rudel, and Vera Kozjak-Pavlovic, (2019) "Biomimetic human tissue model for long-term study of *Neisseria Gonorrhoeae* infection." *Frontiers in Microbiology* 10 (July): 1740.
2. **Heydarian Motaharehsadat**., Schweinlin M., Steinke M., Walles H., Rudel T. and Kozjak Pavlovic V., (2019). Development of an advanced human 3D *in vitro* tissue model to study host interaction with *Neisseria gonorrhoeae*. 3D Infect Tissue Symposium. Würzburg, Germany (**Oral presentation**).
3. **Heydarian Motaharehsadat**, Schweinlin M., Steinke M., Walles H., Rudel T. and Kozjak Pavlovic V., (2018). 3D human tissue models for studying *Neisseria gonorrhoeae* infection. GSLS Eureka symposium, Würzburg, Germany (Poster Prize Winner).
4. **Heydarian Motaharehsadat**, Schweinlin M., Steinke M., Walles H., Rudel T. and Kozjak Pavlovic V., (2018). Establishment and characterization of a 3D endometrial epithelial human tissue model to study *Neisseria gonorrhoeae* infection, Würzburg. Germany (Poster).
5. **Heydarian Motaharehsadat**, Schweinlin M., Steinke M., Walles H., Rudel T. and Kozjak Pavlovic V., (2018). 3D *in vitro* human tissue model for studying *Neisseria gonorrhoeae* infection. 12th International Conference and Workshop on Biological Barriers. Saarbrucken, Germany (Poster).

Acknowledgment

First, I would like to offer my special thanks to my advisors, Dr. Vera Kozjak-Pavlovic, Prof. Dr. Thomas Rudel, and Prof. Dr. Heike Walles for supporting me over the last three years.

I would like to say a big thank to Dr. Vera Kozjak-Pavlovic for her continued guidance, encouragement, and advice. She continuously supported me to pursue various projects and improve the quality of my research.

I am very grateful to Prof. Dr. Thomas Rudel for providing me with this opportunity to work in the chair of microbiology and for his scientific advice and insightful suggestions.

I am also deeply grateful to the member of my Ph.D. committee, Prof. Dr. Heike Walles for her helpful advice and suggestions.

I wish to express my deepest gratitude to my beloved husband and best friend for all his love, support, motivation, and most important for always believing in me. Thank you, Ali, you have been an outstanding inspiration to me**.**

I would like to thank the various members of chair of microbiology especially Tao Yang, Elke Maier, Tobias Kunz, Adriana Moldovan, Franziska Solger, Marie Zachary, Kathrin Stelzner, Nadine Vollmuth, David Kessie, Pargev Hovhannisyan, Sudip Das, Suvagata Roy Chowdhury, Kerstin Paprotka, Susanne Bauer, Heike Czotscher, Manuela Hilpert, Kerstin Kordmann, Prof. Dr. Dagmar Beier, Dr. Martin Fraunholz, Dr. Andreas Demuth, and Prof. Dr. Roy Gross. The Mikbio was like my second home. I want to thank for all the wonderful moments we shared together, support, help, patience and a good mood.

I wish to thank several key people who contributed in this project especially Dr. Matthias Schweinlin, Dr. Maria Steinke, and Dr. Thomas Schwarz (TERM); Dr. Knut Ohlsen, Dr. Tobias Hertlein, Dr. Sina Bartfeld, Özge Kayisoglu, and Sylvie Vandenabeele (IMIB); Dr. Andreas Beilhack, Dr. Zeinab Mokhtari, and Dalia Sheta (IZKF); Prof. Dr. Christian Stigloher, Daniela Bunsen, Claudia Gehrig, Barbara Bauer, and Rosemarie Bott (Biocentre); Prof. Dr. Christine Wulff, Dr. Saskia-L. Herbert, and Andrea Fick (UKW).

I would like to acknowledge GSLS especially Dr. Gabriele Blum-Oehler, for her assistance that provided during my Ph.D. project.

I would like to express the deepest appreciation to my parents who instilled a love of science in my soul. Baba Amir, thank you for supporting me in my ambitions. Maman Roya, thank you for helping me get through my wishes. I see you all the love, sacrifice, and selflessness. I am grateful to my sisters, Mina and Maryam, for their constant love and support.

Last but not least, I acknowledge the Deutsche Forschungsgemeinschaft (DFG) GRK 2157 for providing funding during my Ph.D. study.

Affidavit

I hereby confirm that my thesis entitled “Development of human 3D tissue models for studying *Neisseria gonorrhoeae* infection” is the result of my own work. I did not receive any help or support from commercial consultants. All sources and / or materials applied are listed and specified in the thesis.

Furthermore, I confirm that this thesis has not yet been submitted as part of another examination process neither in identical nor in similar form.

Place, Date Signature